

Hydrogel interfaces for applications in microbial biotechnology

by

Niloufar Fattahi

B.S., Sharif University of Technology, 2015

AN ABSTRACT OF A DISSERTATION

submitted in partial fulfillment of the requirements for the degree

DOCTOR OF PHILOSOPHY

Tim Taylor Department of Chemical Engineering
Carl R. Ice College of Engineering

KANSAS STATE UNIVERSITY
Manhattan, Kansas

2021

Abstract

Hydrogels are three-dimensional, water-swollen, highly crosslinked polymers that can be designed to provide biocompatible and biofunctional interfaces for cells and biomolecules. With facile fabrication and precise control over chemistry, pore size, and mechanical properties, hydrogels have been studied extensively in various areas of biomedical and bioengineering, particularly in drug delivery and tissue engineering applications. However, hydrogels have not been well-studied or well-applied to many emerging applications in microbiology. This thesis explores two new applications involving hydrogel interfaces: (1) photodegradable hydrogels for high-throughput screening and isolation of rare bacteria and (2) hydrogels for protection of electroactive biofilms from environmental shocks in microbial electrolysis cell systems.

The initial portion of this thesis focuses on the use of photodegradable hydrogels for microbial cell screening and rare cell isolation. The photodegradable hydrogel used here was formed with polyethylene glycol (PEG) *o*-nitrobenzyl acrylate and PEG-tetrathiol macromers, which form three-dimensional hydrogels through thiol-acrylate addition reactions to encapsulate heterogeneous populations of bacterial cells. The individual entrapped cells can be cultured into clonal microcolonies due to the suitable hydrogel mesh size for nutrient transport to the cells. Cells are monitored *en masse* and rare cells showing unique growth phenotypes are identified and extracted from the hydrogel interface using a high-resolution light patterning tool. The optimum experimental setup for achieving high throughput observation and clean extraction was developed. Release kinetics with light dose, the effect of light pattern on cell morphology, and the DNA quality of the extracted cells after exposure to 365 nm light patterns was also investigated. We demonstrated the use of this approach as a screening interface by rapidly screening a mutant library

of the Gram-negative bacteria *Agrobacterium tumefaciens* to identify, isolate, and genetically characterize strains with rare growth profiles. The reported method offers an inexpensive and practical approach to cell screening and cell sorting and can be applied to a wide range of applications where isolating phenotypically pure cells from complex, heterogenous mixtures is essential. This includes applications in microbiology, microbial therapeutics, and biomedical diagnostics.

The next section of this thesis focuses on developing PEG-based hydrogels that are designed to protect electroactive biofilms from harsh environmental stressors. The coating was fabricated using PEG-tetrathiol and PEG-divinyl sulfone macromers that form hydrogels with crosslinks resistant to degradation from acid or base hydrolysis, while still promoting nutrient diffusion and electron transport. Methods of fabricating anodes containing electroactive biofilms with the hydrogels are first reported, followed by investigation of the hydrolytic stability of the coatings. Transport of a carbon source (acetate) through the coating is then modeled, and the long-term stability and compatibility of the coating over the biofilm is investigated. Lastly, the effect of the coating on the biofilm recovery from an environmental shock (ammonium exposure) is demonstrated to emphasize the potential benefit of the coating.

Finally, the future directions of hydrogels in these applications are recommended, which include discussion on developing a hydrogel chemistry that is degradable on exposure to a near-infrared (NIR) light source as well as discussion on chemical and biological hydrogel additives that will improve its performance.

Hydrogel interfaces for applications in microbial biotechnology

by

Niloufar Fattahi

B.S., Sharif University of Technology, 2015

A DISSERTATION

submitted in partial fulfillment of the requirements for the degree

DOCTOR OF PHILOSOPHY

Tim Taylor Department of Chemical Engineering
Carl R. Ice College of Engineering

KANSAS STATE UNIVERSITY
Manhattan, Kansas

2021

Approved by:

Major Professor
Dr. Ryan R. Hansen

Copyright

© Niloufar Fattahi 2021.

Abstract

Hydrogels are three-dimensional, water-swollen, highly crosslinked polymers that can be designed to provide biocompatible and biofunctional interfaces for cells and biomolecules. With facile fabrication and precise control over chemistry, pore size, and mechanical properties, hydrogels have been studied extensively in various areas of biomedical and bioengineering, particularly in drug delivery and tissue engineering applications. However, hydrogels have not been well-studied or well-applied to many emerging applications in microbiology. This thesis explores two new applications involving hydrogel interfaces: (1) photodegradable hydrogels for high-throughput screening and isolation of rare bacteria and (2) hydrogels for protection of electroactive biofilms from environmental shocks in microbial electrolysis cell systems.

The initial portion of this thesis focuses on the use of photodegradable hydrogels for microbial cell screening and rare cell isolation. The photodegradable hydrogel used here was formed with polyethylene glycol (PEG) *o*-nitrobenzyl acrylate and PEG-tetrathiol macromers, which form three-dimensional hydrogels through thiol-acrylate addition reactions to encapsulate heterogeneous populations of bacterial cells. The individual entrapped cells can be cultured into clonal microcolonies due to the suitable hydrogel mesh size for nutrient transport to the cells. Cells are monitored *en masse* and rare cells showing unique growth phenotypes are identified and extracted from the hydrogel interface using a high-resolution light patterning tool. The optimum experimental setup for achieving high throughput observation and clean extraction was developed. Release kinetics with light dose, the effect of light pattern on cell morphology, and the DNA quality of the extracted cells after exposure to 365 nm light patterns was also investigated. We demonstrated the use of this approach as a screening interface by rapidly screening a mutant library

of the Gram-negative bacteria *Agrobacterium tumefaciens* to identify, isolate, and genetically characterize strains with rare growth profiles. The reported method offers an inexpensive and practical approach to cell screening and cell sorting and can be applied to a wide range of applications where isolating phenotypically pure cells from complex, heterogenous mixtures is essential. This includes applications in microbiology, microbial therapeutics, and biomedical diagnostics.

The next section of this thesis focuses on developing PEG-based hydrogels that are designed to protect electroactive biofilms from harsh environmental stressors. The coating was fabricated using PEG-tetrathiol and PEG-divinyl sulfone macromers that form hydrogels with crosslinks resistant to degradation from acid or base hydrolysis, while still promoting nutrient diffusion and electron transport. Methods of fabricating anodes containing electroactive biofilms with the hydrogels are first reported, followed by investigation of the hydrolytic stability of the coatings. Transport of a carbon source (acetate) through the coating is then modeled, and the long-term stability and compatibility of the coating over the biofilm is investigated. Lastly, the effect of the coating on the biofilm recovery from an environmental shock (ammonium exposure) is demonstrated to emphasize the potential benefit of the coating.

Finally, the future directions of hydrogels in these applications are recommended, which include discussion on developing a hydrogel chemistry that is degradable on exposure to a near-infrared (NIR) light source as well as discussion on chemical and biological hydrogel additives that will improve its performance.

Table of Contents

List of Figures	xiii
List of Tables	xviii
Acknowledgements	xix
Dedication	xxi
Chapter 1 - Introduction	1
1.1 Synthetic Interfaces for Traditional Applications in Microbiology	1
1.2 Importance of Cell Isolation	2
1.3 Conventional and Merging Methods for Cell Isolation	3
1.3.1 Flow Cytometry	3
1.3.2 Fluorescent Activated Cell Sorting (FACS)	4
1.3.3 Microfluidics	4
1.3.4 Microwell Arrays	7
1.4 Hydrogels	8
1.4.1 Hydrogel Crosslinking Chemistries	9
1.4.1.1 Chain-Growth Polymerization	10
1.4.1.1.1 Chain-Growth Free Radical Photopolymerization	10
1.4.1.2 Step-Growth Polymerization	11
1.4.1.2.1 Michael Type Addition	11
1.4.2 Stimuli Responsive Hydrogels	13
1.4.2.1 Temperature Responsive Hydrogels	13
1.4.2.2 pH Responsive Hydrogels	14
1.4.2.3 Light Responsive Hydrogels	15
1.5 Photodegradable Hydrogels for Cell Isolation	16
1.6 Bioelectrochemical Systems (BESs)	18
1.6.1 Limitations of BESs	19
1.6.2 Polymeric Material to Enhance the Efficiency of BESs	20
Chapter 2 - Objectives	22
2.1 Background	22
2.2 Motivation	24

Chapter 3 - Photodegradable Hydrogel Interfaces for Bacteria Screening, Selection, and Isolation

.....	27
3.1 Overview.....	27
3.2 Introduction.....	28
3.3 Experimental section and protocols.....	29
3.3.1 Bacterial strains and culture protocols.....	29
3.3.2 Preparation of the material needed for hydrogel formation.....	30
3.3.2.1 Photodegradable PEG- <i>o</i> -NB-diacrylate synthesis.....	30
3.3.2.2 Crosslinking buffer.....	30
3.3.2.3 PEG- <i>o</i> -NB-diacrylate solution.....	31
3.3.2.4 Thiol solution.....	31
3.3.3 Preparation of perfluoroalkylated glass slides.....	31
3.3.4 Preparation of thiol functionalized glass coverslips.....	32
3.3.4.1 Cleaning of the glass coverslips using a plasma cleaner.....	32
3.3.4.2 Cleaning and hydroxylation of the coverslips with piranha solution.....	32
3.3.4.3 Thiol functionalization of the coverslips.....	33
3.3.5 Preparation of silicon microwell arrays.....	34
3.3.5.1 Parylene coating.....	34
3.3.5.2 Photolithography.....	34
3.3.6 Hydrogel formation.....	34
3.3.6.1 Bulk hydrogel formation on glass coverslip.....	34
3.3.6.2 Hydrogel formation over microwell arrays.....	36
3.3.7 Material preparation for cell extraction.....	37
3.3.7.1 PDMS holder preparation.....	37
3.3.7.2 Micro syringe and tubing preparation.....	38
3.3.8 Polygon 400.....	38
3.3.8.1 Software preparation.....	38
3.3.8.2 Polygon calibration.....	39
3.3.9 Cell retrieval.....	42
3.3.10 Genomic DNA purification and DNA quality measurement.....	43
3.3.11 Determining cell viability from hydrogel and microwell extracts.....	44

3.4 Representative results	45
3.5 Discussion	50
3.6 Acknowledgement	53
Chapter 4 - Photodegradable Hydrogels for Rapid Screening, Isolation, and Genetic	
Characterization of Bacteria with Rare Phenotypes	54
4.1 Overview	54
4.2 Introduction	56
4.3 Experimental section	60
4.3.1 Materials	60
4.3.2 Synthetic of the photodegradable poly(ethyleneglycol) diacrylate	62
4.3.3 Bacterial strains and culture conditions	63
4.3.4 Transposon mutagenesis	66
4.3.5 Media for screening experiments	66
4.3.6 Thiol surface functionalization	66
4.3.7 Hydrogel preparation and growth monitoring	67
4.3.8 Hydrogel degradation and cell release with the Polygon 400 light patterning device	69
4.3.9 Labeling the hydrogel with fluorescent dye	71
4.3.10 Live/Dead assay	71
4.3.11 Cell retrieval and recovery	72
4.3.12 Agrocin 84 bioassay	73
4.3.13 Genomic DNA Purification	73
4.3.14 Whole genome sequencing	74
4.3.15 Sequence Analysis	74
4.4 Results and discussion	75
4.4.1 High density cell encapsulation and parallel tracking of cell growth	75
4.4.2 Characterization of cell release and cell viability	79
4.4.3 Sequential extraction and recovery of individual microcolonies	83
4.4.4 Screening and identification of rare phenotypes from transposon mutant libraries	85
4.4.5 Follow-up phenotypic and genotypic analysis of rare cells	87
4.5 Conclusion	89
4.6 Acknowledgements	91

Chapter 5 - Polyethylene glycol-based Hydrogel Coating for Improved Performance of Microbial Electrochemical Cells	92
5.1 Overview.....	92
5.2 Introduction.....	93
5.3 Materials and methods	97
5.3.1 Materials	97
5.3.2 Hydrogel crosslinking chemistry and hydrogel hydrolytic stability experiments	97
5.3.3 Diffusion coefficient measurements and COMSOL modeling.....	98
5.3.4 MEC reactor setup and current monitoring.....	101
5.3.5 Parafilm holder for the coating process	102
5.3.6 Hydrogel coating preparation.....	103
5.3.7 Initial testing of coating impacts on current production and longevity of coating	105
5.3.8 Ammonium spike experiments	105
5.4 Results.....	106
5.4.1 Hydrolytic stability of the hydrogels	106
5.4.2 Substrate diffusion coefficient and optimum coating thickness	108
5.4.3 Hydrogel coating effect on microbial activity	110
5.4.4 Protection of anode biofilm against ammonia shock.....	112
5.5 Conclusion	115
Chapter 6 - Summary and Future Recommendations	117
6.1 Photodegradable hydrogels for high-throughput screening, identification, and on-demand isolation of rare microbial cells.	117
6.1.1 PEG-based hydrogels for high throughput screening of microbial cells.	117
6.1.1.1 Future work.....	118
6.1.2 Light responsive PEG-based hydrogels for microbial cell isolation with spatiotemporal control.	119
6.1.2.1 Future work.....	120
6.2 Hydrogel coatings for covering and protecting anode biofilm of bioelectrochemical systems from environmental pressure.....	121
6.2.1 Future work	122
References.....	124

Appendix A - List of materials from Chapter 3	148
Appendix B - List of Abbreviation	150

List of Figures

Figure 3.1. Impact of different light exposure patterns on cell viability and DNA quality of bacteria released from bulk hydrogels. (A) Cell recovery levels for both *E. coli* and *B. subtilis* after extraction using cross patterns and circle patterns. For this experiment extraction was done from the spherical colonies with the same diameter ($26 \pm 1 \mu\text{m}$) to ensure the number of released cells from each colony were equivalent. The extracted solutions were then plated to calculate the CFU/mL acquired from each pattern. Statistical analysis showed no significant difference in CFU/mL obtained from cross and circle patterns for both *E. coli* and *B. subtilis* (P-value > 0.05). (B) Spectrophotometric quantification of DNA quality for isolated *E. coli* cells using cross and circle patterns. Here, statistical analysis did not show a significant difference in DNA quality for the patterns used (P-value > 0.05). (C) Brightfield images of the colonies with equal diameters exposed to cross and circle patterns. 47

Figure 3.2. Representative confocal microscopy images showing light pattern impact on cell isolation from microwell arrays. Adapted with permission from van der Vlies *et al.*¹³⁰ Copyright (2019) American Chemical Society. (A) Microwells with diameter of $40 \mu\text{m}$ containing bacteria (red). (B) Light exposure using circle and ring patterns (blue) for 5 min at $0.7 \text{ mW}/\text{mm}^2$. (C) Diffuse red fluorescence demonstrates that cells are released from irradiated wells. (D) Green fluorescence signal representing the fluorescein-labeled membrane, and red fluorescence signal representing mCherry expressing cells coming from the xy plane along the green line in E. (E) Fluorescence signal coming from the xz plane along the red line in D. Samples in images (C-E) were washed for removal of released cells, then fixed and imaged. Scale bar = $40 \mu\text{m}$ 49

Figure 3.3. Impact of different patterns on cell viability and DNA quality in microwell arrays. (A, B) For both *E. coli* and *B. subtilis*, circle patterns and ring patterns were used for cell extraction from $10 \mu\text{m}$ microwells. Circle pattern with a diameter of $10 \mu\text{m}$ and ring pattern with an inner diameter of $10 \mu\text{m}$ and outer diameter of $20 \mu\text{m}$ were used in this experiment for cell extraction. Microwells with the same diameters were used to ensure that the number of released cells from each microwell was the same. (C) The extracted solutions were then plated to calculate the CFU/mL acquired from each exposure pattern. Statistical analysis

showed no significant difference in CFU/mL obtained from circle and ring pattern for both *E. coli* and *B. subtilis* (P-value > 0.05). (D) Spectrophotometry was used to measure the DNA quality of both *E. coli* and *B. subtilis* cells using circle and ring patterns. Here, statistical analysis did not show any significant difference in the DNA quality for the patterns used (P-value > 0.05). 50

Figure 4.1. ¹H NMR spectrum of PEG-*o*-NB-diacrylate in CDCl₃. 63

Figure 4.2. Optimization of hydrogel thickness. (A) Using 12.7 μm thick spacers results in formation of colonies in one focal plane. (B) Spacers with thickness greater than 12.7 μm show overlay of colonies within the three-dimensional hydrogel. (C) Overlay of colonies can result in cross-contamination during cell release: (i) ring pattern exposed on a desired cell colony, (ii) during light exposure a second colony is observed underneath the target colony, and (iii) cells from the non-target colony are also released causing cross contamination when colonies are overlaid. 69

Figure 4.3. Spatial temporal control of hydrogel degradation. The Polygon400 light patterning tool allows for adjustment of UV light intensity and exposure time across a user-defined pattern enabling control of hydrogel degradation. Inset: representative fluorescent images of patterns degraded with two different light intensity and various exposure times. Hydrogels were stained with fluorescein-5-maleimide after UV irradiation for visualization. 70

Figure 4.4 Setup used for UV light exposure and cell retrieval. During light exposure for cell release, the hydrogel is placed in a PDMS holder and covered with media to prevent dehydration. 71

Figure 4.5 Parallel growth monitoring of individual C58 cells into microcolonies within the hydrogel matrix after seeding. (A) Representative fluorescent images of C58 ML microcolonies at different time points. (B) Microcolony growth for 11 sample microcolonies within the hydrogel as a function of time. 76

Figure 4.6. Growth curve of C58 ML during culture in ATGN media at 28°C and 282 rpm in 96 well plate format (n = 19). 78

Figure 4.7. Hydrogel degradation by bacteria: Entrapped cells within the hydrogel are able to degrade the hydrogel and are released after 5 days incubation in ATGN media. 78

Figure 4.8. C58 ML cell arrangement after release with different light patterns. (A) Ring pattern for extraction of colonies protected within a PEG layer. (B) Broken cross pattern for

extraction of aggregated cells. (C) Cross pattern for extraction of predominantly free cells. For each exposure pattern the following are shown: (i) the projected light pattern (white line) over a targeted colony, (ii) the hydrogel immediately after cell release, and (iii) brightfield and/or fluorescent images of the recovered cells in solution. Patterns were exposed at an intensity of 4.2 mW/mm². 80

Figure 4.9. The efficiency of a line pattern exposure for cell release compared to a broken cross exposure pattern. Use of a broken cross pattern results in complete release of the microcolony, whereas use of a line exposure pattern results in only partial release of the microcolony. 81

Figure 4.10. (A) Microcolony release time from hydrogels at varied 365 nm light intensity. An entire cell mass lift off effect was noted during broken cross pattern exposure, providing a discrete time point for cell release. (B) Red fluorescence signal after staining with the reagents in the live/dead bacterial viability kit. Microcolonies without UV exposure, with broken cross pattern UV exposure (4.2 mW/mm², 40 s), and from chemically treated (70% isopropanol) dead cells are compared. (C) Representative green-red fluorescent images of microcolonies after staining with live/dead assay. Dead cells with compromised membranes appeared red. ImageJ software was used to adjust images for color contrast. For each treatment (n = 3 independent trials), 30 different microcolonies were imaged. 82

Figure 4.11. Sequential extraction of targeted microcolonies from a hydrogel. (A) Brightfield image of a hydrogel with a sample exposure map (white lines) showing exposure locations targeting a blank area or a microcolony with a broken cross pattern. (B) Colony forming units (CFU/mL) of recovered suspensions after washing the hydrogel at various steps and plating. W = initial wash of the hydrogel; B = hydrogel blank; MC = microcolony. All exposures, wash steps, and plating steps onto selective media were performed under identical conditions (n = 3 independent trials). 84

Figure 4.12. The density of recovered cells was not significantly associated with microcolony diameter ($F_{1,42} = 2.03$, $p = 0.16$, adjusted $r^2 = 0.16$; $\beta = 28.78$, $t = 1.42$, $p = 0.16$). 85

Figure 4.13. (A) Schematic of the ML screen: (i) positive control: growth of C58 ML cells within the hydrogel, (ii) hydrogel incubation in presence of CFCE/ATGN for growth of agrocin resistant C58 ML cells, (iii) negative control: C58-GFP incubated in CFCE/ATGN under identical conditions. (B) Representative fluorescent images of the fluorescent micro-

colonies in (i) positive control, (ii) test hydrogels, and (iii) negative control. (C) Representative data for generated micro-colonies in each treatment (n = 3 independent trials).	87
Figure 4.14. (A) Observations of the agrocin 84 bioassay. As expected, NT1 shows no inhibition when co-cultured with K84, and was used as the positive control. The isolated C58 mutant (herein referred to as 100) also shows no inhibition when co-cultured with K84, similar to NT1, while C58 bacteria show a clearing (zone of inhibition) surrounding the K84 at the plate center. K84 bacterial growth is contained inside the red dashed line. The boundary of the zone of inhibition, if present, is denoted by the gray dash line. (B) Most agrocin 84 resistant mutants carry mutations in the <i>acc</i> operon. The location of the <i>acc</i> operon mutations found in seven of the nine isolated mutants is represented with yellow diamonds, with numbers below indicating how many times a mutation in this position was observed. All <i>acc</i> mutants were recovered from different agrocin 84 resistant microcolonies. Mutants with identical mutations were recovered from different hydrogels and so cannot be the result of cross-contamination during recovery. Each gene is shown as an arrow, and they all have been drawn to scale.	88
Figure 5.1. Setup used for diffusion coefficient measurements.....	100
Figure 5.2. Preparation of the parafilm holder for coating process.	103
Figure 5.3. Anode coating procedure. (A) Coating formation over the anode inside the parafilm mold. (B) Coated hydrogel over the anode electrode after gelation. (C) Coated anode electrode placed back inside the reactor.	104
Figure 5.4. (A) Hydrolytic stability of PEGVS hydrogels at different pH values. Hydrogels (n=3) were incubated in pH 3, 7, and 10 at 25 °C for > 10 weeks. (B) Comparison of hydrolytic stability of PEGVS and PEGDA hydrogels at pH 3. (C) Comparison of hydrolytic stability of PEGVS and PEGDA hydrogels at pH 7.	108
Figure 5.5. (A) The cumulative mass release of acetate from PEGVS hydrogels with the initial concentration of 0.3 mM. (B) Early time ($M_t/M_\infty < 0.6$) release profile plotted as a function of the square root of time that is used to determine the diffusion coefficient of the acetate through the PEGVS hydrogel using equations (2) and (3).	109
Figure 5.6. (A) Substrate concentration profile of a hollow cuboid representing the hydrogel coating over the anode biofilm, showing the diffusion of the substrate from the media	

through the walls. The dark red color on the outer surface of the cuboid shows the higher concentration of the substrate, which is the same as in the external solution. The dark blue color on the inside of the cuboid represents the lower concentration of the substrate available to the anode biofilm. (B) Two-dimensional concentration profile of the cuboid from the top view. (C) Effect of substrate consumption rate on maximum allowable coating thickness..... 110

Figure 5.7. Current density comparisons between electrodes with and without a hydrogel coating for (A) trial 1 and (B) trial 2, showing a consistent 1.5-2.5 A/m² gap. 111

Figure 5.8. 6.8 g/L NH₄-N spike. Pre-spike current density difference changes from 55-65% to 75-85% difference post spike and media replacement..... 113

Figure 5.9. 10.8 g/L NH₄-N spike. Post spike current difference from 75-85% to 80-90% in trial 1 and 67-77% to 80-90% in trial 2..... 114

Figure 5.10. Variance reduction between the current density of the uncoated and coated electrode before and after ammonium spike..... 115

List of Tables

Table 4.1. Strains and plasmid used in this study.	65
---	----

Acknowledgements

First and foremost, I would like to express my deepest gratitude to my Ph.D. advisor, Dr. Ryan Hansen, for his guidance, encouragement, and endless support. Without his inspiration and assistance, this work would not have been possible. I am so fortunate to have the opportunity to have his supervision and knowledgeable advice from the beginning of this research, helping me grow as a scientist.

I would also like to thank all my graduate committee members, Dr. Tom Platt, Dr. Prathap Parameswaran, Dr. John Schlup, and Dr. Jishu Shi, for their assistance and their fruitful recommendations throughout this research.

Special thanks to Dr. Andre van der Vlies for his outstanding mentorship, vision and for teaching me how to be a better researcher. His continuous support and insights were critical factors to making this research possible.

I am also thankful to work with a fantastic group of undergraduate students, graduate students in Hansen Lab, and other collaborators, including Dr. Mohammadali Masigol, Niloy Barua, Priscila Guzman, and Evan Heronemus.

I want to acknowledge and thank all friends, faculty, and staff at Tim Taylor Department of Chemical Engineering at Kansas State University for their support and for making this journey possible.

I am grateful to my family, especially my parents Nahid Golbaz, Alireza Fattahi, my brother Behzad, and my husband, David Mertz, for their endless love, support, and encouragement to pursue my dreams. Mom and Dad, I cannot thank you enough for your unconditional love and everything that you have sacrificed for me to be where I am today. David, I cannot imagine going through graduate school without your support. Thanks for constantly pushing me to be a better version of myself and motivating me to better balance my work and personal life. My amazing parents-in-law, Bob, and Mary Mertz, thanks for always make me feel at home and supporting me during these past couple of years. I feel so blessed to be a part of your family.

Lastly, I would like to thank all my friends, especially Alaleh Alivar, Efaf Mansouri, and Arghavan Momeni, who have always been there for me through the best and the worst. I thank them for their unconditional support and encouragement.

Dedication

To my dearest parents,

Nahid Golbaz and Alireza Fattahi

To my beloved husband,

David Mertz

Chapter 1 - Introduction

1.1 Synthetic Interfaces for Traditional Applications in Microbiology

Since the Industrial Revolution, there has been a rapid development in advanced materials research, which has led to the widespread use of synthetic polymers.¹ Due to their tunable chemical and physical properties, synthetic polymers have been widely used in various applications such as drug delivery,² biomedical implants,³ tissue engineering,⁴ antibacterial coating,⁵ food sciences,⁶ and water treatment.⁷ Innovations in polymer synthesis have led to developing a broad range of synthetic interfaces with different structures such as polymer brushes or hydrogel networks.⁸ These biomaterials are of great interest because of the engineered properties, which may include biodegradation, sensitivity to various external stimuli, mechanical properties, and cross-linking density.⁹

In microbiology, the primary use of synthetic polymers has been in antimicrobial and antifouling applications. Biofouling occurs when non-specific microbes or proteins adhere or adsorb onto material surfaces.¹⁰ Biofouling often leads to constant challenges in a broad range of industries and for any surfaces which is in direct contact with biological samples. When biofouling occurs on biomedical materials for *in vivo* use, such as devices, implants, or tissue engineering scaffolds, it can lead to harmful impacts on health, like chronic infection.¹¹ Another example of the damaging influence of biofouling is the unwanted adsorption of organisms onto surfaces in the marine environment, which causes severe technological impacts such as increasing the corrosion rate of the manufactured materials underwater.¹² To address biofouling issues, antimicrobial or antifouling interfaces have shown to assist in preventing the non-specific adsorption of proteins or organisms.¹³

Synthetic polymers are also utilized to sense, detect, and capture microorganisms due to their ability for modification and functionalization with desired biomolecules and their intrinsically high attachment points for various bioconjugation chemistries.¹⁴ Continuous advancements in polymer chemistry and better control over the polydispersity of the synthesized materials result in an accurate display of affinity ligands on synthesized polymers improving cell capture.¹⁴ While synthetic material interfaces have been well-explored in antifouling, sensing, and capture applications, there has been considerably less attention given to developing synthetic interfaces for other applications in microbiology. **Chapter 1** of this thesis provides background on 1) current cell isolation techniques, and 2) bioelectrochemical systems and highlights how polymeric material interfaces can offer beneficial enhancements to both systems.

1.2 Importance of Cell Isolation

A significant and widespread challenge in cellular biology is identification of genetic characteristics that are responsible for certain cell functionality, or phenotype.¹⁵ To correlate phenotype to genotype, understanding the degree and significance of cellular heterogeneity is crucial.¹⁵ However, most laboratory methods only analyze bulk cell populations where cell populations are considered homogeneous.¹⁶ Therefore, cell analysis from bulk populations distorts the properties and unique phenotype of individual cells, while analyzing single cells or small clonal populations can uncover rare molecular biomarkers and other factors regulating the phenotype of individual cells.¹⁷ Analyzing individual or clonal cell populations requires isolation methods that can physically separate them from the bulk population.¹⁸ Additionally, cell isolation from a heterogeneous mixture is a crucial step towards engineering bacterial communities that can be designed to enable the production of new materials or improvement of established compounds in

different areas of biotechnology and bioremediation.^{19,20} Currently, there are several techniques that are used for cell isolation and detection such as flow cytometry, microfluidics and others.²¹

1.3 Conventional and Merging Methods for Cell Isolation

1.3.1 Flow Cytometry

Flow cytometry is a powerful and high-throughput single-cell analysis technology utilized in various applications. Flow cytometry has been used in studying bacteria physiology, such as in *Mycobacterium tuberculosis*,²² screening of cellular libraries,²³ and for diagnostic applications such as the diagnosis of leukemias and lymphomas.²⁴ This optical-based technology can detect and measure multiple cellular parameters in a sizeable and heterogeneous population of cells, by tagging various receptors with fluorescence markers or by sensing light scattering. In flow cytometers cells are partitioned into droplets and flow in a stream through a channel and laser beam. When the laser hits the moving cells, photonic detectors sense the scattered light and fluorescence signal.²⁵ The scattered signal is correlated to the structural and morphological characteristics of cells, while the acquired fluorescent signal from the cells is related to the presence and quantity of the cellular marker that was targeted.²⁶ Although flow cytometry is used in various fields, it has several downsides, such as being limited in distinguishing the cell subgroup with similar marker expression and the need for several dilution steps before the analysis, lowering the device's sensitivity. This is why flow cytometers are often used in conjunction with other techniques such as qPCR to obtain precise results.²⁷

1.3.2 Fluorescent Activated Cell Sorting (FACS)

Fluorescence-activated cell sorting (FACS) is a type of flow cytometry with the ability to sort cells from a population based on the signals from fluorescently labeled proteins or fluorescence in situ hybridization probes.²⁸ In FACS individual cells are encapsulated in droplets. Droplets are then charged and electrostatically deflected into collection containers.²⁹ FACS provide exceptional high-throughput beneficial for applications with abundant cells. In the field of microbiology, FACS has been used for applications including isolation of microbial populations for molecular analysis,³⁰ single-cell screening for bacterial promoters with appropriate expression properties,³¹ and rapid detection of specific microbes.²⁹ However, FACS demands expensive equipment due to their complex sorting mechanism. Therefore FACS is often limited to core research facilities, requiring highly trained personnel for its operation.^{32,33} Another limitation of FACS is the necessity of having more than 10,000 cells in each suspension, which is impractical for applications dealing with a limited number of cells.³⁴ Aerosol production by the cell sorter before the sorting process leading to possible sample contamination is among other drawbacks of FACS.³⁵

1.3.3 Microfluidics

For the last two decades, microfluidics has been a rapidly developing field for a myriad of applications in biology and biotechnology.³⁶⁻³⁸ Microfluidic devices are commonly fabricated using soft lithography methods that involve placing a polydimethylsiloxane (PDMS) layer over a silicon master substrate, then curing in an oven. The PDMS device then contains patterned microchannels that can be attached to a polymer surface, glass slide, or an additional PDMS layer. Fluids can be introduced to the system and pass through channels, while the small channel

dimensions (typically ranging between 10 nm to several hundred micrometers³⁹ in width and channel aspect ratios between 0.5 and 10^{40,41}) ensure low Reynolds numbers and laminar flow, which provide well controlled hydrodynamic conditions⁴² and a remarkable degree of control over the chemical and physical microenvironment of the cells.⁴³ Microfluidics also have the ability of confining single cells into micron-scale chambers and lower dilution effects to increase detection sensitivity.⁴⁴ Micron-scale sizes, lower consumption of reagents, and the control over the cellular microenvironment, make microfluidic platforms a suitable high-throughput technology.⁴⁵

Microfluidic devices integrated with microvalves and droplet assays are among the primary devices used for single-cell studies as they allow spatial and temporal control. Droplet microfluidics has become a popular platform for studying bacteria as these devices can generate, manipulate, and screen droplets that carry single bacteria cells or small populations of bacteria in a high-throughput manner as they can generate droplets at rates as high as 20,000/sec.⁴⁶ These platforms use a two-phase system. In this system, aqueous microdroplets that are 0.05 pL to 1 nL in volume are surrounded by an immiscible oil, isolating cells from each other and eliminating the risk of cross-contamination that is likely to happen in other microfluidic approaches.⁴⁷⁻⁴⁹ These features can pave the way for fundamental bacteria studies, rapid detection of cells and improve rare cell cultivation ability.^{50,51} Different research groups have used these devices for various applications including identification of pathogens,⁵² antibiotic resistance,⁵³ cultivation of unknown microbes,⁵⁴ study microbial interactions,⁵⁵ study microbial physiology,⁵⁶ and detection of metabolic activity of bacteria.⁵⁷ For instance, Mao *et al.* took advantage of the laminar flow in microfluidic channels to create gradients of repellents and attractants to study bacterial chemotaxis.⁵⁸ They reported the higher sensitivity of their microfluidic system by three orders of magnitude compared to a conventional capillary-based chemotaxis assay. In another study,

Boedicker *et al.* used single cell isolation in microfluidic droplets to discover that individual *Pseudomonas aeruginosa* cells could self-activate through diffusive quorum sensing pathways that were classically considered to be an intercellular phenomena.⁵⁹ Cottinet *et al.*⁶⁰ developed a drop-based microfluidic platform to study microbial growth in microdroplets in parallel. The growth of individual cells in each droplet allowed for heritable phenotype changes in single cells to be amplified and quantified, even though these changes could not be detected at the single-cell level. Jeong *et al.*⁶¹ developed a microfluidic static droplet assay to study quorum sensing. Their approach was used to study the impact of population ratio on cell-cell interaction between the signal sender cells, SCs, (production of signal molecules), and receiver bacteria. Leung *et al.*⁶² developed a programmable droplet-based microfluidic device with wettability control over the flow for single-cell studies. Their platform could sort bacteria phenotypically and analyze them at a single-cell level by integrating a cell sorting module and applying an elution process downstream to analyze the recovered samples.

While droplet microfluidics is considered a high-throughput platform, they face considerable limitations. For instance, small volumes of droplets cause a high surface area to volume ratio. Droplets are produced by a comminatory water and oil system, and the higher surface-to-volume ratio means water and oil are more in contact at their interface. Since the interface must be stable, it is crucial to use a suitable surfactant, which is often difficult.⁴⁸ In addition, labeling droplets in specific, confined regions of the device requires a need for complex control strategies for multiple fluid streams, and difficulty in monitoring target cells in droplets that pass through the device are other cons of these platforms.⁶³ Moreover, bacteria in microdroplets are devoid of a host surface, which is often present in natural habitats and biofilms environments. However, perhaps most critical limitation in these systems comes from the fact that

cells confined within droplets are not easily retrieved from the platform. This limits the analysis of these cells to on-chip measurements, which most often is with microscopic observation. However, powerful molecular information that could be provided from "-omic" technologies is inhibited without cell retrieval for off-chip analysis. This includes genomic analysis (ex. 16S amplicon sequencing, whole genome sequencing), proteomic analysis, transcriptomic analysis, and metabolomic analysis. Without retrieval capabilities, connecting molecular information, such as genotype with phenotype will continue to be difficult.

1.3.4 Microwell Arrays

Recently, bacterial microarrays have been used to partition, trap, and culture single bacteria cells in microwells. Microwell arrays are of great interest for unique high-throughput screening assays (THS) that monitor dynamic cellular responses. Microwells can be observed in parallel in an array format, depending on the microscope's field of view.^{64,65} For example, a novel microwell array was developed by Lim *et al.*⁶³ in which a fluid array was used to insulate bacteria in microwells and allowed for selective extraction of cells of interest based on their phenotype for additional culture using capillary tubes. In this platform, they seeded the microwells with bacteria solution, and for compartmentalization of the microwells, the platform was inverted into an oil. Due to the immiscible properties of oil and aqueous solution and their different specific gravity, the aqueous solution containing bacteria was compartmentalized. This platform was further used for the growth-based screening of a mutant library. Random mutants were sorted based on their nutrient consumption as implication of their growth rate. Zhang *et al.*⁶⁶ proposed an agarose-based microwell array that allowed nutrient transport and cell growth. To get individual bacteria in each microwell, they optimized the size of the wells and density of the inoculation culture. This resulted in having a clonal population of bacteria in microwells, which facilitated the observation and

detection process. The proposed platform was used to monitor functional lipase-expressing bacteria.

While microwell arrays hold a great potential for cell screening applications, they still require to be prepared in microfabrication facilities, which not all laboratories can easily access. As with droplet microfluidics, retrieval of cells from wells for "-Omics" analysis remains difficult, particularly when wells are relatively small (diameters $<100\ \mu\text{m}$), at which point they cannot be picked from wells or extracted in a clean or specific manner. The limitations of cell retrieval after observation in these formats have motivated the work presented in this thesis involving the use of photodegradable hydrogels for cell retrieval.

1.4 Hydrogels

Hydrogels are three-dimensional water-swollen cross-linked polymeric networks that are created by hydrophilic polymer chains.⁶⁷ These cross-linked structures can encapsulate and immobilize biomolecules, active agents, etc., and release these material on an environmental cue. Hydrogels can be made of both natural and synthetic materials.⁶⁸ Two examples of natural hydrogels that are found in nature are gelatin and agar and have been widely used in various microbiology applications. However, the physical and biochemical features of natural hydrogels can often be difficult to modify and control with a high degree of precision. On the other hand, synthetic hydrogels have wide-ranging tunable physical and chemical properties, making them more favorable for designing scaffolds of various tissue types in different fields such as biomedical, pharmaceutical, and biotechnology.⁶⁹ Synthetic hydrogels also have a high water content, and they can be designed to mimic natural living tissue and show high biocompatibility with cells.⁶⁷ The majority of synthetic hydrogels use poly(ethylene glycol) (PEG) as the hydrogel

backbone due to the remarkable advantages PEG offer for hydrogels.⁷⁰ The cross-linked network of these hydrophilic biomaterials can offer well-controlled viscoelastic properties and can be used to tune diffusive transport and interstitial flow properties.⁷¹ Due to their excellent biocompatibility and non-cytotoxic properties,⁷² PEG hydrogels also provide an effective chemistry for cell encapsulation.⁷³ PEG-containing hydrogels are also known to be excellent antifouling materials.⁷⁴ PEG is, in fact, the most often used polymer for antifouling purposes⁷⁵ as it reduces the non-specific adsorption of proteins, cells, and bacteria. One of the most successful applications of these hydrogels has been for marine antifouling purposes. With these beneficial properties, PEG-based hydrogel materials can also be used for cell screening applications. Polyacrylamide (PAA) hydrogels are among other well studied hydrogels. These hydrogels have been utilized for different applications including food packaging, water treatment,⁷⁶ and to explore the influence of hydrogel stiffness on cell morphology.⁷⁷ Other synthetic hydrogels employ polypeptide chains, such as Arg–Gly–Asp (RGD) peptides, as the hydrogel backbone to provide adhesion sites to promote adhesion and proliferation of mammalian cells.⁷⁶ In one study, Zhou *et al.* reported the development of a peptide-based bioactive hydrogel as a three-dimensional cell scaffold. Here, the hydrogel was fabricated through combination of Fmoc-FF (Fluorenylmethoxycarbonyl-diphenylalanine) and Fmoc-RGD. The developed hydrogel allowed the culture of human dermal fibroblast within the hydrogel matrix for studying the morphology and viability of the cells. Due to simple and inexpensive nature of these hydrogels, they hold promise for cell screening in tissue regeneration, and other biological applications.⁷⁶

1.4.1 Hydrogel Crosslinking Chemistries

PEG-based hydrogels are made by different polymerization mechanisms including chain polymerizations and step polymerizations,⁷⁸ which are described here.

1.4.1.1 Chain-Growth Polymerization

Chain growth polymerization reactions require initiators such as free radical initiators or anionic and cationic initiators.⁷⁹ Initiators are activated to generate free radicals on light exposure, heat, or free redox reactions. Chain polymerizations occur by propagating free radicals through unsaturated vinyl or acrylate bonds on the PEG macromer with only monomers reacting with the active site of growing chains.⁸⁰ Cross-linking via chain-growth polymerization is usually completed in a relatively short time, seconds to minutes.⁸¹

1.4.1.1.1 Chain-Growth Free Radical Photopolymerization

Photopolymerization is a category of free-radical polymerization where light is used to initiate the polymerization. Photoinitiated crosslinking is a suitable method for hydrogel formation *in situ* as it offers spatiotemporal control over the hydrogel formation.⁸² Rapid polymerization rate and polymerization under physiological conditions are other advantages of photopolymerized hydrogels. With the mentioned benefits, PEG hydrogels generated by the photoinitiated polymerization have shown potential for cell encapsulation applications.⁸³

However, hydrogels formed by chain-growth polymerization are also known to contain network non-idealities compare to those made through step-growth polymerization.⁸⁴ For example, the arbitrary nature of radical propagation and termination in chain-growth polymerization causes cross-link functionality heterogeneity across the hydrogel.⁸⁵ Moreover, chain growth polymerization initiated by radicals are inhibited by oxygens, which is often a limiting factor when cells are present.⁸⁶ This is due to the relatively stable nature of peroxide radicals that slows the polymerization rate, and due to oxygen molecules forming reactive oxygen species which can put oxidative stress on cells.⁸¹

1.4.1.2 Step-Growth Polymerization

Unlike chain-growth polymerization, step-growth polymerization forms more homogenous hydrogels with uniform crosslinking densities.⁸⁷ This is because the polymerization occurs when at least two multifunctional monomers with mutually reactive groups act as cross-linking points and are reacted together. This polymerization usually does not require free-radical initiators and can proceed on mixing of monomer precursors under ambient conditions.⁸⁴

1.4.1.2.1 Michael Type Addition

Michael addition is the nucleophilic addition of a nucleophile to an α,β -unsaturated carbonyl compound.⁸⁸ Michael-type addition reaction is the most widespread bioconjugation reaction,⁸⁹ which usually uses thiols as nucleophiles and electron-poor double bonds as electrophiles such as (meth)acrylates, acrylamides, vinyl sulfones and maleimides.⁹⁰ Among various Michael-type addition reactions, thiol-acrylate, thiol-maleimide, and thiol-vinyl sulfone reactions have been broadly studied.⁹¹

Thiol-acrylate reaction has been extensively used for hydrogel fabrication and surface functionalization.⁹² Thiol-acrylate reactions have especially been used for formation of hydrolytically degradable hydrogels as the ester groups present in their chemistry is susceptible to hydrolysis. Yom-Tov *et al.* investigated the impact of different hydrogel preparation techniques on thiol-acrylate hydrogel properties. They reported that manipulation of the hydrogel preparation method, could result in achieving desired properties, such as polymerization time, crosslinking structure, etc. for specialized biomedical applications.⁹³ These tunable properties of thiol-acrylate hydrogels are mainly achieved by changing the thiol-to-acrylate molar ratio. Khan *et al.* developed a biodegradable thiol-acrylate hydrogel as a three-dimensional cell culture platform for *in vitro*

applications. Here they investigated the impact of different formulation for hydrogel preparation on viability and growth of breast cancer cells cultured over time to find the optimum formulation.⁹⁴ Hubbell and co-workers used the step-growth polymerization method to form a series of degradable hydrogels by cross-linking acrylated star PEG polymers and dithiols through a Michael-type addition reaction for protein drug delivery.⁹⁵ In another study, Elia *et al.* reported the development of a hydrogel through thiol-acrylate addition reaction for *in situ* delivery of loaded growth factors to localized sites in a mouse model.⁹⁶

Maleimides, another reactive groups with thiols, are widely used in bioconjugation of peptides due to their rapid reaction and high specificity for thiol groups under physiological condition.⁹⁷ Phelps *et al* investigated the potentials of a thiol-maleimide hydrogel for regenerative medicine and reported the promise of these interfaces for cell delivery due to fast crosslinking reaction (1-5 minutes) suitable for clinical use and *in situ* gelation under mild reaction conditions. Although, the fast polymerization reaction of thiol and maleimide is of great interest for tissue engineering, rapid polymerization rate can lead to heterogenous hydrogel network and crosslinking gradient⁹⁸ which is reported to potentially decrease the reproducibility in the cell response such as correlating cell function to hydrogel stiffness.⁹⁸ Moreover, retro-Michael type addition can occur between thiol-maleimide linkage even at physiological pH and temperature, decreasing the hydrogel stability.⁹⁹

In contrast, thiol-vinyl sulfone reaction results in a very stable thioether bond that is not prone to hydrolysis and that offers significantly greater stability for applications requiring a range of different environments.¹⁰⁰ In one study, Liu *et al.* developed a biologically inert hydrogel through the thiol-vinyl sulfone addition reaction. The hydrogel was generated through mixing a 4-arm PEG- vinyl sulfone and a multi-arm, macromer with terminal thiol groups. The hydrogel in

this study was used as a cell encapsulation matrix to study the epithelial cyst formation. The polymerization rate of the developed hydrogel was suitable for *in situ* cell encapsulation, holding promise for other potential *in situ* applications.¹⁰¹

1.4.2 Stimuli Responsive Hydrogels

Stimuli-responsive hydrogels, or "smart" hydrogels, are designed to respond to various external or internal stimuli to undergo changes in their network structure, mechanical strength, swelling behavior, or permeability. Some of these stimuli are temperature, pH, light, magnetic field, and electric current.¹⁰² These smart hydrogels have proven to be extremely useful in drug delivery, tissue engineering, and cell encapsulation,^{103–105} and are reviewed here.

1.4.2.1 Temperature Responsive Hydrogels

Temperature-responsive hydrogels are one of the most studied stimuli-responsive hydrogels. These hydrogels change their swelling and shrinking behavior upon shifts in the surrounding fluid temperature¹⁰⁶ and can be categorized as negative or positive temperature-responsive systems.⁶⁹ Negative temperature hydrogels that exhibit a lower critical solution temperature (LCST) shrink at temperatures above the LCST as these polymers become hydrophobic because of enhanced polymeric interactions.^{107–109} LCST systems are used in different applications such as reversible switches for sensors, drug delivery carriers and diagnostics. For instance, hydrogels showing an LCST lower than human body temperature have the potential to be injected into the human body, as they can be tuned to be liquid at room temperature and shrink or gel once introduced to body fluids due to an increase in temperature.¹¹⁰ Guenther *et al.* used a temperature-responsive gel in their hydrogel-based chemical sensors. The hydrogel used in their system experienced changes in its swelling behavior to bend a thin silicon

membrane, leading to an electrical output voltage of the sensor chip.¹¹¹ Another example of LCST systems is the one developed by Uchiyama *et al.* who used a temperature-responsive polymer with fluorescent units to measure the local temperature in organelles of living cells utilizing the variances in fluorescence intensity made by dehydration.¹¹² Unlike LCST systems, positive temperature hydrogels exhibiting an upper critical solution temperature (UCST) contract by cooling below the UCST due to phenomena such as hydrogen bonding and electrostatic interactions. UCST systems can also be used in applications such as sensors and protein separation.¹¹³ For instance, Danko *et al.* reported the preparation of a thermo-responsive hydrogel using carboxybetaine and sulfobetaine based monomers. The developed hydrogel was able to turn transparent above UCST, offering the potential to serve as a simple means of thermal warning detection for required cooling.¹¹⁴

1.4.2.2 pH Responsive Hydrogels

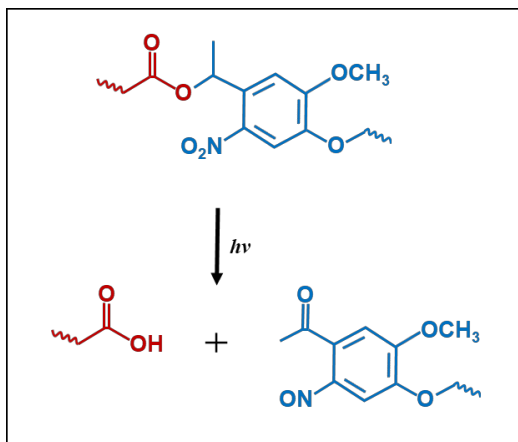
pH-responsive hydrogels are another category of smart hydrogels that have been widely studied and applied. These hydrogels have ionic pendant groups capable of accepting and donating protons because of changes in the environmental pH. Ionization of the pendant groups and the quick transformation in their net charge generate electrostatic repulsive forces controlling pH-dependent swelling or deswelling of the hydrogel.¹¹⁵ pH-responsive hydrogels are also suitable for specific drug and therapeutic delivery since different human body locations, such as blood vessels and the gastrointestinal tract, have various pH values and can support a good base for releasing pH-responsive drugs.^{115,116} In one study, Xu *et al.* developed a pH-responsive hydrogel by combining poly(L-lactide)-co-polyethyleneglycol-co-poly(L-lactide) dimethacrylates with acrylic acid and N-isopropylacrylamide. The hydrogels were loaded with two drugs and had the ability to shrink at pH 1.2 and swelling at pH 7.4 with each pH favoring one of the drugs to be released in a

slow release or rapid release pattern. The developed hydrogel with pH triggered differential drug release functionality successfully killed d HeLa cells while inhibiting the growth of *Escherichia coli*.¹¹⁷

1.4.2.3 Light Responsive Hydrogels

Light proves to be an advantageous stimulus for controlling the behavior of biomaterials as it can be tuned spatially and in terms of light intensity, exposure time, and wavelength.^{118,119} Light-responsive polymers usually undergo degradation or bonding reactions as a response to the light energy.¹²⁰ In photoreleasable hydrogels, degradation occurs upon photocleavage of the covalent bonds. These hydrogels are created by integrating photoresponsive moieties such as *o*-nitrobenzyl (*o*-NB) groups (**Scheme 1.1**) into the hydrogel network.¹²¹ The *o*-NB moiety and its derivatives have found the most widespread use in photoresponsive hydrogels.¹²² *o*-NB groups cleave at the ester bond upon UV light exposure and result in the production of aldehydes and carboxylic acids (**Scheme 1.1**).¹²³ Photocleavage wavelength can also be manipulated through functionalization of the benzene group to achieve photoresponse to light wavelength from 350 to 450 nm.¹²¹ These properties allow for direct hydrogel degradation manipulation, which is favorable in many applications where spatiotemporal control over degradation is required.¹²⁴ For instance, photodegradable hydrogels are a good candidate for therapeutics, where controlled drug release is essential. Their three-dimensional structure allows encapsulation of different drugs, and the light-triggered gel-to-sol transition results in the release of the loaded drugs.¹²⁵ Another application of photodegradable hydrogels is in wound dressing, where hydrogels are required to attach to the tissue for a specified time and then get removed or degrade gradually. Villiou *et al.* designed a photodegradable hydrogel suitable for wound dressing applications. The developed

hydrogel was capable of cross-linking *in situ*, encapsulating cells, adhering to tissue, and on-demand releasing of cells upon light exposure and ultimately detaching from the tissue.¹²⁶



Scheme 1.1. Cleavage mechanism of *o*-nitrobenzyl groups upon UV light exposure.

1.5 Photodegradable Hydrogels for Cell Isolation

Photodegradable hydrogels provide biocompatible cell capture and release with the ability of selective release of target cells. Recently, LeValley *et al.* developed a patterned, antibody-conjugated photodegradable PEG-based hydrogel for cell capture and on-demand cell release. Using this photodegradable hydrogel allowed them to capture target cells from whole blood with enhanced purity due to the selective release of cells.¹²⁷ Shin *et al.* also functionalized a photodegradable hydrogel with antibodies to isolate specific cells from a heterogeneous cell population and further took advantage of photodegradability of the hydrogels for selective release of cells down to the single-cell level.¹²⁸ Variations in reactivity of *o*-NB derivatized linkers enabled Kasko and Griffin¹²⁹ to establish a series of macromers integrated with *o*-NB groups in their backbone to form hydrogels with different photodegradation rate constants at 370 nm, capable of

encapsulating and releasing human mesenchymal stem cells without compromising the cell viability. While these materials have been reported for isolation of mammalian cells, they have not been applied to the microbial kingdom until very recently. Van der Vlies *et al.*¹³⁰ provided the first report of photodegradable hydrogels for isolating populations of bacteria after observation of cell growth in a microwell format. Here, a model bacterium, *Agrobacterium tumefaciens*, was seeded inside the microwells. The bacteria were then sealed inside the wells by attachment of a photodegradable hydrogel layer with a suitable pore size for nutrient exchange required for cell growth. Cell growth was monitored overtime utilizing fluorescence measurements. Selected wells were exposed to light for membrane degradation and cell release. The high control over hydrogel degradation, ability to screen, identifying populations with a desired or rare behavior, and selective well opening make this cell isolation method proper for applications requiring follow-up genetic analysis.¹³⁰ Building off of this progress Barua *et al.*¹³¹ used the same cell isolation method from microwell arrays to discover synergistic or antagonistic interactions between rhizosphere bacteria. In this study, microwell arrays were used for trapping a focal species expressing fluorescence with multi-species communities at various ratios to track the growth of the focal species. Using this approach, the microwell arrays were applied to simultaneously screen positive and negative interactions between a plant growth-promoting rhizobacteria and a rhizosphere isolate. Target wells with rare behavior were then opened using a light patterning device and 16S rRNA sequencing was done on the isolates.¹³¹

Microwell arrays allow cell screening and isolation in a well-controlled manner. However, they still need microfabrication requiring expert personnel and fabrication facilities, which not every laboratory have access to. To develop a more translational method for cell screening and isolation, Fattahi *et al.* used the same photodegradable hydrogel interfaces, with the difference of

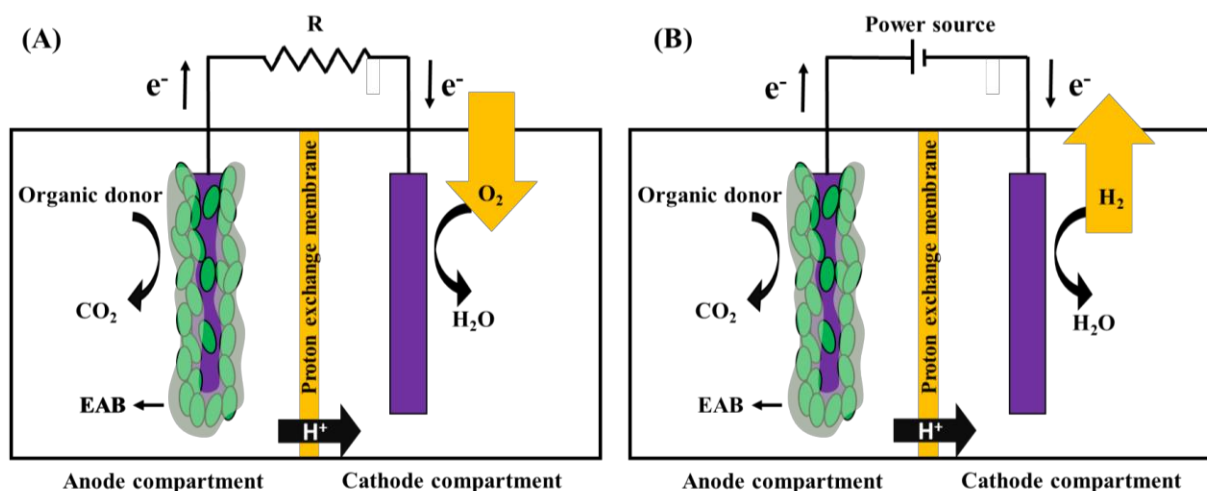
cell entrapment within the hydrogel matrix. Here, hydrogel interfaces were fabricated over glass coverslips. Hydrogel permeability allowed for formation of microcolonies from individual encapsulated cells. Hydrogels were then screened for cell colonies with unique growth profile, and selective colony extraction was done using a light patterning device with micron-scale resolution. This method allowed screening a model mutant library of bacteria, *Agrobacterium tumefaciens* C58, to saturation, identification of rare mutants showing desired phenotype, cell extraction with precision, and follow up genetic analysis to map mutation.¹³²

Hydrogels, owing to their exceptional properties, including great biocompatibility, swelling ability, and the tunable network properties, have attracted a great interest for use in different applications. Specially, the continues enhancement in polymer synthesis increases the chemical and physical tunability of hydrogels. Thus, these interfaces can be designed to meet the requirements of the target industry or research area, such as many microbiology, biomedical, and biotechnology applications.

1.6 Bioelectrochemical Systems (BESs)

With the gradual depletion of non-renewable energy resources, there is a great need to enhance and develop new types of renewable energy sources.¹³³ Bioelectrochemical systems (BESs) are one of the promising candidates that fit within this category. BESs are electrochemical cells that use microorganisms to oxidize organic compounds present in waste, like wastewater, which results in the production of electrons through this oxidizing process. The produced electrons are then used to either generate energy or value-added compounds.^{134,135} Two main categories of BESs are microbial fuel cells (MFCs), where electrons are produced by microorganisms, and microbial electrolysis cells (MECs), where microorganisms consume electrons (**Scheme 1.2**).¹³⁶

While both systems have a similar anodic reaction with bacterial anode oxidizing a carbon source, the reaction occurring at the cathode differs. In MFCs, the cathode reaction results in electricity production. On the other hand, in MECs, cathode reaction leads to the formation of value-added products such as hydrogen gas.¹³⁷



Scheme 1.2. Schematic representation of (A) a microbial fuel cell (MFC), and (B) a microbial electrolysis cell (MEC).

1.6.1 Limitations of BESs

Although BESs are a good candidate for producing green energy, they face several challenges such as lower efficiency and decreased production rate preventing them to be fully applicable to large-scale applications.¹³⁸ To overcome these issues, it is important that the operation of these systems provide more benefits than the cost associated with using these systems. Therefore, a crucial step towards making these systems practical is to maximizing the efficiency of BESs to lower their operation cost.¹³⁹

The microbial community, and particularly the abundance and viability of electroactive bacteria (EAB), play a crucial role in electroactivity of the biofilm and efficiency of these systems.¹⁴⁰ EAB are capable of extracellular electron transfer (EET), which enables them to transfer electrons to or from a solid substrate such as electrodes.¹⁴¹ EAB are also known as exoelectrogens and anode-respiring bacteria (ARB). Retaining a well-balanced microbial composition on the anode with an affluent EAB population is crucial for efficient electron transfer and achieving maximum current densities in BESs.¹⁴² A major limiting factors in the performance of BESs is decreased activity of the EAB and ARB within the anode-bound biofilm over time. It is known that harsh environmental conditions such as variations in pH values,¹⁴³ temperature fluctuations,¹⁴⁴ and high salinity¹⁴⁵ can compromise the viability and activity of the EAB.

1.6.2 Polymeric Material to Enhance the Efficiency of BESs

Recently, various studies have reported on techniques protecting the electroactive anode biofilm from harsh environmental stressors. Anode biofilm protection by immobilizing the biofilm on the anode using a protective layer is one of the techniques used for this purpose. Recently, Du *et al.*¹⁴³ used polydopamine (PDA) to encapsulate bacteria cells on the anode to protect them against severe acid shock. Using this method, they could achieve a limiting current density that was 1900% higher than their control system with a non-immobilized anode. They reported the bacteria protection ability of PDA against acid shock was potentially due to their biocompatibility, high stability, and formation of a hard shell on the bacteria surface protecting the cells inside. They believe this could be due to rich functional groups of the PDA binding it closely to the bacterial cells.

There have been a couple of recent reports of hydrogel biomaterials that provide a biocompatible and protective matrix in BESs.¹⁴² These interfaces allow for nutrient transport to the electroactive biofilm and diffusion of waste materials out of the interface. Hydrogels also provide protections against environmental stressors such as a broad range of temperature, pH, solvents, and toxins.^{142,146} Gandu *et al.*¹⁴² is among the research groups that used alginate combined with chitosan or only alginate to immobilize the anode biofilm in an BES operating in wastewater. Their studies showed that using BESs containing immobilized anode biofilm increased the chemical oxygen demand (COD) removal from 40% to 78% compared to systems with non-immobilized anode biofilm. After microbial diversity analysis, they observed that in their immobilized anode, the electroactive bacteria, *Geobacter*, accounted for 90 % of the microbial composition on the anode. In contrast, in systems with the non-immobilized anode, this number was 73%. In another study conducted by Luo *et al.*¹⁴⁷ anode biofilm was encapsulated using agarose gel, a natural polymer, to investigate the performance of the BES under high substrate concentration, which is known to inhibit the activity of the EAB and lower the yield of the system. The agarose immobilized anode used in their studies showed higher power density compared to the non-immobilized anode. The immobilized anode showed a power density of 610 and 370 mW/m² at a substrate concentration of 5 and 10 g/L, while these values for the untreated anode were 343 and 240 mW/m², respectively. These three have motivated the use of our PEG-based hydrogels as a protective layer against environmental shocks in BESs, as described in **Chapter 5**.

Chapter 2 - Objectives

2.1 Background

Poly(ethylene glycol) (PEG) based hydrogels have been one of the most broadly studied among the synthetic hydrogels.⁷⁰ The cross-linked network of these hydrophilic biomaterials can offer well-controlled viscoelastic properties and can be used to tune diffusive transport and interstitial flow properties.⁷¹ Due to their excellent biocompatibility and non-cytotoxic properties,⁷² PEG hydrogels also provide an effective chemistry for cell encapsulation.⁷³ PEG-containing hydrogels are also known to be excellent antifouling materials.⁷⁴ PEG is, in fact, the most often used polymer for antifouling purposes⁷⁵ as it reduces the non-specific adsorption of proteins, cells, and bacteria. One of the most successful applications of these hydrogels has been for marine antifouling purposes. With these beneficial properties, PEG-based hydrogel materials can also be used for cell screening applications. To connect phenotype to genotype determination, it becomes crucial to isolate the targeted cells after identification from the screen. However, most established methods for cell screening lack the ability to recover the target cells from the platform. This highlights a significant need for development of cell screening methods that also allow for selective cell isolation for genetic analysis after microscopic observation.

The motivation behind the final portions of this thesis to investigate the methods for improving the efficiency of bioelectrochemical systems (BESs) stem from the great potential of this technology to serve as a sustainable environmentally benign source of energy.¹³³ Despite the promises that BESs holds, they face several problems that constrain this technology to laboratories and prevent them to be commercialized. In these systems, electroactive bacteria (EAB) capable of harvesting energy from waste material are one of the key components of the system efficiency.¹⁴⁸

As mentioned in (**Chapter 1**), environmental shocks such as pH shock,¹⁴³ temperature fluctuations,¹⁴⁴ and high salinity¹⁴⁵ can compromise the metabolic activity of the EAB. The well-known sensitivity of EAB to environmental pressure, and the direct dependence of the current density on anode biofilm metabolic activity, makes MFC systems, a category of BESs, a good candidate as toxicity sensors especially for water monitoring.¹⁴⁹ For instance, introducing toxic substances such as Pb_2^+ would affect the biofilm metabolic activity and lower the current density of the MFC. However, even in MFC sensors that environmental stressors experienced by the biofilm is the key feature of the system, repeated exposure to toxins or high concentrations of toxins can affect the anode biofilm metabolic activity in an irreversible way decreasing the sensor sensitivity. Therefore, for BESs operation in actual environment, that can potentially contain high concentrations of toxins or experience extreme conditions related to temperature, pH, etc., the EAB metabolic activity needs to be maintained or have the ability to re-acclimate after extreme environmental shocks. To this end, there is a great need for development of methods capable of protecting EAB from extreme conditions, and ultimately increasing the efficiency of the system.

Only a few studies have utilized polymeric hydrogel materials for improving the efficiency of BESs by providing a protective barrier around the anode biofilm. However, the long-term stability of these hydrogels has not been well-characterized. For BESs to be practically applicable to most applications, they need to have the ability to remain stable in the environment for weeks to months during operation. Otherwise, there is a continuous need for changing the material after a short period of time, increasing the operation cost. Therefore, there is a great need to further investigate the polymeric material with high stability that can potentially answer the current limitations for commercialization of BESs.

2.2 Motivation

The first section of this thesis focuses on the development of a facile, high-throughput method for cell isolation that is translational to common microbiological labs with no fabrication need. Incorporating stimuli responsive, photocleavable chemical moieties into the hydrogel network enables cleavage of covalent bonds, degradation of the network structure, and release of bacteria cells from the hydrogel. With this, it is hypothesized that photodegradable polymeric materials can be designed with small (10-20 nm) pore sizes to encapsulate and culture cells in a bulk format that effectively serves as a miniaturized version of standard plating methods, allowing for cell screening and isolation of selected cell population in a defined chemical environment with high spatiotemporal control using a patterned light source. The second portion of the thesis emphasizes an inexpensive method for encapsulation of electroactive anode biofilms in BESs with a hydrogel coating. Here we hypothesize that the hydrogel can be designed with high pH stability, nutrient diffusion to keep the biofilm viable, and can be used to protect the biofilm from environmental shocks. Successful development of this coating will open the door to a new application of PEG-based hydrogels that may address some of the critical limitations in current BESs associated with reduced biofilm activity over time.

The goals motivating this research are outlined by the following objectives:

Aim 1: Characterize the degree of control over the cell isolation and cell viability after light exposure using photodegradable hydrogels. Hydrogel degradation using a UV light source with programable features, such as user defined light patterns, and light dose will be evaluated. Different light intensity, exposure time, and release patterns will be tested to achieve appropriate release mechanism for different applications. Purity of this extraction method and procedures to

minimize the chance of contamination are demonstrated. DNA quality measurements will be conducted to evaluate the influence of UV light exposure on cell viability using various light patterns. The advantages, and limitations of this isolation method will be compared to existing approaches.

Aim 2: Demonstrate the potential of PEG-based hydrogels for high throughput screening of mutant libraries. Bacteria can be mutated randomly; however, only rarely might a strain have a mutation that affects function. Traditional methods for screening mutant libraries (ML) for discovering strains with unique function are time-consuming and laborious as they involve potentially observing tens of thousands of different colonies after plating mutant libraries on solid media in order to ensure that every gene mutation has been accounted for in the screen. Therefore, early portions of this thesis focus on developing PEG hydrogels to serve as a miniaturized version of a standard plating methods, reducing the labor and materials cost by increasing the throughput. The studies will describe preparation of PEG hydrogels as a three-dimensional cell culture matrix capable of encapsulating cells while having a proper pore size to provide sufficient nutrients transfer required for cell growth. Optimum preparation procedure of the hydrogels will be discussed along with the important experimental factors, such as cell seeding density to increase the high-throughput and the effect of light pattern and intensity on cell release. A model system based on interactions between *Agrobacterium tumefaciens* C58 (C58) and the biocontrol agent *Rhizobium rhizogenes* K84 (K84), a potent antagonist against *A. tumefaciens*, the causative agent of crown gall disease will be used to screen, identify, and isolate the rare C58 mutants resistant to antagonizing K84. The genome of the isolated strains is mapped with whole genome sequencing to identify the mutations responsible for resistance. This model system will provide a first display

of a phenotype-to-genotype demonstration using the photodegradable hydrogel screening approach for bacteria cells.

Aim 3: Demonstrate the use of hydrolytically stable PEG hydrogels on enhancing the efficiency of BESs by protecting the anodic biofilm from environmental shocks. It is hypothesized that using hydrogel coating can protect the anode biofilm from environmental shocks that affect the biofilm metabolic activity. The hydrolytic stability of the PEG hydrogel containing divinyl sulfone chemistry will be evaluated. A simple and practical method for coating the hydrogel layer over the anode electrode will be investigated. After anode coating, the effect of the protective coating on biofilm activity will be studied. The addition of an ammonia spike in the system will be used as a model of a toxic shock to assess the impact of the protective layer on the biofilm activity compared to an uncoated control system.

Chapter 3 - Photodegradable Hydrogel Interfaces for Bacteria

Screening, Selection, and Isolation¹

3.1 Overview

Biologists have long attempted to understand the relationship between phenotype and genotype. To better understand this connection, it is crucial to develop technologies that enable both cellular observation and screening with cell isolation for downstream genetic analysis. Here, we describe the use of photodegradable poly(ethylene glycol) hydrogels for screening and isolation of bacteria with unique growth phenotypes from heterogeneous cell populations. The method relies on encapsulating or entrapping cells with the hydrogel, followed by microscopic screening, then use of a high-resolution light patterning tool to enable spatiotemporal control of hydrogel degradation to release cells into solution for retrieval. Applying different light patterns allows for control over the morphology of the extracted cell, and patterns such as rings or crosses can be used to retrieve cells with minimal direct UV light exposure to ensure minimal DNA damage to the isolates. Moreover, the light patterning tool delivers an adjustable light dose to achieve various cell release rates and allows for degradation at high resolution, enabling release with micron-scale precision. Here, we demonstrate the use of this material to screen and retrieve bacteria from both bulk hydrogels and from microfabricated, lab-on-a-chip devices. The method is inexpensive, simple, and can be used for emerging applications in microbiology, including isolation of

¹ Manuscript: Fattahi, N.; Barua, N.; Van der Vlies, A. J.; Hansen, R. Photodegradable hydrogel interfaces for bacteria screening, selection, and isolation. Submitted to *Journal of Visualized Experiments*.

antagonistic or symbiotic collections of bacteria and isolation of bacterial strains with rare growth profiles for genomic characterization through 16S amplicon or whole-genome sequencing.

3.2 Introduction

Isolation of cells with unique behaviors from a heterogeneous cell population is fundamental for obtaining genetic information in biology.¹⁵⁰ Some of the most established methods of cell isolation include flow cytometry, fluorescent activated cell sorting (FACS), and microfluidics.¹⁵¹ Although these isolation methods are of high value in cell analysis, they are often labor-intensive, experimentally complex, expensive, and troubled by high cell loss, making them infeasible for practical implementation or for applications where the number of cells is limited.¹⁵² Recently, microfluidic flow cytometry has obtained much attention, which compare to conventional flow cytometry, allows for a significant reduction in the sample volume required.¹⁵³ However, further innovation on practical cell screening and isolation techniques is required for widespread use in many laboratories.

In microbiology, selection of rare or unique cells from heterogenous mixtures after observation is important in many applications. This includes selection of phenotypically rare strains from mutant libraries,⁶³ selection of keystone microorganisms from complex microbial communities,^{18,154} or selection of phenotypically rare but important bacteria from isogenetic populations. Isolation of viable but non-culturable cells (VBNC) from a bacteria population is one important example of the latter, where cells with the VBNC phenotype are often hidden in bacteria populations at ratios between $1:10^2$ to $1:10^5$.^{155,156} Due to the widespread difficulties in bacteria isolation, much remains unknown about many phenotypically rare microorganisms. These

limitations emphasize the need for cell isolation techniques to first identify the target cell or cells from a mixture and then retrieve and isolate them for downstream analysis.¹⁵⁷

This paper presents a material-based approach for bacteria screening and isolation. The method uses photodegradable hydrogels for cell encapsulation, culture, microscopic observation, and then on-demand release and recovery of targeted bacteria with unique phenotypes. This is a key procedure in novel microbial screening and selection applications that we have recently reported.^{130–132} Hydrogels are designed to contain 10 nm mesh size, where each crosslink contains photocleavable poly(ethylene glycol) (PEG)-*o*-nitrobenzyl groups. This allows the material to encapsulate cells either within bulk hydrogels or to trap them within microwell surfaces while enabling diffusion of nutrients and waste products to and from cells during culture. Exposing the surface to a patterned UV light source with an upright microscope enables local ablation of the hydrogel entrapping individual microcolonies, triggering selective cell release and recovery for downstream analysis, which may include genomic, proteomic, or transcriptomic analysis. The method is demonstrated here with a model Gram-negative organism (*Escherichia coli*) and a model Gram-positive organism (*Bacillus subtilis*) but has been readily extended to a variety of other bacteria.

3.3 Experimental section and protocols

3.3.1 Bacterial strains and culture protocols

1. Streak colonies of *Bacillus subtilis* (strain 1A1135, Bacillus Genetic Stock Center) on ATGN (0.079 M KH₂PO₄, 0.015 M (NH₄)₂SO₄, 0.6 mM MgSO₄·7H₂O, 0.06 mM CaCl₂·2H₂O, 0.0071 mM MnSO₄·H₂O, 0.125 M FeSO₄·7H₂O, 28 mM glucose, pH: 7 ± 0.2, 15 g/L Agar) agar

plates supplemented with 100 µg/ml spectinomycin and *E. coli* (strain 25922, ATCC) on ATGN agar plates supplemented with 100 µg/mL ampicillin.

2. Pick colonies of both strains from ATGN agar plates and start overnight cultures at 37 °C while shaking at 215 rpm in ATGN liquid medium for 24 hours. Store the cell cultures in 50% glycerol at -80 °C for future use.

3. Pick colonies of both strains from glycerol stocks using sterile inoculation loops and incubate in ATGN liquid media for 24 hours at 37 °C and 215 rpm.

3.3.2 Preparation of the material needed for hydrogel formation

3.3.2.1 Photodegradable PEG-*o*-NB-diacrylate synthesis

NOTE: The in-house synthesis of the PEG-*o*-NB-diacrylate has been well-described and previously reported.^{130,158} Alternatively, because the synthesis is routine, it can be outsourced from a chemical synthesis facility.

3.3.2.2 Crosslinking buffer

1. Take the recipe of the selected medium for the bacterial strain and prepare media with 2X nutrients.

2. Add phosphate, i.e., NaH₂PO₄, to the medium to a final concentration of 100 mM.

3. Adjust the pH value to 8 using 5 M NaOH (aq).

4. Sterilize the buffer solution and store at -20 °C until further use.

NOTE: Leave out any transition metals present in the media, as these metals catalyze the oxidation of the thiols to a disulfide.

3.3.2.3 PEG-*o*-NB-diacrylate solution

1. For each mg of the aliquot PEG-*o*-NB-diacrylate (3,4K MW) powder add 3.08 μ L ultrapure water to reach 49 mM concentration of PEG-*o*-NB-diacrylate (98 mM acrylate concentration).
2. Vortex the solution until it is well mixed.
3. Store this solution at -20 °C until further use.

3.3.2.4 Thiol solution

1. For 4-arm PEG-thiol (10K MW) preparation, add 4 μ L of ultrapure water per mg powder to reach a 20 mM concentration (80 mM of thiol concentration).
2. Vortex this solution until it is well-mixed.
3. Store this solution at -20 °C until further use.

3.3.3 Preparation of perfluoroalkylated glass slides

1. Place up to 5 glass slides (25 \times 75 \times 1 mm) inside a polypropylene slide mailer.
2. Sonicate the slides with a 2 % (w/v) alconox solution for 20 minutes.
3. Rinse the slides within 3 times with ultrapure water and sonicate these slides in water for 20 minutes. Then dry the slides using a stream of N₂.
4. Plasma clean both sides of the glass slides according to the protocol in **Section 3.3.4.1** for 2 minutes.
5. Place the plasma cleaned slides back into the slide mailer and fill the container with a 0.5 % (v/v) solution of trichloro(1H, 1H, 2H, 2H,-perfluorooctyl)silane in toluene. Allow these glass slides to be functionalized for 3 hours at room temperature.
6. After slides are functionalized, rinse the slides within the slide mailer, first with toluene

and next ethanol (3 times with each solvent).

7. Dry each functionalized slide using a N₂ stream.

3.3.4 Preparation of thiol functionalized glass coverslips

3.3.4.1 Cleaning of the glass coverslips using a plasma cleaner

1. Place 18×18 mm coverslips in a petri dish.
2. Place the petri dish in a plasma cleaner chamber, and power the plasma cleaner on and place the petri dish inside the chamber.
3. Turn the vacuum pump on to clear the air within the chamber until the pressure gauge reads 400 mTorr.
4. Open the metering valve to let air into the chamber until the pressure gauge reaches a steady pressure (800-1000 mTorr). Then, select RF with "Hi" mode and allow the coverslips to be exposed for 3 minutes.
5. After 3 minutes, turn off the RF and the vacuum pump.
6. Take the petri dish out of the chamber, flip the coverslips, and place them back in the chamber to plasma clean the other side of the glass coverslip.
7. Repeat steps 2 to 5 to plasma clean the untreated side of the glass coverslip.
8. After completing the process, remove the petri dish from the chamber and turn the plasma cleaner and vacuum pump off.

3.3.4.2 Cleaning and hydroxylation of the coverslips with piranha solution

NOTE: Piranha solution (Caution! Strongly Corrosive) is a 30:70 (v/v) mixture of H₂O₂ and H₂SO₄.

1. Place a 100 × 50 mm Pyrex dish on a magnetic stirrer under a fume hood and add 14 mL of H₂SO₄ to the dish.
2. Gently place a stirring bar inside the dish. Then, turn on the stirrer and put the setup on slow to avoid splashing the acid.
3. Gently add 6 mL of H₂O₂ to the dish and allow the solution to get well mixed.
4. Remove the stirring bar from the dish. Next, gently place the coverslips inside the dish and set the temperature to 60-80 °C.
5. After 30 minutes, gently remove the coverslips using forceps and submerge them in DI water 2 times to wash out the piranha solution residues.
6. After rinsing with water, store the coverslips in DI water at room temperature until further use.
7. Neutralize the piranha solution and pour it down the sink.

3.3.4.3 Thiol functionalization of the coverslips

1. Prepare a 5 % (v/v) solution of 269 mM of (3-mercaptopropyl) trimethoxysilane (MPTS) solution in dry toluene.

NOTE: Use at least 10 mL of solution for each coverslip.

2. Add 10 mL of the solution to individual 50 mL falcon tubes and place one cleaned coverslip in each falcon tube and submerge it within the solution.

NOTE: One coverslip per falcon tube is used to assure the thiolation of both sides of the substrate without being disturbed by other substrates.

3. After 4 hours, wash each coverslip (four washes per coverslip) with toluene, a 1:1 (v/v) ethanol: toluene mixture, and ethanol.

NOTE: This is done by immersing each coverslip sequentially into falcon tubes containing the mentioned solutions.

4. After rinsing the substrate, submerge them in ethanol and store them at 4 °C for further use.

NOTE: The method used here could be laborious due to treating the coverslips one at the time. An alternative method is using Columbia jars that fit several slides at the time and are compatible with the functionalizing solution.

NOTE: Thiol functionalization is needed for having a covalent bond between the hydrogel and base coverslip surface.

3.3.5 Preparation of silicon microwell arrays

3.3.5.1 Parylene coating

NOTE: Silicon wafers were coated with parylene using the standard protocol described in previous research articles.^{159,160}

3.3.5.2 Photolithography

NOTE: Standard photolithography techniques described by Barua *et al.*¹³¹ were applied to fabricate microwell arrays on silicon wafers.

3.3.6 Hydrogel formation

3.3.6.1 Bulk hydrogel formation on glass coverslip

Hydrogel precursor solution

1. Add 12.5 μL of the crosslinking buffer to an Eppendorf tube, followed by 5.6 μL of PEG-*o*-NB-diacrylate crosslinker to the tube. Lastly, add 6.9 μL of PEG-tetrathiol to the mixture.

NOTE: Adding the PEG-tetrathiol to the mixture initiates the crosslinking reaction. Thus, the hydrogel precursor solution should be used immediately after mixing.

Cell encapsulation in the hydrogel precursor solution

NOTE: For cell encapsulation, before step 1, inoculate the crosslinking buffer with the desired cell density. As reported previously.¹³² It was observed that cell density of 7.26×10^7 CFU/mL in the crosslinking buffer correlates to acquiring ~ 90 cells/ mm^2 across the hydrogel.

1. Place the thiolated base coverslip on a clean petri dish. Place two spacers on the two opposing sides of the coverslip.
2. Fix the spacers on the base coverslip by taping the spacers to the petri dish.
3. Pipette the desired volume of the precursor solution on a non-reactive perfluoroalkylated glass slide.
4. Place the perfluoroalkylated glass slide on the base coverslip (**Scheme 3.1c**). Wait 25 minutes at room temperature for the hydrogel formation to complete.
5. After gelation, gently remove the perfluoroalkylated glass slide. The hydrogel will stay attached to the base coverslip.

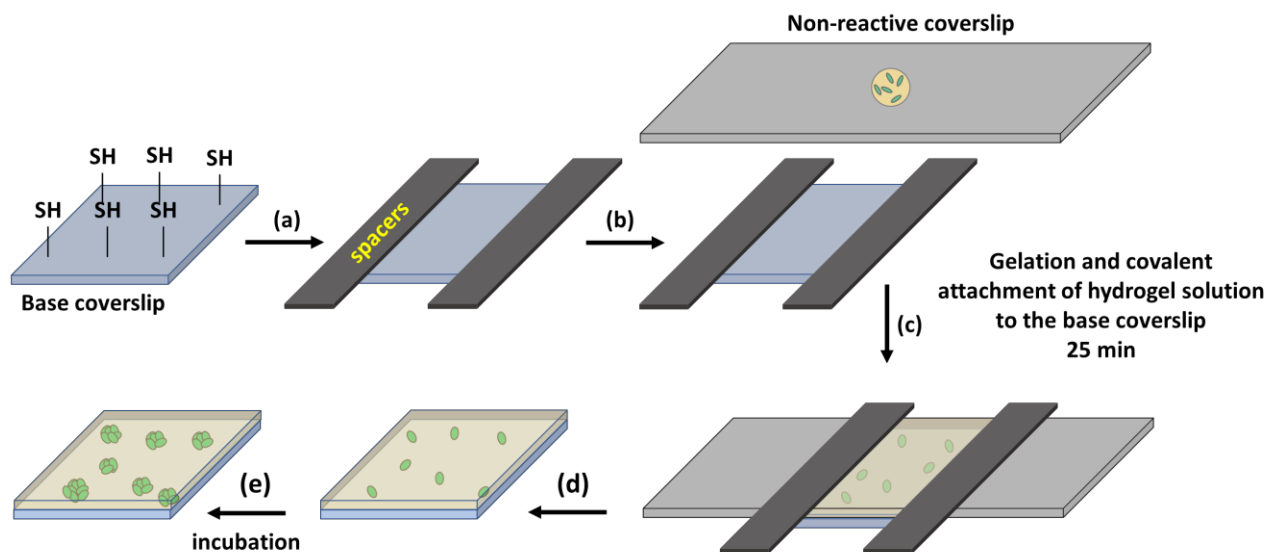
NOTE: for 18 \times 18 mm coverslips to obtain a 12.7 μm thick membrane, use ~ 7 μL of the precursor solution (**Scheme 3.1a, b**).

NOTE: Using higher volume of precursor solution may result in hydrogel underneath the base coverslip. This may cause the base coverslip to stick to the petri dish and break upon attempt of removal. Also, hydrogel residue underneath the coverslip is problematic for microscopy.

NOTE: Gentle removal of the non-reactive perfluoroalkylated glass slide is required, as fast

removal can damage the hydrogel.

6. Place the substrate in a 60×15 mm petri dish in specified media for culture. Here, ATGN media supplemented with 100 µg/ml spectinomycin for *B. subtilis* and 100 µg/ml ampicillin for *E. coli* at 37 °C for 24 hrs.



Scheme 3.1. Hydrogel formation on thiolated glass coverslips. (a) Spacers with the thickness of 12.7 µm are placed on the edges of a base coverslip containing reactive thiol groups. (b) Hydrogel precursor solution is pipetted over a non-reactive fluorinated glass slide. (c) The non-reactive glass slide is placed on the spacers for the formation of 12.7µm thick hydrogel. (d) The non-reactive glass slide is gently removed, leaving the hydrogel attached to the base coverslip. (e) The prepared hydrogel can be incubated in media for cell culture.

3.3.6.2 Hydrogel formation over microwell arrays

1. 700 µL of OD₆₀₀= 0.1 cell suspensions were seeded over the microwell array substrates, and parylene lift-off method was applied to remove cells from the background by using the protocol described by Timm *et al.*¹⁶¹

2. Prepare the hydrogel precursor solution by adding 5.6 μL of the PEG-*o*-NB-diacrylate with 12.5 μL pH 8 phosphate buffered saline ATGN and mixing with 6.9 μL of the PEG-tetrathiol solution.
3. Pipette 12.5 μL of the precursor solution on a non-reactive perfluoroalkylated glass slide and place two 38 μm steel spacers on two opposing sides of the microwell array substrate inoculated with cells.
4. Invert the perfluoroalkylated glass slide with the precursor solution droplet and place the droplet in the middle of the microwell substrate. Then, incubate for 25 minutes at room temperature for hydrogel formation.
5. Gently remove the glass slide from the microwell substrate. The hydrogel membrane should remain attached to the microwell substrate.
6. Place the substrate in a 60 \times 15 mm petri dish in specified media, here, ATGN media supplemented with 100 $\mu\text{g}/\text{ml}$ spectinomycin for *B. subtilis* and 100 $\mu\text{g}/\text{ml}$ ampicillin for *E. coli* at 37 $^{\circ}\text{C}$ for 24 hrs.

3.3.7 Material preparation for cell extraction

3.3.7.1 PDMS holder preparation

1. Tape a stack of 10 18 \times 18 mm coverslips together and glue this stack of coverslips to the bottom of a petri dish.
2. Fabricate PDMS holders by mixing PDMS precursor and curing agent at a ratio of 10:1 followed by degassing the mixture in a vacuum desiccator. Next, pour this mixture in the petri dish

and incubate in the oven for 90 minutes at 80 °C.

3. After curing PDMS, cut around the taped block to remove the PDMS holder and place the PDMS holder on a glass slide for easier handling for microscopy.

4. NOTE: This will result in a PDMS holder that fits the coverslips and the microwells and require less liquid volume for cell extraction.

3.3.7.2 Micro syringe and tubing preparation

1. Cut 20 cm of 0.05" ID PTFE tubing and attach one end of the tubing to a 100 μ L microliter syringe.

NOTE: For extraction, avoid using pipettes as drawing the released cells via a pipette tip can damage the hydrogel surface and can lead to contamination.

3.3.8 Polygon 400

3.3.8.1 Software preparation

NOTE: The following steps described in this section are identical for both bulk hydrogels, and microwell arrays except for the light exposure patterns described in this section.

1. Turn on the microscope. Then, turn on the Polygon400 device.

2. Turn on the BioLED Analog and Digital control module. Next, turn on the BioLED Light Source Control Module.

3. Open the microscope software, Infinity Analyze, and Polygon software, PolyScan2. When the Hardware configuration window is opened, select the Load button.

NOTE: You should see three devices here to be loaded. (Third-party camera, a control module, and the Polygon400).

4. Press the Start button.

NOTE: The PolyScan2 software window will now open.

5. Select the first option, the Device Control, button on the left sidebar of the window.

3.3.8.2 Polygon calibration.

NOTE: Calibration must be done with the same microscope objective and filter that will be used for light exposure.

NOTE: Set the microscope objective to 10X magnification. This magnification allows enough working distance between the microscope lens and the sample surface. It also allows for monitoring and recording the retrieval process in real-time through the image window.

1. Set the microscope lens, and filter to the settings that will be used for light exposure and place the calibration mirror under the microscope.
2. In the Device Control window, press the LED Control tab. Turn on the LED #1 and set the light intensity to the desired number.
3. Press the Polygon tab in the Device Control window. Then, press the Show Grid button.

NOTE: A grid pattern will be projected on the calibration mirror.

4. Adjust the microscope focus and camera exposure to obtain high image quality of the grid and rotate the camera to align the grid lines parallel to the camera window frame if needed.

5. Select the Calibration Wizard button under the Polygon tab and follow the instructions provided by the software in this window.

NOTE: A third-party camera Setup window will be opened.

6. A calibration Type Selection window will be opened. Select "Automatic Calibration" and press Next.

7. When the Pre-calibration Adjustment window opens, follow the software instructions, and press the "Next" button.

8. When the Mapping Information window opens, save this calibration accordingly in the desired folder.

NOTE: This is done by putting in the date, microscope name, Objective Lens, Filter.

9. After calibration, press the "Working Area Definition" button under the Polygon tab to define the Polygon working area if needed.

10. Press the Sequence Design button on the left-sidebar of the software window. Then, press the Profile Sequence Editor button.

11. When the Profile Sequence Editor window opens, select the New Profile option under the Profile List.

NOTE: Now, a Pattern Editor window will be opened.

12. Prepare the desired pattern for light exposure by choosing different pattern shapes and sizes or manually drawing the pattern, if desired.

Circle and broken cross patterns for bulk hydrogel.

1. For circle patterns, define a circle with a 30 μm diameter over a target bacteria colony so it covers the whole colony. Choose the shape fill color white.
2. For broken cross patterns, choose the rectangle shape from the pattern drawing window with the dimensions of 3 \times 8 μm . Place 4 rectangles with this dimension on the edges of the target colony, while half the patterns have an overlay with the colony.

Circle and ring patterns for microwell arrays

1. For circle patterns, draw a 10 μm diameter circle around the well perimeter. Choose the shape fill color white.
2. For ring pattern, draw a circle of diameter 20 μm and place it over the well and choose the shape fill color white. Draw another circle pattern of diameter 10 μm with fill shape color black and place it around the perimeter of the well.
3. Edit the pattern and modify the shapes based on the desired extraction method. Ensure that the desired pattern exists within the Polygon working area.
13. Place the sample in a PDMS holder and pipette the defined media on top of the sample to prevent sample dehydration and provide a carrier solution for released cells. Then, replace this with the calibration mirror.
14. Here, light patterns can be designed while the camera view is showing the sample surface to test different patterns for cell extraction.
15. Save the defined pattern. After saving the defined pattern, select the “Session Control”

section. In this section, under the Polygon tab, add the saved sequence.

16. After adding the sequence, choose the option to simulate the pattern to view and adjust for the desired location of exposure.

NOTE: Sample location can be adjusted here to assure the pattern is projected precisely on the targeted area.

17. Next, adjust the light intensity to 60 % and the exposure time to 40 sec under the LED control tab and start the exposure process.

18. Monitor the hydrogel degradation in real-time to ensure cell release.

3.3.9 Cell retrieval

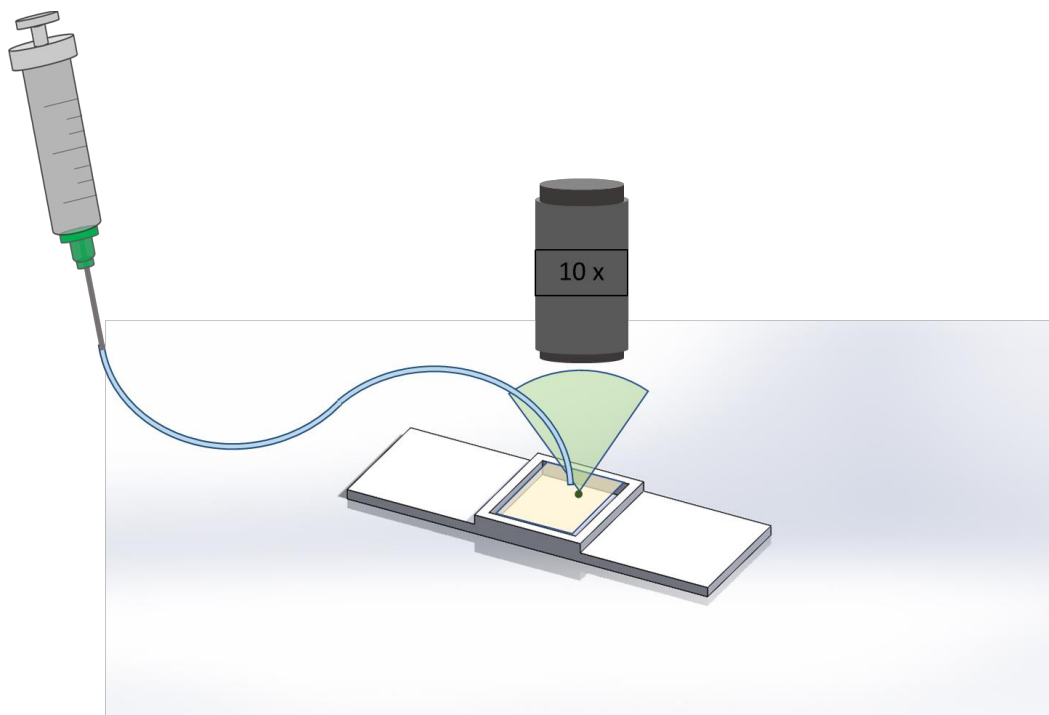
NOTE: Cell retrieval procedure is identical for both microwell arrays and bulk hydrogels.

1. After light exposure and cell release, cells can be collected using a microliter syringe and microfluidic tubing (**Scheme 3.2**).

2. Change the microscope filter from brightfield to FITC. This allows for visualizing the exposed area of the sample by the naked eye.

3. Once the exposed area is located, place the end of the tubing upon the irradiated spot. Then change the microscope filter back to brightfield to monitor cell retrieval in real-time.

4. Use the syringe attached to the other end of the tubing to carefully withdraw the released cells. Suction 200 μ L of solution. Next, Insert the solution into an Eppendorf tube for DNA analysis or plating.



Scheme 3.2. Schematic representation of the extraction method for collecting cells released from the hydrogel. Here, immediately after UV exposure, hydrogel degradation, and cell release, the microscope is used to illuminate the sample with a FITC filter, resulting in a bright spot covering the area where released occurred. This assists the user in identifying the spatial location for sample collection. After visualizing this area, tubing attached to a microliter syringe is placed at this spot for sample collection. Brightfield microscopy at 10X magnification is used to monitor the end of the tubing in real-time for precise cell collection.

3.3.10 Genomic DNA purification and DNA quality measurement

1. Use DNeasy Blood and Tissue kit to extract DNA from bacteria isolates.
2. Follow the manufacturer's specification described in DNeasy Blood and Tissue kit handbook 18 up to the last step, step 7, requiring elution with Buffer AE.
3. For the elution step follow the manufacturer's specification, with the difference of using 100 μL Buffer AE instead of 200 μL .

4. Repeat elution once as described in step 11.1.2. This step leads to increased overall DNA yield.
5. Measure DNA quality by using a Nanodrop spectrophotometer.
6. Turn on the NanoDrop.
7. After the device initialization, on the home page, select the “dsDNA” option on the screen.
8. Next, lift the pedestal arm, and clean the pedestal position with DI water and Kimwipes.
9. Pipette 2 μL of a blank solution, here AE buffer, on the pedestal position and gently bring the pedestal arm down and select “Blank” on the screen.
10. Next, lift the pedestal and clean the pedestal position with DI water and Kimwipes to remove any residues from the previous measurement.
11. Load your sample (2 μL) on the pedestal position, bring the pedestal arm down, and select the Measure button on the screen.
12. Redo steps 10 and 11 for all samples.
13. Once the measurement is done, select “End Experiments” on the screen.
14. Insert your flash drive into the device and press “Export Data” on the screen.

3.3.11 Determining cell viability from hydrogel and microwell extracts

1. Dilute the bacterial suspensions by a dilution factor of 10^5 using a 96-well plate.

2. Pipette 10 μL , 10^5 of the diluted bacterial suspension and spot three times on ATGN plates for each bacteria suspension. Tilt the plates to spread the cells on agar surfaces. Air-dry the ATGN plates containing the bacterial suspensions.
3. Incubate the plates at 37 °C for 48 hrs. Count and record the Colony Formation Units (CFUs) numbers. Count all three spreads of bacterial suspensions on each plate.

NOTE: Perform steps 1 to 3 in a biological safety cabinet to avoid contamination of the plate.

3.4 Representative results

To investigate the ability of UV light to trigger controlled hydrogel degradation for cell release, the percent gel degradation was calculated after UV light exposure with various light intensity and exposure times. A representative example of how these two parameters affect hydrogel degradation is shown in **Figure 4.3** (appearing in next chapter). As evident, patterned light provided by the Polygon 400 tool provides spatial-temporal control of hydrogel degradation at a resolution that can enable release of only a small number of cells.

For cell extraction, different light patterns were used to investigate cell release (**Figure 4.8** appearing in next chapter). It was observed that different patterns influenced the morphology of the released cells. This is potentially beneficial for various applications. For instance, exposing a ring pattern around the target colony, results in release of the entire colony still encapsulated in a protective PEG hydrogel and without direct UV light exposure (**Figure 4.8A**), which may preserve cells and provide easy downstream purification. In contrast, by exposing part or all of the colony to UV light, cells can be extracted either as aggregated cell clusters (**Figure 4.8B**) or as free, individual cells (**Figure 4.8C**).

Starting with screening from bulk hydrogels, bacteria samples were encapsulated, cultured, and imaged following the established protocols. A representative example of bacteria cell colonies in bulk hydrogels is shown in **Figure 4.2** (appearing in next chapter), where cells were seeded at an OD₆₀₀ of 3.63×10^7 , resulting in a microcolony density of 90 colonies/mm² throughout the hydrogel. As seen in **Figure 4.2B**, hydrogel thicknesses greater than 12.7 μm can result in the formation of overlapping colonies in the vertical direction, which may result in extraction of multiple colonies. **Figure 4.2C** shows how cross-contamination can occur during extraction due to overlay of colonies. Here, a top colony is targeted, while an underlying colony also is extracted with it. Therefore, using 12.7 μm spacers is recommended for hydrogel preparation.

Given the potential damage to bacteria with UV light, the effect of varied UV light micropatterns on cell viability was further studied using model Gram-positive bacteria (*B. subtilis*) and model Gram-negative bacteria (*E. coli*). Each was encapsulated within bulk hydrogels and cultured into microscale colonies, verifying their compatibility with the hydrogel. Targeted microcolonies of equivalent sizes (26 ± 1 μm diameter) were then exposed to a constant light dose (168 mJ/mm²), either in the form of circle patterns exposing entire microcolonies to UV light or cross-patterns that degrade only hydrogel edges to minimize light exposure to cells. Cells were then recovered and plated to quantify the CFU/mL recovered from each colony. **Figure 3.1A** shows that no significant difference in cell recovery level was found. To further investigate the integrity of the cells, DNA was extracted from *E. coli* samples and analyzed using a Nanodrop spectrophotometer. DNA quality levels fall within a A₂₆₀/A₂₈₀ range between 1.8 and 2.0 as shown in **Figure 3.1B**, which is in the ideal range for genomic sequencing.¹⁶² This demonstrates that using UV for release under the described conditions has minimal effect on the integrity of recovered cells from the bulk hydrogels.

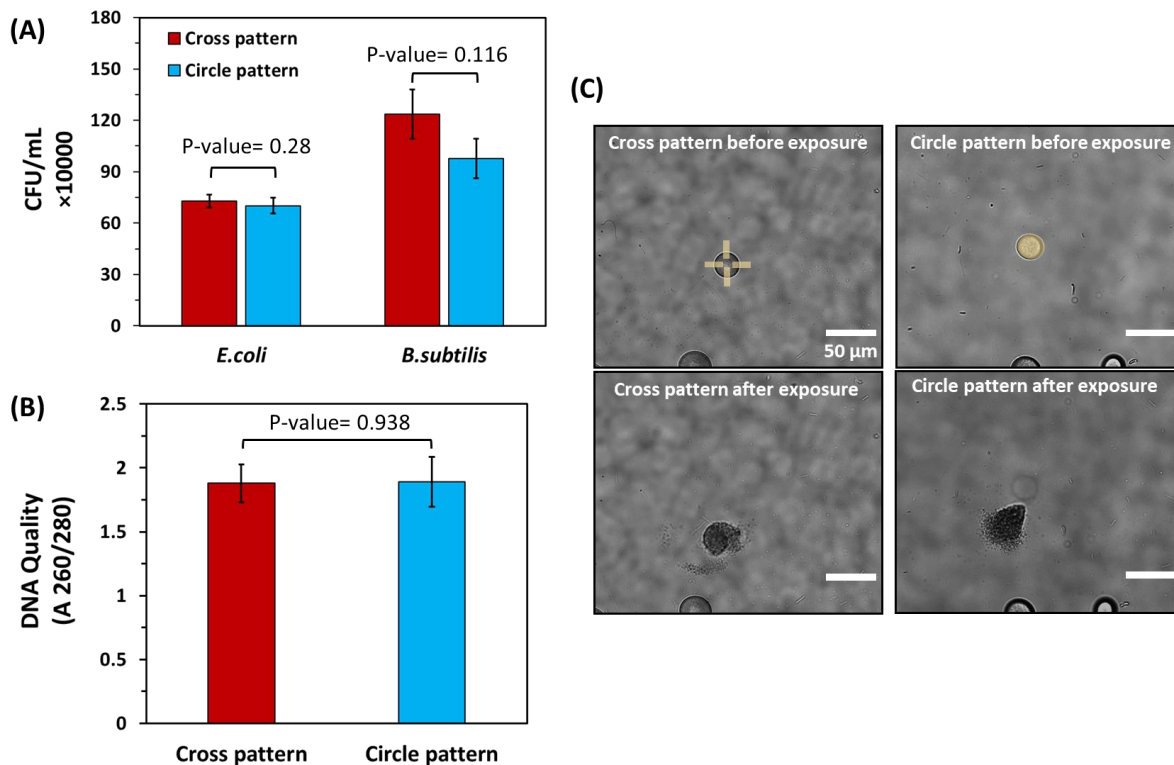


Figure 3.1. Impact of different light exposure patterns on cell viability and DNA quality of bacteria released from bulk hydrogels. (A) Cell recovery levels for both *E. coli* and *B. subtilis* after extraction using cross patterns and circle patterns. For this experiment extraction was done from the spherical colonies with the same diameter ($26 \pm 1 \mu\text{m}$) to ensure the number of released cells from each colony were equivalent. The extracted solutions were then plated to calculate the CFU/mL acquired from each pattern. Statistical analysis showed no significant difference in CFU/mL obtained from cross and circle patterns for both *E. coli* and *B. subtilis* (P-value > 0.05). (B) Spectrophotometric quantification of DNA quality for isolated *E. coli* cells using cross and circle patterns. Here, statistical analysis did not show a significant difference in DNA quality for the patterns used (P-value > 0.05). (C) Brightfield images of the colonies with equal diameters exposed to cross and circle patterns.

Microwell arrays provide an alternative screening interface that has been useful for studying bacteria growth under spatial confinement,¹⁶³ and most recently for discovery of symbiotic and antagonistic interactions between different bacterial species.¹³¹ Cellular extraction from wells for genomic analysis such as 16S amplicon sequencing is also important in these applications. Using the same tool, UV light can be exposed over a well containing cells of interest,

either as circle or as ring patterns (**Figure 3.2**). The latter ensures hydrogel degradation only at the microwell perimeter to prevent direct irradiation of cells. Unlike the bulk hydrogel format, cell extraction here has only been observed in the shape of cell clusters.¹³¹

To quantify bacteria cell viability and DNA quality after extraction in this format, *B. subtilis* and *E. coli* cells were seeded, cultured, then released from microwell arrays using circle and ring patterns (**Figure 3.3A, B**). Released cells were then plated on ATGN agar plates and the DNA quality of the extracted cells was quantified. To ensure that a consistent number of cells was present during each extraction, microwells with similar fluorescent intensities (~ 6000 A.U.) and therefore similar number of cells were targeted for release. As shown in **Figure 3.3C**, the number of viable cells extracted using circle pattern was not significantly different from the number of viable cells extracted using ring pattern for either bacteria. Also, the DNA quality levels were not significantly different between the circle and ring patterns for either bacteria as shown in **Figure 3.3D**. Hence, similar to findings in bulk hydrogels, the application of UV light at the intensity and duration specified here had a negligible impact on the viability and DNA integrity of cells extracted from the microwell arrays. These findings demonstrate that viable bacteria cells can be selectively retrieved from microwells with minimal damage, essential for downstream genomic analysis.

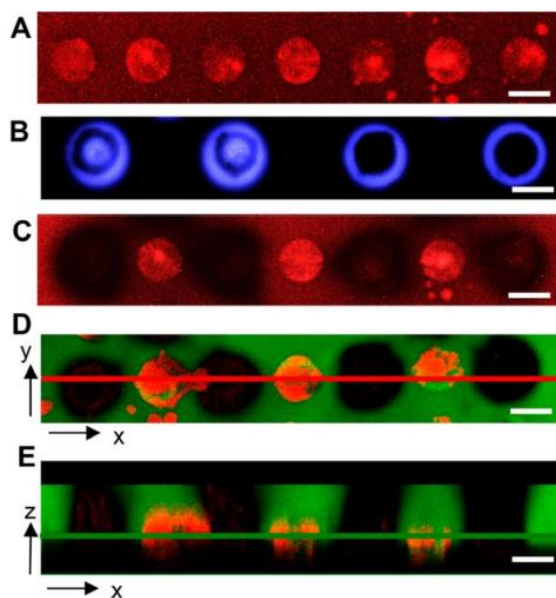


Figure 3.2. Representative confocal microscopy images showing light pattern impact on cell isolation from microwell arrays. Adapted with permission from van der Vlies *et al.*¹³⁰ Copyright (2019) American Chemical Society. (A) Microwells with diameter of 40 μm containing bacteria (red). (B) Light exposure using circle and ring patterns (blue) for 5 min at 0.7 mW/mm^2 . (C) Diffuse red fluorescence demonstrates that cells are released from irradiated wells. (D) Green fluorescence signal representing the fluorescein-labeled membrane, and red fluorescence signal representing mCherry expressing cells coming from the xy plane along the green line in E. (E) Fluorescence signal coming from the xz plane along the red line in D. Samples in images (C-E) were washed for removal of released cells, then fixed and imaged. Scale bar = 40 μm .

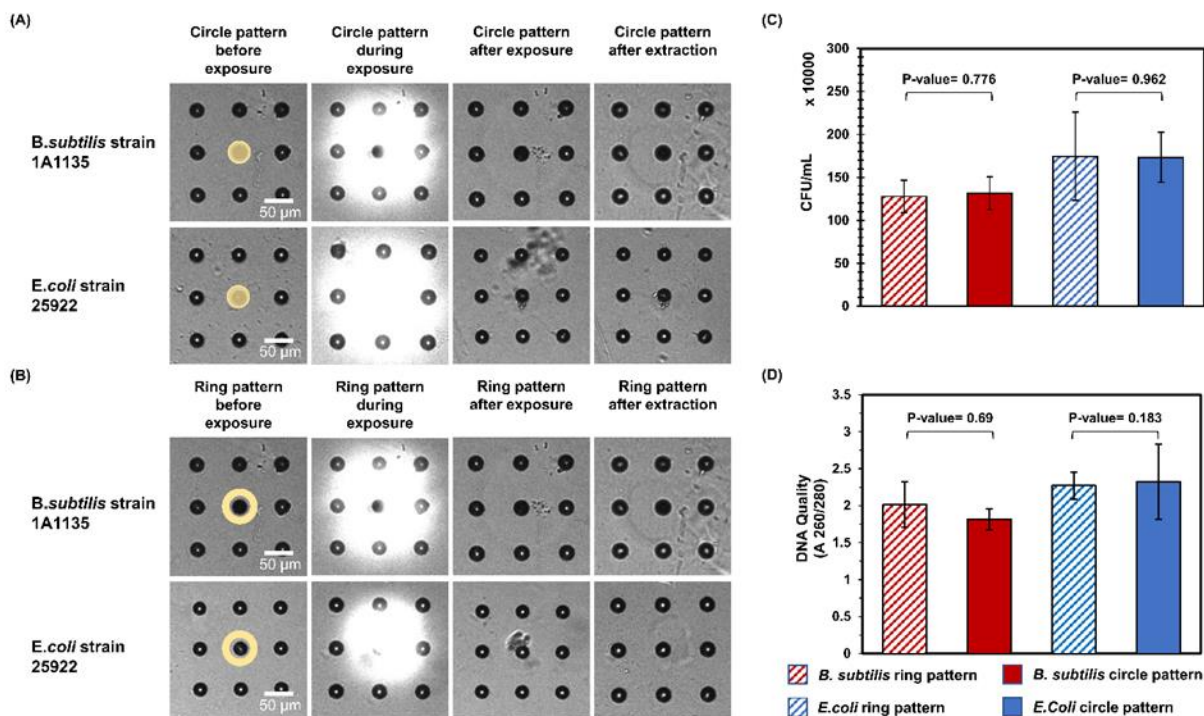


Figure 3.3. Impact of different patterns on cell viability and DNA quality in microwell arrays. (A, B) For both *E. coli* and *B. subtilis*, circle patterns and ring patterns were used for cell extraction from 10 μm microwells. Circle pattern with a diameter of 10 μm and ring pattern with an inner diameter of 10 μm and outer diameter of 20 μm were used in this experiment for cell extraction. Microwells with the same diameters were used to ensure that the number of released cells from each microwell was the same. (C) The extracted solutions were then plated to calculate the CFU/mL acquired from each exposure pattern. Statistical analysis showed no significant difference in CFU/mL obtained from circle and ring pattern for both *E. coli* and *B. subtilis* (P-value > 0.05). (D) Spectrophotometry was used to measure the DNA quality of both *E. coli* and *B. subtilis* cells using circle and ring patterns. Here, statistical analysis did not show any significant difference in the DNA quality for the patterns used (P-value > 0.05).

3.5 Discussion

This manuscript demonstrates the use of photodegradable hydrogels for bacteria isolation from both bulk hydrogels and microwell arrays, each format with its own set of unique advantages and drawbacks. The separation process in both methods has been successfully used to isolate

bacteria that display unique growth behavior for downstream genotyping after culture and microscopic observation, which is a critical capability for connecting genotype to phenotype. To date, genomic characterization of bacteria extracted from these interfaces has included 16S amplicon sequencing to identify multi-species collections bacteria from environmental microbiomes that generate emergent growth behavior, and for whole genome sequencing to identify genetic mutations in rare cells present within mutant libraries.

Cell recovery and extraction in both formats occurs in an open-plate environment, thus effort is required to harvest cells efficiently while minimizing the chance of contamination from the external environment.¹⁵¹ To this end, care must be taken to acquire enough cells from the target colonies while also minimizing the volume of the extraction solution. To obtain enough cells for plating and recovery or for extraction of DNA material, we found that hydrogels must be cultured long enough to reach colony diameters of at least 10. To lower the required volume for cell extraction, we observed that using a microliter syringe and tubing (**Scheme 3.2**) was more efficient than pipetting. The tubing allowed the isolates to be drawn from the release point more accurately, requiring less solution volume and lowering the chance of contamination.¹⁵¹

Using bulk hydrogels for cell screening and isolation provides the most straightforward and simple experimental setup. Bulk photodegradable hydrogels form rapidly (25 minutes) after mixing the precursors over transparent glass coverslips to encapsulate cells in a 3-D cell culture matrix that is easily imaged and monitored with a standard upright or inverted fluorescence microscope. Thus, the method has potential to be highly translational to common microbiological laboratories that do not have microfabrication resources or expertise. Extraction with high spatial precision requires that the fluorescent microscope is coupled to a Polygon400 light patterning tool (~\$22K). The drawback to this format is that cells are randomly oriented throughout the three-

dimensional hydrogel. Therefore, cells can appear out of the focal plane when imaging with higher magnification objectives, and extraction can be difficult if cell colonies are oriented too close to each other or if there is an overlay of colonies. Depositing a thin hydrogel (<13 μm) as described here is essential to mitigate these drawbacks.

In contrast, microwell arrays provide an alternative screening interface which provides a more well-controlled interface, as bacteria cells are partitioned into discrete microwells that serve as small culture or co-cultures sites.^{130,131,163} Microwell dimension, pitch, and density are well-controlled using standard photolithographic microfabrication approaches. Compared to bulk hydrogels, bacteria can be extracted from microwell arrays with a high degree of specificity and lower chance of cross-contamination, as the cells are only present at predefined locations, not randomly dispersed throughout the hydrogel. The concentration and ratios of bacteria cells in the seeding solution can also be varied to control the quantity and composition of the microwell inoculum, this seeding process has been well-characterized in previous reports. This capability gives the user flexibility in the experimental design of the screen.¹⁶³

The primary drawback of the screening with the microwell array format is the added time, and expertise required for microfabrication. We estimate that in our lab, fabrication of microwells costs ~\$10 per array, which includes material costs and cleanroom expenses. In addition, due to constraints associated with Bosch etching during fabrication, microwell arrays are traditionally made from silicon, which can cause imaging difficulties since the substrates are non-transparent. Moreover, a high amount of light scattering from the silicon surface can limit imaging within the microwells and can decrease pattern resolution during membrane exposure with UV light from the Polygon tool, as evident in **Figure 3.3A**, and **B**. Similar microwells have been fabricated on quartz

substrates to address these types of limitations,¹⁶⁴ however the fabrication is considerably more difficult.

3.6 Acknowledgement

This research was supported by the National Science Foundation (Award #1944791).

Chapter 4 - Photodegradable Hydrogels for Rapid Screening, Isolation, and Genetic Characterization of Bacteria with Rare Phenotypes²

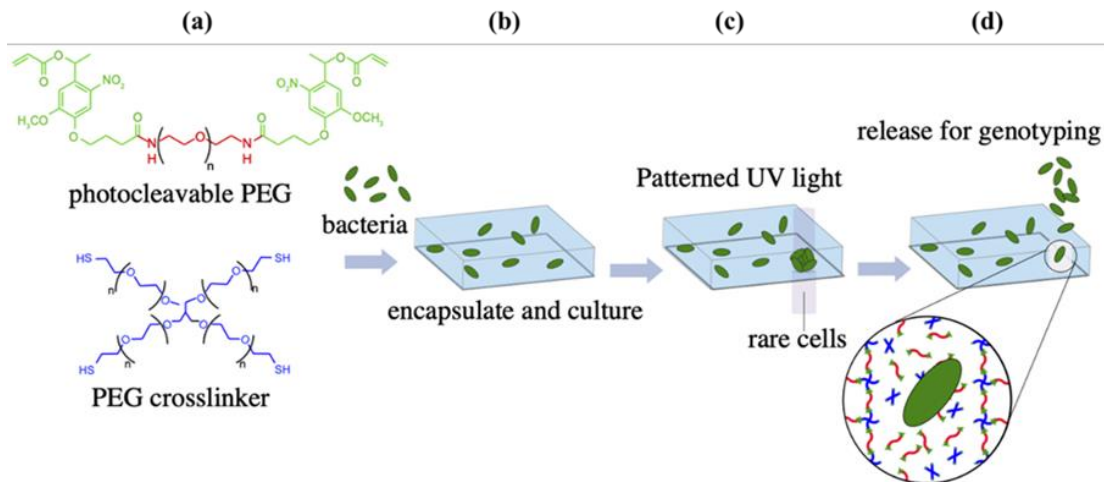
4.1 Overview

Screening mutant libraries (MLs) of bacteria for strains with specific phenotypes is often a slow and laborious process that requires assessment of tens of thousands of individual cell colonies after plating and culturing on solid media. In this report, we develop a three-dimensional, photodegradable hydrogel interface designed to dramatically improve the throughput of ML screening by combining high-density cell culture with precision extraction and the recovery of individual, microscale colonies for follow-up genetic and phenotypic characterization. ML populations are first added to a hydrogel precursor solution consisting of polyethylene glycol (PEG) *o*-nitrobenzyl diacrylate and PEG-tetrathiol macromers, where they become encapsulated into 13 μm thick hydrogel layers at a density of 90 cells/ mm^2 , enabling parallel monitoring of 2.8×10^4 mutants per hydrogel. Encapsulated cells remain confined within the elastic matrix during culture, allowing one to track individual cells that grow into small, stable microcolonies ($45 \pm 4 \mu\text{m}$ in diameter) over the course of 72 h. Colonies with rare growth profiles can then be identified, extracted, and recovered from the hydrogel in a sequential manner and with minimal damage using

² Manuscript: Fattahi, N.; Nieves-Otero, P. A.; Masigol, M.; Van der Vlies, A. J.; Jensen, R. S.; Hansen, R. R.; Platt, T. G. Photodegradable Hydrogels for Rapid Screening, Isolation, and Genetic Characterization of Bacteria with Rare Phenotypes. *Biomacromolecules* 2020. <https://doi.org/10.1021/acs.biomac.0c00543>. Reproduced with permission from the American Chemical Society. Copyright 2020 American Chemical Society.

a high-resolution, 365 nm patterned light source. The light pattern can be varied to release motile cells, cellular aggregates, or microcolonies encapsulated in protective PEG coatings. To access the benefits of this approach for ML screening, an *Agrobacterium tumefaciens* C58 transposon ML was screened for rare, resistant mutants able to grow in the presence of cell free culture media from *Rhizobium rhizogenes* K84, a well-known inhibitor of C58 cell growth. Subsequent genomic analysis of rare cells (9/28,000) that developed into microcolonies identified that seven of the resistant strains had mutations in the *acc* locus of the Ti plasmid. These observations are consistent with past research demonstrating that the disruption of this locus confers resistance to agrocin 84, an inhibitory molecule produced by K84. The high-throughput nature of the screen allows the *A. tumefaciens* genome (approximately 5.6 Mbps) to be screened to saturation in a single experimental trial, compared to hundreds of platings required by conventional plating approaches. As a miniaturized version of the gold-standard plating assay, this materials-based approach offers a simple, inexpensive, and highly translational screening technique that does not require microfluidic devices or complex liquid handling steps. The approach is readily adaptable to other applications that require isolation and study of rare or phenotypically pure cell populations.

KEYWORDS: High-throughput screening, hydrogels, mutant libraries, rare cell isolation, bacteria



Scheme 4.1. Photodegradable hydrogel interface for cell screening and isolation. (a) Hydrogel precursor material. (b) Hydrogel gelation and cell encapsulation. (c) UV light exposure on target cell colony. (d) Cell extraction and recovery.

4.2 Introduction

The identification and isolation of microorganisms with rare or unique functions from heterogeneous populations is a critical step required to connect an organism's genotype with its phenotype.¹⁸ These connections will enable researchers to gain a fundamental, predictive understanding of microbe function, to identify biomarkers that relate to specific diseases, and to engineer bacteria for applications in biotechnology. While phenotypic heterogeneity is prevalent in many microbial populations and communities, including among cells in populations that are genetically homogeneous or nearly homogeneous,^{15,165} practical microbiological methods for screening and isolating phenotypically uniform groups of microbial cells are underdeveloped. This technical limitation poses a challenge to genotype-to-phenotype determination, which thus remains a broad knowledge gap in microbiology and biology more generally.¹⁶⁶ Established methods of microbial cell isolation include flow-based sorting techniques such as fluorescence-

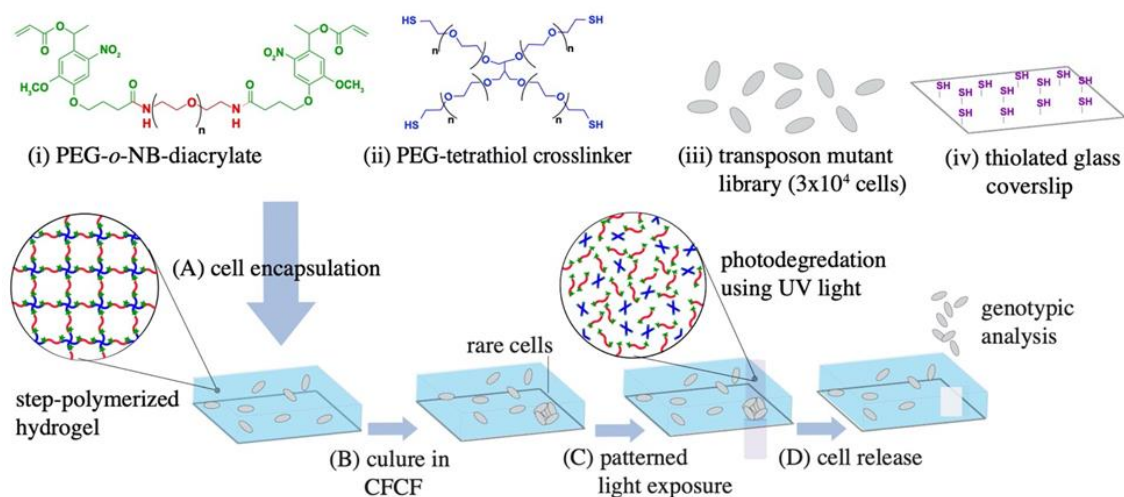
activated cell sorting (FACS), which relies on a signal from fluorescently labeled proteins or fluorescence in situ hybridization probes to isolate cells with specific features from its environment.^{167,168} FACS allows for high-throughput, single cell analysis capable of sorting of up to 50,000 cells per second.¹⁶⁹ However, subsequent cultivation and enrichment of recovered cells is often inhibited, as the labeling step compromises cell viability.¹⁶⁶ Further, FACS is limited by the inability to sort cells by time dependent cellular properties.¹⁷⁰ Consequently, FACS is not directly amenable to growth-based screening. In addition, FACS is an impractical option for many laboratories due to its high cost (~\$100–200/h) and availability often being limited to core research facilities. Motivated by these limitations, numerous micro- and nanoscale devices have been developed to isolate and study bacteria in recent years.^{171–173} One common approach uses droplet-based microfluidic devices to partition cells into picoliter droplets, offering control over the chemical microenvironment and high-throughput, single cell analysis.⁵⁶ However, most devices have several limitations, a major one being that retrieval of individual cells from the device is difficult.¹⁷⁴ Ultimately, this inhibits follow-up genotyping and other -omics level characterizations after on-chip observation. These constraints impose a major limitation for screening and discovery applications. Recently, Lim *et al.* developed an innovative microwell platform for rapid screening of *E. coli* mutant libraries for mutants with growth rate differences,⁶³ demonstrating the benefits of off-chip recovery of individual cell populations for follow-up genotypic analysis. However, many micro- and nanoscale approaches require complex fabrication and liquid handling capabilities; thus, they often fail to translate into nonexpert microbiology laboratories.¹⁶⁶

Hydrogel materials can provide an alternative strategy to microbe screening and isolation.^{158,175} Here, individual cells from a suspension are encapsulated into an elastic,

nanoporous hydrogel matrix, most commonly alginate or agarose, that facilitates diffusive biomolecular exchange.¹⁷⁶ Cells can then be cultured into high-density microcolonies, where enough biomass accumulates for cell preservation and follow-up characterization. Cells can be encapsulated into microscale hydrogel droplets using bulk emulsions¹⁷⁷ or 3D-bioprinters.¹⁷⁸ However, sorting and isolation of individual droplets containing a desired cell or cell population still remains a limitation and is most often achieved using FACS.¹⁷⁹ Photodegradable hydrogels enable an alternative mode of targeted cell recovery, thereby alleviating limitations associated with other hydrogel materials. Photodegradable hydrogels are designed to erode on exposure to light, enabling on-demand release of encapsulated cargo or manipulation of the biochemical and biophysical features of the microenvironment.¹⁸⁰ Because light can be patterned at single micron length scales, the approach affords a high level of spatial and temporal control over on-demand release.¹⁸¹ This capability provides a distinct advantage for microbial selection and isolation applications in which specific cells must be released and retrieved from a screening interface with a high spatial precision. Recently, we reported the use of photodegradable hydrogels as a membrane to retrieve cell populations loaded and cultured in a microwell array format.¹³⁰ The hydrogel was generated by combining a poly(ethylene glycol)-*o*-nitrobenzyl diacrylate (PEG-*o*-NB-diacrylate) macromer with a four-arm PEG-thiol macromer, which generates a cross-linked PEG network through thiol–acrylate Michael-type addition reactions.⁸⁶ Using a patterned 365 nm light source, cell populations cultured in individual microwells can be released from wells and into solution on-demand and then plated and recovered.

Building off of these findings, here we investigate the use of photodegradable hydrogels to screen and isolate phenotypically rare bacteria strains present in mutant libraries (MLs) for follow-up genotypic analysis (**Scheme 4.2**). The approach uses thiol–acrylate reactions to encapsulate a

ML population into a three-dimensional PEG matrix over a thiolated glass coverslip. Encapsulated cells are cocultured in a defined media for screening, and individual cells with unique growth profiles are targeted for removal and downstream analysis. Each step in the screening procedure, including parallel growth monitoring of bacterial microcolonies, the effect of light pattern and exposure on the arrangement and viability of bacteria released from the hydrogels, and sequential extraction of multiple microcolonies, is developed toward high-throughput screening and recovery of viable cells. This enabled observation and recovery of any one of 3×10^4 mutants across a ~ 310 mm² hydrogel area, a throughput that can accommodate enough mutant strains to rapidly screen even large bacterial genomes to saturation in a single assay (e.g., *Streptomyces sp.*, genome of ~ 8.7 – 11.9 Mbps,¹⁸² requiring around 60,000 mutants to achieve saturation). This capability offers a significant reduction in the time and labor required to screen to saturation using standard plating techniques. To demonstrate the benefits and feasibility of this approach, a ML of *Agrobacterium tumefaciens* C58 is screened for resistance to the antagonistic impacts of cell free culture fluid (CFCF) from *Rhizobium rhizogenes* K84. K84 produces multiple chemicals inhibiting the growth of C58, including the bacteriocin agrocin 84.^{183,184} While C58 cells are susceptible to agrocin 84, rare mutations give rise to agrocin-resistant mutants. To identify these rare mutations, the phenotype of tens of thousands of mutants must first be evaluated. In a single test, we were able to screen, identify, and then isolate nine resistant C58 mutants from a ML containing $\sim 28,000$ unique strains. Subsequent analysis of whole genome sequences identified mutations in the acc locus of the Ti plasmid conferring agrocin 84 resistance. This serves as the first example of a successful phenotype-to-genotype determination using this rapid screening approach.



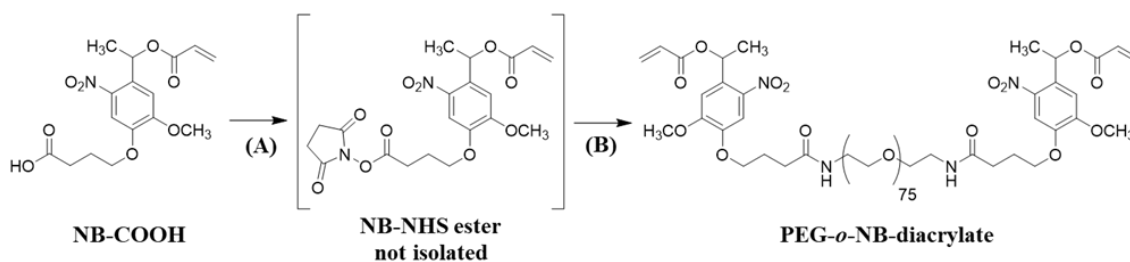
Scheme 4.2 Overall approach to screening and isolation of rare cells from transposon mutant libraries. Precursor materials consisting of (i) PEG-*o*-NB-diacrylate, (ii) PEG-tetrathiol crosslinker, (iii) a bacteria transposon mutant library and (iv) a thiolated glass coverslip is prepared. (A) Precursor components are then mixed, resulting in the formation of a step-polymerized photodegradable hydrogel layer over the coverslip. (B) Cells are cultured in cell free culture fluid (CFCF) from an antagonistic species, to identify mutants with rare growth profiles. (C) Patterned light is then used to spatially degrade portions of the hydrogel. (D) Releasing resistant cells into solution for recovery and follow-up genotyping.

4.3 Experimental section

4.3.1 Materials

Pentaerythritol tetra (mercaptoethyl) polyoxyethylene (4 arm PEG, $((\text{CH}_2)_2\text{-SH})_4$) was purchased from NOF America Corporation. PEG-diacrylate (PEGDA, MW 3400) was purchased from Laysan Bio. Fluorescein-5-maleimide was purchased from Cayman. Ethanol (EtOH), isopropanol, dimethylformamide (DMF), dichloromethane (CH_2Cl_2), diethyl ether (Et_2O), sodium hydrogen sulfate (NaHSO_4), anhydrous sodium sulfate (Na_2SO_4), and acetic acid (AcOH) were purchased from Fisher. D-(+)-Glucose, biotin ($\text{C}_{10}\text{H}_{16}\text{N}_2\text{O}_3\text{S}$), (3-mercaptopropyl)

trimethoxysilane, sodium phosphate monobasic dihydrate ($\text{NaH}_2\text{PO}_4 \cdot 2\text{H}_2\text{O}$), sodium hydroxide (NaOH),alconox detergent, toluene anhydrous, N-hydroxysuccinimide (NHS), dicyclohexyl carbodiimide (DCC), PEG-diamine (MW 3400), deuterated chloroform (CDCl_3), phosphorpentoxide (P_4O_{10}), 4 Å molecular sieves, ninhydrin, and triethylamine (Et_3N) were purchased from Sigma-Aldrich. Silica TLC plates were from Merck. Ammonium sulfate ($(\text{NH}_4)_2\text{SO}_4$), magnesium sulfate heptahydrate ($\text{MgSO}_4 \cdot 7\text{H}_2\text{O}$), calcium chloride dihydrate ($\text{CaCl}_2 \cdot 2\text{H}_2\text{O}$), manganese(II) sulfate monohydrate ($\text{MnSO}_4 \cdot \text{H}_2\text{O}$), kanamycin sulfate, spectinomycin sulfate, and iron(II) sulfate (FeSO_4) were purchased from VWR. DNeasy Blood & Tissue Kits were purchased from QIAGEN. The LIVE/DEAD BacLight Bacterial Viability Kit was purchased from ThermoFisher Scientific. All chemicals were used as received unless stated otherwise. 4 Å molecular sieves were heated under vacuum at 200 °C for 4 h to remove water. CH_2Cl_2 was dried with 4 Å molecular sieves. Et_3N was distilled from ninhydrin at atmospheric pressure and stored over KOH pellets. NHS, DCC, and PEG-diamine were dried under vacuum in the presence of P_4O_{10} at 40 °C for 19 h. NB-COOH (**Scheme 4.3**) was prepared as previously reported.¹⁵⁸ The ninhydrin staining solution was prepared by dissolving 300 mg of ninhydrin in 97 mL of EtOH and 3 mL of AcOH and stored in the dark.



Scheme 4.3 Synthesis of PEG-*o*-NB-diacrylate. (A) NHS and DCC, $\text{CH}_2\text{Cl}_2/\text{DMF}$, 0°C → room temperature, 21 hrs. (B) PEG-diamine and Et_3N , $\text{CH}_2\text{Cl}_2/\text{DMF}$, 20 h.

4.3.2 Synthetic of the photodegradable poly(ethyleneglycol) diacrylate

PEG-*o*-NB-diacrylate was prepared with slight modifications from that previously reported²³ and is shown in Scheme S1. 519 mg (1.5 mmol) of NB-COOH and 175 mg (1.5 mmol) of NHS were dissolved in 4 mL of DMF and 8 mL of CH₂Cl₂. The clear solution was cooled on ice for 15 min, and a solution of 304 mg (1.5 mmol) of DCC in 2 mL of CH₂Cl₂ was added dropwise over the course of 5 min. After stirring for 21 h at room temperature, a solution of 508 mg (0.15 mmol, 0.30 mmol NH₂ groups) of PEG-diamine and 51 μ L (0.37 mmol) of Et₃N in 9 mL of CH₂Cl₂ was added dropwise over the course of 10 min to the turbid reaction mixture. After stirring for 20 h, spotting of the reaction mixture on a silica TLC plate followed by ninhydrin staining and heating showed the absence of amine groups. The mixture was concentrated in a flow of nitrogen to remove CH₂Cl₂, and the residue was diluted with 16 mL of 1 M NaHSO₄ (aq). The suspension was passed through a glass filter, and the white residue was washed with 9 mL of 1 M NaHSO₄ (aq). The slightly hazy filtrate was then passed through a syringe filter (0.45 μ m). After the syringe filter was washed with 1 M NaHSO₄, the clear yellow filtrate (30 mL) was extracted with CH₂Cl₂ (5 \times 30 mL). The extracts were combined, dried over Na₂SO₄, filtered through Whatman paper, and concentrated under reduced pressure at 30 $^{\circ}$ C. The oily residue was dissolved in 8 mL of CH₂Cl₂, and the solution was slowly diluted by adding 200 mL of Et₂O. The precipitate was collected on a glass filter, washed with Et₂O (3 \times 10 mL), and dried. This Et₂O precipitation was repeated one more time to yield PEG-*o*-NB-diacrylate (539 mg) as a light-yellow solid. ¹H NMR (CDCl₃) δ 7.58 (s, CH_{aromat}), 7.00 (s, 1H, CH_{aromat}), 6.52 (m, CH), 6.45 (bs, NH), 6.44 (d, CH=CH_{trans}), 6.16 (dd, CH=CH₂), 5.87 (d, CH=CH_{cis}), 4.10 (t, CH₂CH₂CH₂O), 3.92 (s, OCH₃), 4.22–3.20 (CH₂CH₂O + OCH₂CH₂N), 2.39 (t, CH₂CO), 2.17 (m, CH₂CH₂CH₂), 1.65 (d, CH₃CH). The degree of functionalization using MW = 3400 was 80% by comparing the integral ratios of

the aromatic and CH₂CH₂O PEG protons. The ¹H NMR spectrum is shown in **Figure 4.1**. ¹H NMR spectra were measured on a Varian System 500 MHz spectrometer in deuterated chloroform (CDCl₃). A total of 32 scans was collected, and the D1 was set to 10 s. Chemical shifts (δ) are reported in ppm and are referenced against the residual CHCl₃ peak at 7.26 ppm.

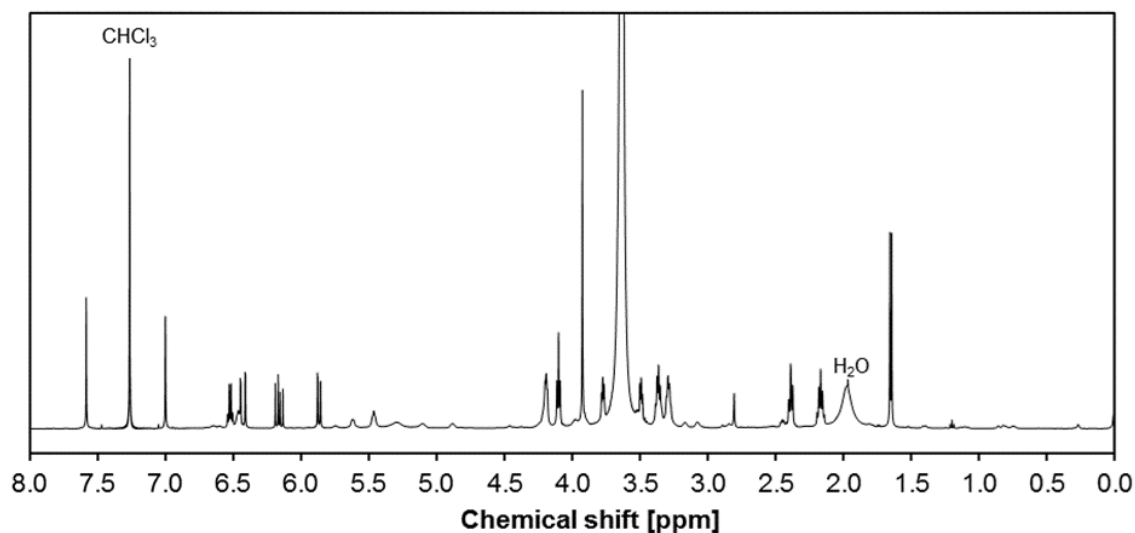


Figure 4.1. ¹H NMR spectrum of PEG-*o*-NB-diacrylate in CDCl₃.

4.3.3 Bacterial strains and culture conditions

All strains and plasmids used in this study are described in **Table 4.1**. Wildtype *A. tumefaciens* C58 (herein referred to as C58) was used for the live/ dead assay. *A. tumefaciens* C58 cells constitutively expressing the fluorescent protein GFPmut3 (herein referred to as C58-GFP) were used as controls in the hydrogel experiments. Populations of fluorescent *A. tumefaciens* C58-GFP *Himar1* mutant library cells (described below and herein referred to as C58 ML) were used in seeding, culture, and screening experiments within the hydrogels. *A. tumefaciens* strain NT1 was used as an agrocin 84 resistant control in the agrocin 84 bioassay. Unless noted otherwise, the

A. tumefaciens strains were grown on AT minimal medium¹⁸⁵ supplemented with 0.5% (w/v) glucose and 15 mM ammonium sulfate (ATGN). *Rhizobium rhizogenes* strain K84 (herein referred to as K84) bacterial cells were cultured in suspension at 28 °C (215 rpm) for 24–48 h to reach an OD₆₀₀ of 0.7 in ATGN media supplemented with kanamycin (150 µg/mL), spectinomycin (100 µg/mL), biotin (2 µg/mL), and iron as Fe (II) sulfate (0.022 mM). The optical densities of bacteria cultures (100 µL) at 600 nm (OD₆₀₀) were measured using an Epoch2 microplate reader (Biotek) in 96-well plates for all experiments. After K84 reached an OD₆₀₀ of 0.7, the bacterial culture was centrifuged at 2000 g for 10 min and the supernatant containing cell free culture fluid (CFCF) from K84 was sterile filtered two times, first with a 0.45 µm syringe filter and a second time with a 0.2 µm syringe filter, before being used in screening experiments.

Table 4.1. Strains and plasmid used in this study.

Strain/Plasmid	Relevant Features	Reference
<i>E. coli</i>		
S17-1/λ pFD1	Carries pFP1 (used as <i>Himar1</i> conjugal donor)	(¹⁸⁶)
<i>Agrobacterium tumefaciens</i>		
C58	Carries pTiC58 and pAtC58; Agrocin 84 sensitive	(¹⁸⁷)
C58-GFP	Carries pTiC58, pAtC58, and pJZ383; Agrocin 84 sensitive	(¹⁸⁸)
NT1	pTiC58- cured derivative of C58; Agrocin 84 resistant	(¹⁸⁷)
<i>Rhizobium rhizogenes</i>		
K84	Carries pAtK84b and pAgK84; produces agrocin 84	(¹⁸⁹)
Plasmids		
pFD1	<i>Himar1</i> transposon vector	(¹⁸⁶)
pJZ383	<i>Ptac::gfpmut3</i>	(¹⁹⁰)

4.3.4 Transposon mutagenesis

The mariner transposon *Himar1* was used to mutagenize C58-GFP cells using previously described methods.¹⁹¹ In brief, *E. coli* S17-1/ λ pir pFD1 and C58-GFP cells were mixed and incubated overnight at 28 °C on a 0.2 μ m polyethersulfone (PES) disk filter (PALL) placed on a LB plate. Following incubation, cells were collected and frozen at -80 °C in 25% glycerol.

4.3.5 Media for screening experiments

8 \times ATGN media was prepared as the undiluted base media. For unconditioned media, 8 \times ATGN was diluted to 1 \times with sterile ultrapure water and then supplemented with iron (0.022 mM), biotin (2 μ g/mL), kanamycin (150 μ g/mL), and spectinomycin (100 μ g/mL). For conditioned media, 8 \times ATGN was diluted with the CFCF acquired from K84 (Section 4.3.3) to get 1 \times ATGN that was subsequently supplemented with iron (0.022 mM), biotin (2 μ g/mL), kanamycin (150 μ g/mL), and spectinomycin (100 μ g/mL).

4.3.6 Thiol surface functionalization

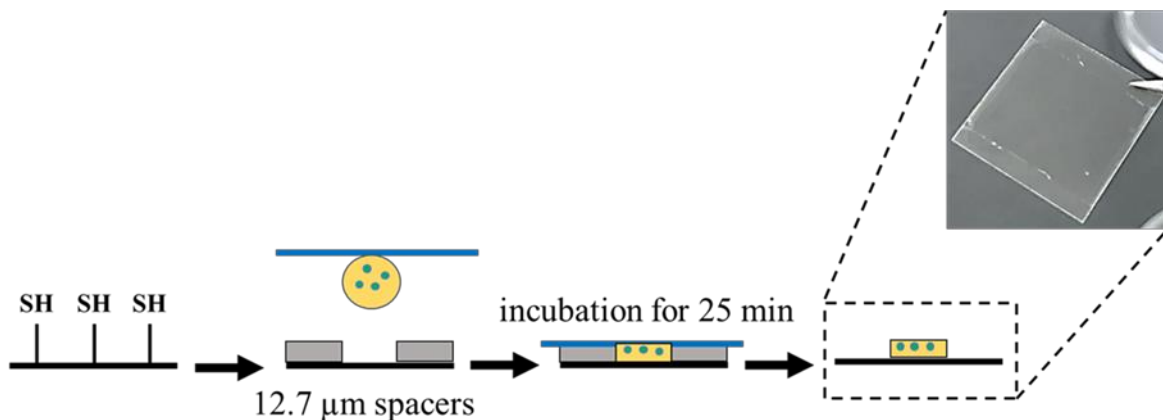
Thiol functionalized surfaces can be used as a route for secondary surface modifications through thiol–acrylate addition reactions¹⁹² and are used here to provide covalent attachment of the hydrogel to the coverslip surface. Glass coverslips (1.8 \times 1.8 cm) were cleaned with oxygen plasma for 3 min using a PDC-001-HGP Plasma Cleaner (Harrick Plasma). Coverslips were then cleaned and hydroxylated in Piranha solution, a 30:70 (v/v) mixture of H₂O₂ and H₂SO₄, at 60–80 °C for 30 min.¹⁹³ (Caution! Strongly corrosive.) Coverslips were then rinsed and stored in ultrapure water at room temperature. For functionalization with thiol groups, coverslips were then dried under a N₂ stream and immersed into a 269 mM (3-mercaptopropyl) trimethoxysilane (MPTS)

solution in dry toluene (5 v/v) for 4 h at room temperature. Substrates were then rinsed with toluene, ethanol/toluene (1:1), and ethanol, 4 times each.¹⁹³ They were then dried under a N₂ stream and stored at 4 °C for further use.

4.3.7 Hydrogel preparation and growth monitoring

All hydrogels were made in 1× ATGN phosphate buffer, pH 8. This was made by first adding NaH₂PO₄ to 2× ATGN and adjusting to pH 8 using 5 M NaOH (aq); the solution was then sterile filtered and stored at −20 °C until further use. Bacteria were encapsulated into the hydrogels by first inoculating 1 mL of 2× ATGN media with 2 μL of cells from the 25% glycerol stock stored frozen at −80 °C, for both the C58 ML and the C58-GFP control. This resulted in a C58 ML concentration of 3.63×10^7 CFU/mL in 1× ATGN media, pH 8. Then, a hydrogel precursor solution was prepared by adding photodegradable PEGDA (Mn 3400 Da, 8.4 μL, 49 mM) in water into 18.75 μL of the inoculated ATGN. Lastly, PEG-tetrathiol (Mn 10 000 Da, 10.35 μL, 20 mM) in water was added to the mixture, resulting in an equimolar acrylate–thiol ratio. The concentrations of acrylate and thiol groups in the final solution were each 22 mM. The final solution volume was 37.5 μL. The cell suspension was added to a thiol-functionalized coverslip (**Section 4.3.6**) to allow for covalent attachment of the hydrogel to the glass surface through thiol–acrylate addition (**Scheme 4.4**). First, 7 μL of the cell suspension was pipetted onto a chemically inert perfluoroalkylated glass slides, made as previously reported.¹³⁰ This coverslip was then contacted with the thiolated coverslip, separated by a fixed distance of 12.7 μm using Stainless Steel Thickness Gage Blades (Precision Brand). The solution was incubated for 25 min at room temperature to allow for cross-linking of the PEG polymers and hydrogel formation. After gelation, the thiolated glass slide and attached hydrogel were gently removed from the perfluoroalkylated glass slide. Care was taken during this step to prevent the hydrogel from

rupturing. With these conditions, it was noted that spacers thicker than 12.7 μm resulted in an overlay of cells, which was not desired because cell colonies above or beneath the target colony are also released during light exposure, which may result in cross-contamination during cell retrieval (**Figure 4.2**). For screening experiments, hydrogels were placed in 60 \times 15 mm Petri dishes and cultured in ATGN media or ATGN/CFCF media in an incubator at 28 $^{\circ}\text{C}$. For growth monitoring, cells were cultured in ATGN media at 28 $^{\circ}\text{C}$ in a live cell incubation chamber (Tokai Hit) placed over a Nikon Eclipse Ti-E inverted fluorescence microscope. Time lapse fluorescence images of the bacteria during growth into microcolonies within the hydrogel were taken with a 10 \times , NA 0.3 or 20 \times , NA 0.45 lens using NIS-Element software. Growth rates were quantified using Growthcurver software.¹⁹⁴



Scheme 4.4. Hydrogel preparation. Hydrogel precursor solution with seeded bacteria is placed on a glass slide which is then placed on a thiol functionalized coverslip with desired spacers for hydrogel formation and cell encapsulation.

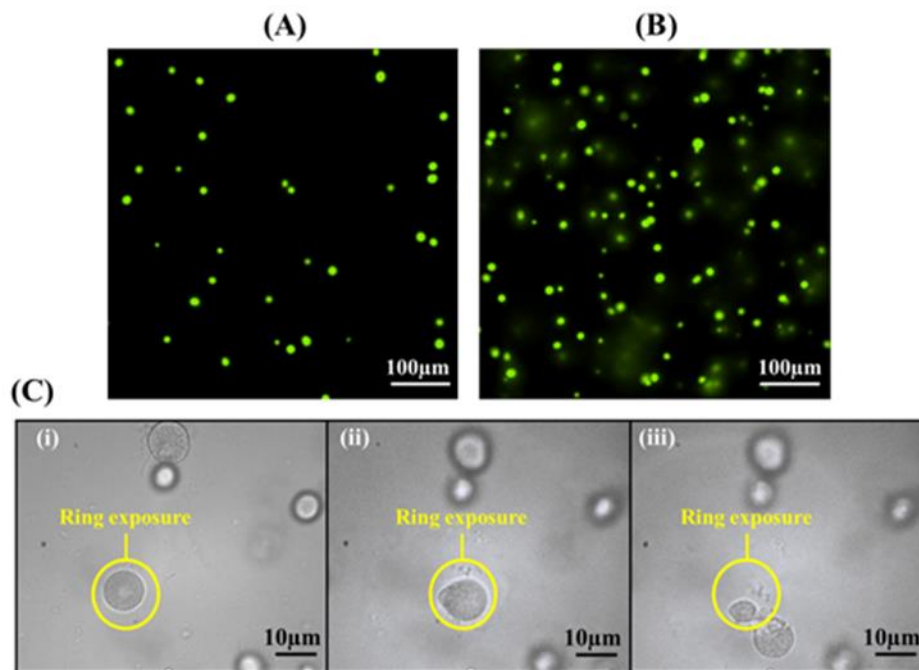


Figure 4.2. Optimization of hydrogel thickness. (A) Using 12.7 μm thick spacers results in formation of colonies in one focal plane. (B) Spacers with thickness greater than 12.7 μm show overlay of colonies within the three-dimensional hydrogel. (C) Overlay of colonies can result in cross-contamination during cell release: (i) ring pattern exposed on a desired cell colony, (ii) during light exposure a second colony is observed underneath the target colony, and (iii) cells from the non-target colony are also released causing cross contamination when colonies are overlaid.

4.3.8 Hydrogel degradation and cell release with the Polygon 400 light patterning device

Hydrogels were exposed to various patterns of UV light from a 365 nm LED light source using the Polygon 400 patterned illumination tool (Mightex Systems) configured to an Olympus BX51 upright microscope. The tool exposes 365 nm light at micron-scale resolution across a user-defined area for a given exposure time, enabling spatiotemporal control of hydrogel degradation (Figure 4.3). Intensity of the 365 nm irradiated light was controlled using Mightex PolyScan2 software and varied between 0.7 and 7 mW/mm^2 . Prior to hydrogel degradation, the tool was

calibrated to the specific objective using a mirror and the calibration software to obtain a clean and sharp pattern exposed on the mirror with the selected objective. Hydrogels were then placed in a PDMS holder and covered with ATGN media to prevent the hydrogel from dehydration (**Figure 4.4**). Targeted microcolonies were identified with the microscope and then focused on within the three-dimensional hydrogel. This focusing step was important to maintain a sharp UV exposure pattern over the targeted cells, as regions above and below the focused region of the hydrogel become exposed to out of focus UV light, causing the degradation pattern to become scattered in these regions. This is an inherent limitation of the upright microscope. Exposure occurred with a 10 \times , NA 0.3 or 20 \times , NA 0.5 objective. Brightfield images and movies were taken during photodegradation using Infinity Capture Software.

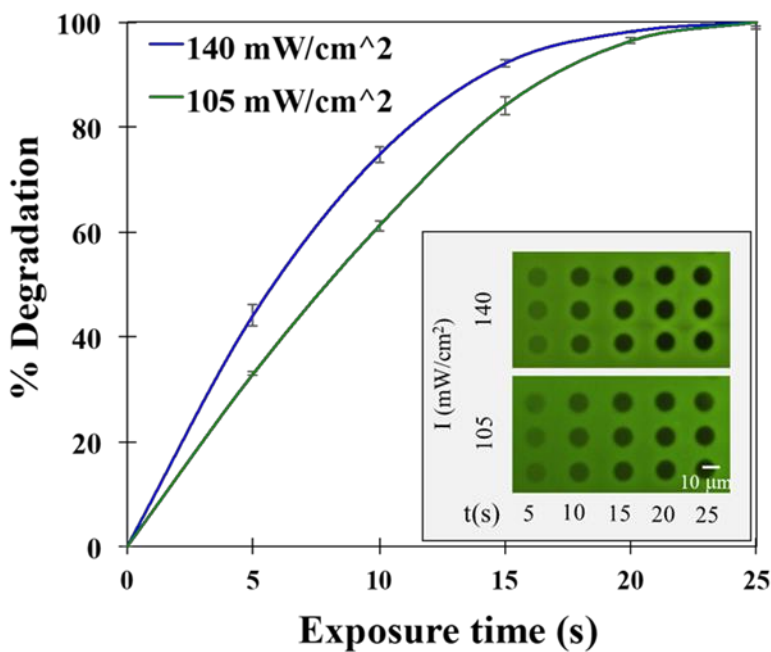


Figure 4.3. Spatial temporal control of hydrogel degradation. The Polygon400 light patterning tool allows for adjustment of UV light intensity and exposure time across a user-defined pattern enabling control of hydrogel degradation. Inset: representative fluorescent images of patterns degraded with two different light intensity and various exposure times. Hydrogels were stained with fluorescein-5-maleimide after UV irradiation for visualization.

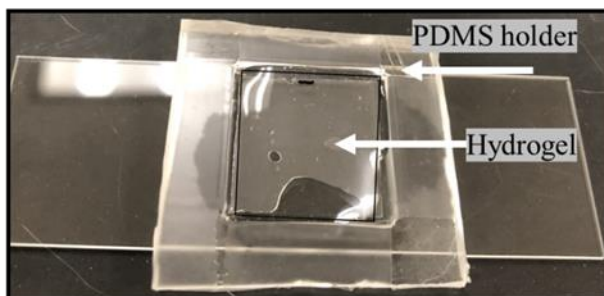


Figure 4.4 Setup used for UV light exposure and cell retrieval. During light exposure for cell release, the hydrogel is placed in a PDMS holder and covered with media to prevent dehydration.

4.3.9 Labeling the hydrogel with fluorescent dye

Fluorescence microscopy was used to image the hydrogel after UV light exposure and degradation by labeling with fluorescein-5-maleimide, which couples to pendant thiol groups within the hydrogel.¹⁹⁵ 4 μ L of a 10 mM stock solution of fluorescein maleimide in DMF was added to 1 mL of PBS buffer (pH 7.3) and then added to the hydrogel for 2 h at room temperature in a dark environment. The hydrogel was then rinsed with 1 \times PBS to remove unbound fluorophores and imaged.

4.3.10 Live/Dead assay

To investigate cell viability after exposure of microcolonies to UV light, a live/dead assay was used. Here, C58 cells were encapsulated in hydrogels containing non-photodegradable PEGDA (Mn = 3400 Da) instead of PEG-*o*-NB-diacrylate; thus, colonies remained within the hydrogel after UV exposure for staining and imaging. The stain mixture was prepared as recommended by the manufacturer. 300 μ L of the mixture was added over each hydrogel and incubated in the dark for 15 min. SYTO 9 labels both intact and compromised cells, while

propidium iodide labels only cells with damaged membranes, resulting in the reduction of expressed fluorescence by SYTO 9.¹⁹⁶ After staining, the hydrogels were washed thoroughly with a 0.85 wt % NaCl solution and imaged using the inverted fluorescence microscope. The percentage of live cells (p) was estimated from the fluorescence intensity data according to eq 1:

$$p = 100 - \left(\frac{r_{UV} - r}{r_{dead} - r} \right) \times 100 \quad (1)$$

Where r_{UV} is the measured red signal following UV exposure, r is the red signal measured when the hydrogel is not exposed to UV, and r_{dead} is the red signal of the dead cell control. For this control, cells were killed by incubating the hydrogel in 70% isopropanol at room temperature for 20 min. The hydrogel was then washed with ultrapure water before staining.

4.3.11 Cell retrieval and recovery

Immediately after light exposure, the free end of a 20 cm long PTFE tubing, 0.05 in. ID, was placed over the irradiated spot. The other end was attached to a 100 μ L syringe that was used three times to aspirate the media containing the released cells. For every exposed microcolony, 300 μ L of solution was collected and transferred into an Eppendorf tube. For each sequential microcolony extracted, the syringe, tubing, PDMS holder, and the hydrogel were washed with ultrapure water at least 3 times to minimize cross-contamination. Following cell retrieval, 300 μ L of the bacterial solution was plated onto selective media for recovery. The plating process was also expected to dilute PEG degradation biproducts. 100 μ L of the solution was plated on ATGN supplemented with kanamycin and spectinomycin. Cells from the mutant library are expected to be resistant to both antibiotics. In contrast, C58-GFP, the parental strain used to generate the mutant library, is resistant only to spectinomycin. The presence of both antibiotics allowed for the

recovery of mutants, decreasing the chance of contamination from other sources. After inoculation, the plates were incubated at 28 °C for 3 to 5 days.

4.3.12 Agrocin 84 bioassay

Agrocin 84 bioassays were performed to determine if recovered mutants are resistant to agrocin 84, a bacteriocin produced by K84 that strongly antagonizes C58. The bioassay protocols were adapted from those reported by Hayman *et al.*^{197,198} K84 and recovered C58 ML mutants (**Section 4.3.11**) were grown in liquid ATGN as previously described for 24 h. All cultures were normalized to an OD₆₀₀ of 0.6 in ATGN media. Tubes containing 10 mL of molten agar (65 °C) were inoculated with 35 µL of the C58 mutant cultures. The tubes were vortexed vigorously for 10 s and then poured onto sterile 60 × 15 mm Petri dishes. Once the agar solidified, 7.5 µL of the K84 cells (OD₆₀₀ = 0.6) was spotted in the center of the plate and allowed to air-dry. Once the K84 cells had dried completely, the plates were wrapped with a plastic wrap to prevent drying of the media, and they were incubated at 28 °C for 72 to 120 h.

4.3.13 Genomic DNA Purification

QIAGEN's DNeasy Blood & Tissue Kit was used to purify bacterial genomic DNA from cellular debris and any residual PEG byproduct. The manufacturer's protocol, including the Gram-negative bacteria pretreatment, was followed with minor modifications. Proteinase K incubation was performed for 60 min at 56 °C, and 4 µL of RNase A (100 mg/mL) was added following proteinase K incubation. Lastly, two sequential elution steps via centrifugation were included: the first elution used 150 µL of Buffer AE while 50 µL of Buffer AE was used for the second elution. Genomic DNA samples were stored at -20 °C.

4.3.14 Whole genome sequencing

Genomic DNA samples were sent to the Microbial Genomic Sequencing Center (MiGS) in Pittsburgh, PA. Samples were received and immediately frozen until the library preparation began. Qubit fluorometric quantification was used to quantify DNA concentrations. All samples were normalized to the same concentration and enzymatically fragmented using an Illumina tagmentation enzyme. Unique indices were attached to each pool of fragmented genomic DNA using PCR, and the resulting barcoded pools were combined to multiplex on an Illumina NextSeq 550 flow cell.

4.3.15 Sequence Analysis

Bioinformatic analyses were performed on Beocat, the High-Performance Computing cluster at Kansas State University. Once sequencing reads were acquired from the MiGS, read mapping was performed by aligning the reads to the C58 reference genome using the Burrows-Wheeler Aligner's SmithWaterman Alignment (BWA-SW) algorithm.¹⁹⁹ The BWA-SW algorithm aligns long sequences (up to 1 Mb) against a large reference genome in a fast and accurate manner. A variant calling applying the Genome Analysis Toolkit (GATK) was then applied. GATK is a pipeline that compares the alignment of our reads to the C58 genome at a more detailed level while simultaneously performing a base quality score recalibration, indel realignment, duplicate removal, and SNP and INDEL discovery.²⁰⁰ Additionally, the GATK pipeline applies standard hard filtering parameters or variant quality score recalibration that result in the identification of mutations with high confidence. The purpose of the read mapping and variant calling is to find the mutation responsible for agrocin 84 resistance. Once the mapped reads and the variants were generated, regions with mutations were identified.

4.4 Results and discussion

4.4.1 High density cell encapsulation and parallel tracking of cell growth

The first step in developing the hydrogel interface involved achieving high-density encapsulation of viable bacteria cells within the hydrogel for growth monitoring. C58 ML cells were seeded across a 1.8×1.8 cm glass coated with a hydrogel, initially $12.7 \mu\text{m}$ thick, that reached $140 \mu\text{m}$ in its swollen state after incubation. Given the genome size of *A. tumefaciens* C58 (approximately 5.67 Mbps),²⁰¹ the observation of 28,000 mutants within a single hydrogel was desired to ensure that the genome could be screened to saturation with 99% certainty.²⁰² Using fluorescence microscopy, it was found that seeding bacteria at a concentration of 3.63×10^7 CFU/mL encapsulated bacteria at a density of 90 CFU/ mm^2 , meeting this requirement.

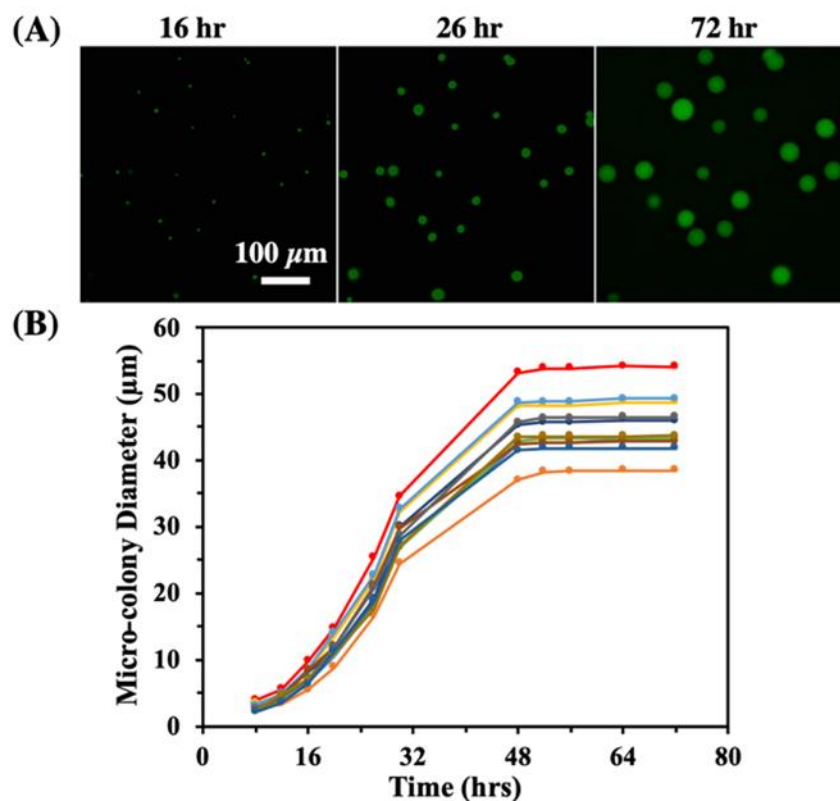


Figure 4.5 Parallel growth monitoring of individual C58 cells into microcolonies within the hydrogel matrix after seeding. (A) Representative fluorescent images of C58 ML microcolonies at different time points. (B) Microcolony growth for 11 sample microcolonies within the hydrogel as a function of time.

As shown in **Figure 4.5A**, after encapsulation, cells appeared randomly dispersed and the vertical overlap of cells was minimal, which was desired to prevent the extraction of multiple colonies during the light exposure step. Hydrogel thicknesses greater than 12.7 μm resulted in the vertical overlap of cells (**Figure 4.2B**). After encapsulation, parallel growth tracking of individual cells into microcolonies during culture in ATGN media was achieved. Microcolonies become visible under 20× magnification, 8 h after encapsulation. They then grow ($k = 0.18 \text{ h}^{-1}$) in diameter for approximately 40 h (**Figure 4.5B**). These observations suggest that there was sufficient mass transfer to support cell growth. Hydrogel mesh size (ξ), a critical determinant of mass transfer

within the hydrogel,²⁰³ was calculated to be 10 nm on the basis of the equation described by Canal and Peppas,²⁰⁴ small enough for the immobilization of bacteria cells but large enough for the diffusive exchange of nutrients (e.g., glucose) and waste products. Similar growth trajectories were observed when monitoring the growth of free cells in a 96-well plater reader (**Figure 4.6**), suggesting that cell confinement or diffusion limitations had a minimal effect on growth within the hydrogel environment. Cells developed into spherical microcolonies due to deformation of the elastic PEG matrix caused by the local increase in cell numbers and through chemical or enzymatic modes of hydrogel degradation.²⁰⁵ These measurements were performed several times (n = 26) with 92% of the trials resulting in microcolony growth. At later time points (~5 days), bacteria were observed to escape hydrogel encapsulation (**Figure 4.7A**). While chemical hydrolysis of thioether–ester linkages may play a role in hydrogel degradation,²⁰⁶ follow-up studies have indicated that hydrogels remain capable of immobilizing inert, 1 μm fluorescent beads at neutral pH over 5 days (**Figure 4.7B,C**). Others have also reported minimal mass loss in similar thiol–acrylate PEG hydrogels over a 5-day time period at neutral pH.⁹⁴ These observations suggest that bacteria within the microcolonies were the cause of the eventual breakdown of the hydrogel matrix.

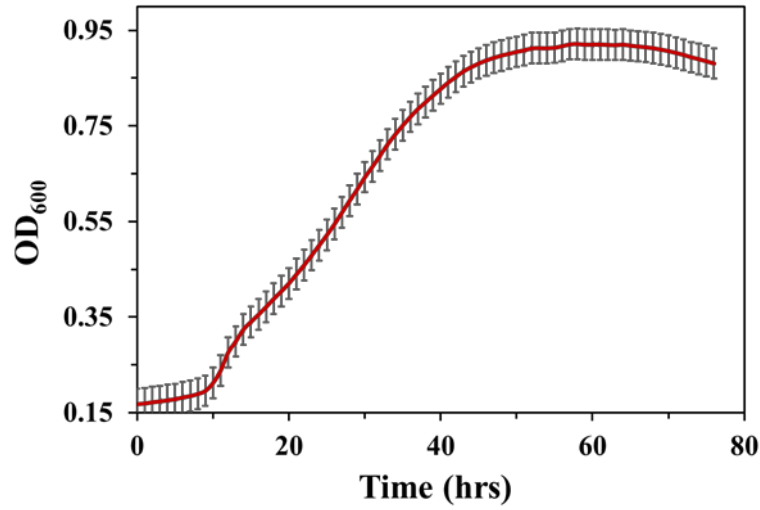


Figure 4.6. Growth curve of C58 ML during culture in ATGN media at 28°C and 282 rpm in 96 well plate format (n = 19).

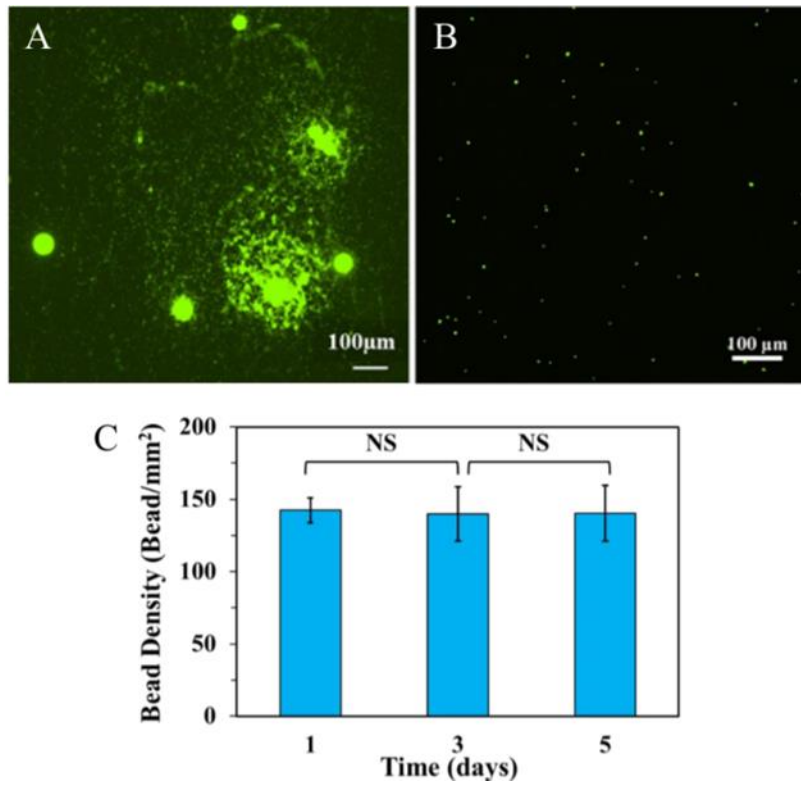


Figure 4.7. Hydrogel degradation by bacteria: Entrapped cells within the hydrogel are able to degrade the hydrogel and are released after 5 days incubation in ATGN media.

4.4.2 Characterization of cell release and cell viability

Using light for extraction has the advantage of spatiotemporal control of cell release, as the patterned illumination tool allows for projection of user-defined, two-dimensional patterns over any microcolony within the hydrogel. Here, the arrangement of cells released into solution after exposure with different patterns was investigated. Microscale patterns including lines, rings that outline the microcolony perimeter, a cross, or a broken cross pattern were investigated. Patterns with greater coverage of the colony such as circles were avoided to minimize unnecessary UV light exposure in an effort to preserve bacteria viability and DNA quality. The recovered cells present in the extract solution were then imaged in brightfield and fluorescence modes to examine the cell arrangement (**Figure 4.8**). Light patterning offered control of the arrangement for cells liberated from the hydrogel interface. Ring patterns degraded the hydrogel immediately surrounding the microcolony, forming a hydrogel island that immediately detached from the interface. Examination of the extract solution revealed that cells remained encapsulated as microcolonies in the detached hydrogel (**Figure 4.8Aiii**). This pattern offers the advantage that extracted cells are not directly exposed to UV light and that they remain preserved in a larger, protective PEG layer, being potentially useful for downstream separation or processing steps. Cross patterns instead appeared to liberate cells as either aggregates or free cells (**Figure 4.8Biii, Ciii**), as these exposure patterns etched a direct path for cellular transport out of the hydrogel. Here, it was noted that the entire cell mass was liberated into the media covering the hydrogel as the membrane became compromised (**Figure 4.9**). Inspection of the recovered cells in the extract solution revealed that broken cross patterns favored aggregated cells, whereas cross patterns contained extract solutions dominated by free cells. Other patterns, such as individual lines

patterned at the microcolony edge, also caused a burst of free cells into solution; however, some of the cells appeared to remain in the hydrogel after exposure (**Figure 4.9**). Because removal of a maximum number of target cells with a minimum direct exposure to UV light was desired, the broken cross pattern was selected for further use.

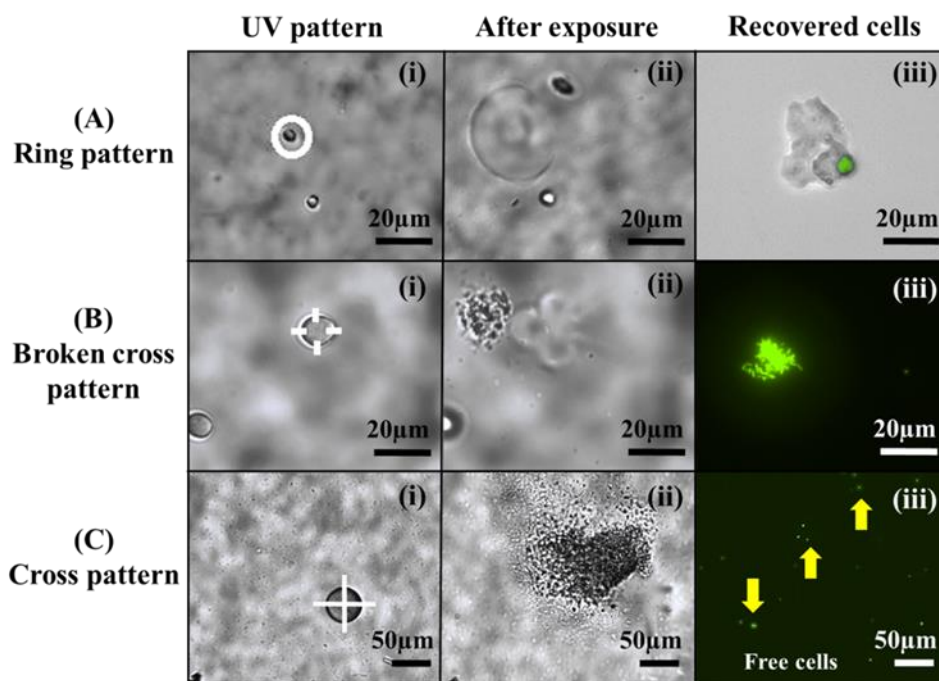


Figure 4.8. C58 ML cell arrangement after release with different light patterns. (A) Ring pattern for extraction of colonies protected within a PEG layer. (B) Broken cross pattern for extraction of aggregated cells. (C) Cross pattern for extraction of predominantly free cells. For each exposure pattern the following are shown: (i) the projected light pattern (white line) over a targeted colony, (ii) the hydrogel immediately after cell release, and (iii) brightfield and/or fluorescent images of the recovered cells in solution. Patterns were exposed at an intensity of 4.2 mW/mm^2 .

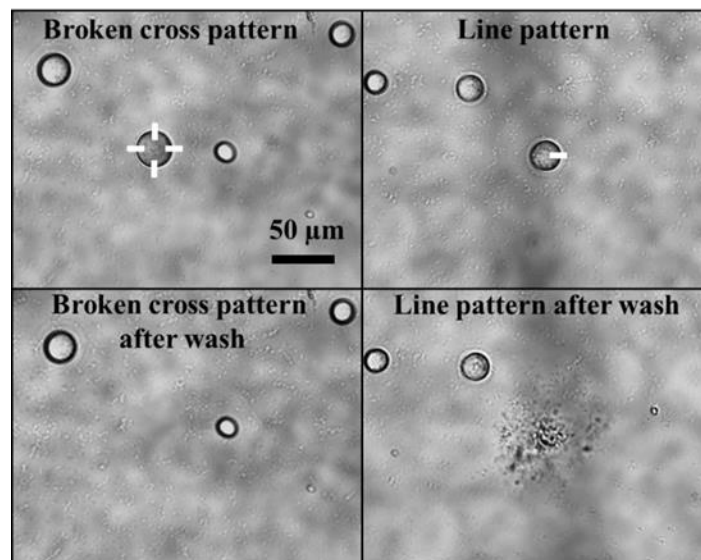


Figure 4.9. The efficiency of a line pattern exposure for cell release compared to a broken cross exposure pattern. Use of a broken cross pattern results in complete release of the microcolony, whereas use of a line exposure pattern results in only partial release of the microcolony.

After establishing that using broken cross pattern exposure results in lift off of the entire cell mass, we investigated how varied light intensities affected release time, defined here as the exposure time until microcolony burst is observed (**Figure 4.10A**). Step growth hydrogels are characterized by rapid erosion rates due to the low levels of network connectivity;²⁴ here, degradation and cell release were noted in <180 s for all exposure intensities studied. Cell release time showed significant decreases with increasing light intensity up to an intensity of 4.2 mW/mm^2 ($p < 0.05$), this trend was expected as exposure time required for reverse gelation of the hydrogel is inversely proportional to light intensity.²⁴ Beyond this, only minor decreases in release time were noted and a minimum light dose for release was found at $168 \pm 14 \text{ mJ/mm}^2$, corresponding to an intensity of 4.2 mW/mm^2 . Since 365 nm light can be cytotoxic to bacteria through the generation of reactive oxygen species,⁴⁶ the effect of broken cross pattern exposure (4.2 mW/mm^2 , 40 s) on cell viability was characterized using a live/dead assay (**Figure 4.10B, C**). Here, C58 cells

were first seeded within a hydrogel generated with PEG diacrylate without the photocleavable *o*-NB moiety and cultured into microcolonies, and the colonies were then exposed to broken cross patterns of light. Removal of the *o*-NB group from the network backbone ensured that the microcolonies would remain in place during exposure so they could be subsequently stained and observed with fluorescence microscopy. The comparison of red signal indicating nonviable cells showed no significant difference between unexposed and exposed cells, both of which were significantly less than the dead cell control ($P < 0.01$). This suggests that the majority of cells remain viable during the extraction step for recovery and genomic analysis. Given these findings, these exposure conditions were used in the remaining studies.

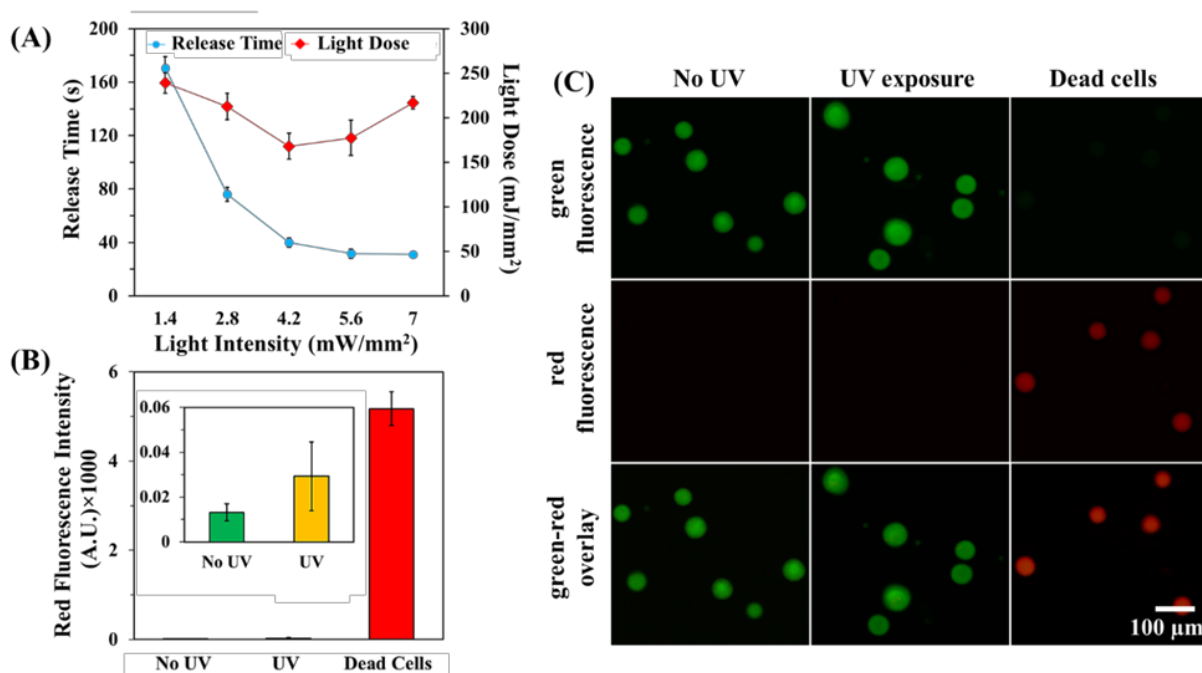


Figure 4.10. (A) Microcolony release time from hydrogels at varied 365 nm light intensity. An entire cell mass lift off effect was noted during broken cross pattern exposure, providing a discrete time point for cell release. (B) Red fluorescence signal after staining with the reagents in the live/dead bacterial viability kit. Microcolonies without UV exposure, with broken cross pattern UV exposure (4.2 mW/mm², 40 s), and from chemically treated (70% isopropanol) dead cells are compared. (C) Representative green-red fluorescent images of microcolonies after staining with live/dead assay. Dead cells with compromised membranes appeared red. ImageJ software was used

to adjust images for color contrast. For each treatment ($n = 3$ independent trials), 30 different microcolonies were imaged.

4.4.3 Sequential extraction and recovery of individual microcolonies

Isolation of bacteria for pure cultures is one of the most important requirements in microbiological techniques because it enables extraction of pure genetic material, allows for follow-up biological and biochemical testing, and eliminates confounding observations that can arise from other bacteria. Here, the ability to generate pure cultures exclusively from the bacteria targeted for extraction was evaluated. Hydrogels were first seeded and cultured for microcolony development and placed inside a PDMS holder (**Figure 4.4**).

Designated areas of the hydrogel were exposed to UV light and then immediately washed with wash buffer to remove the released cells. Wash solutions were plated on selective media to quantify colony forming units (CFU/mL) in each wash solution. To verify the presence or absence of contaminating bacteria in the media prior to extraction, hydrogels were initially washed prior to light exposure. Additionally, as a negative control, areas of the hydrogel where no colonies were present were exposed to UV light under the same conditions used for cell release. This was done before and after every microcolony extraction, and washes from these blank areas were processed and plated in an identical manner as those solutions containing an extracted microcolony. In this way, carryover and cross-contamination during subsequent microcolony extraction could be identified. Using this approach, the purity of four sequentially extracted microcolonies was accessed (**Figure 4.11**). The initial washings of the hydrogels and negative controls generated from the opening of the hydrogel in areas lacking colonies showed little or no recovery after plating (**Figure 4.11B**). Conversely, solutions extracted from selected microcolonies showed significant

growth after plating, with average measurements ranging from 90 ± 28 CFU/mL (MC1) to 260 ± 98 CFU/mL (MC4). The number of cells (CFU/mL) in the wash buffer after microcolony extraction showed no significant association with microcolony size (**Figure 4.12**). A small amount of carryover (<5 CFU/mL) was noted in blank solutions after the first microcolony extraction, suggesting that cross-contamination from a previously opened microcolony is a possibility during sequential extraction; however, these levels were minimal, representing $<1\%$ of cells recovered from a typical microcolony. These observations demonstrate that the extraction method allows for targeted and clean recovery of bacteria colonies, enabling one to sample and isolate multiple colonies from a single screen, if desired.

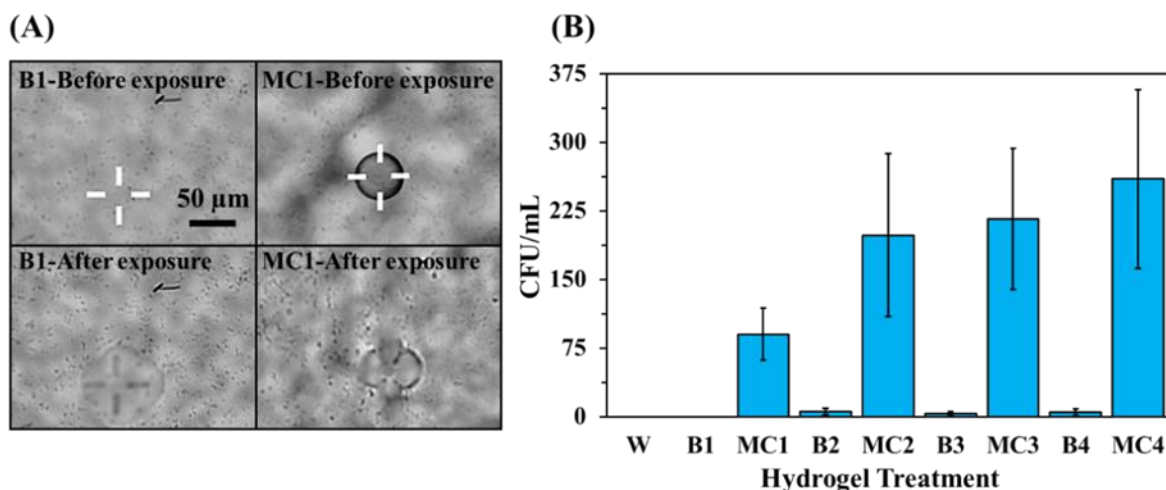


Figure 4.11. Sequential extraction of targeted microcolonies from a hydrogel. (A) Brightfield image of a hydrogel with a sample exposure map (white lines) showing exposure locations targeting a blank area or a microcolony with a broken cross pattern. (B) Colony forming units (CFU/mL) of recovered suspensions after washing the hydrogel at various steps and plating. W = initial wash of the hydrogel; B = hydrogel blank; MC = microcolony. All exposures, wash steps, and plating steps onto selective media were performed under identical conditions ($n = 3$ independent trials).

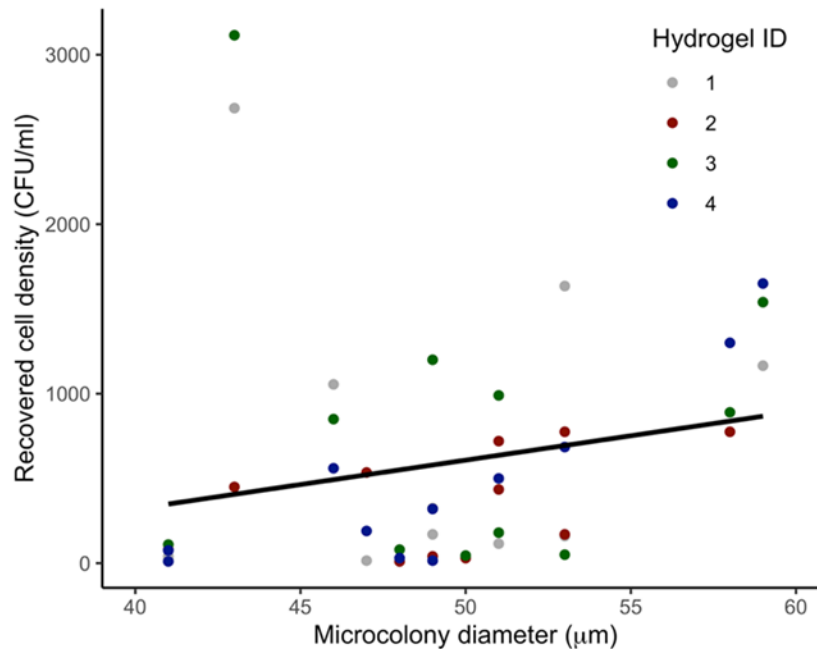


Figure 4.12. The density of recovered cells was not significantly associated with microcolony diameter ($F_{1,42} = 2.03$, $p = 0.16$, adjusted $r^2 = 0.16$; $\beta = 28.78$, $t = 1.42$, $p = 0.16$).

4.4.4 Screening and identification of rare phenotypes from transposon mutant libraries

Following the characterizations in **Sections 4.4.1-4.4.3**, the photodegradable hydrogels were evaluated for use in a model ML screening application. The screen involved seeding and culturing C58 ML cells in media supplemented with cell free culture fluid (CFCF) from K84, which contains agrocin 84, a well-known bacteriocin with activity against C58.^{183,185} During this screen, three separate hydrogels were prepared from the same hydrogel precursor solution. This included a positive control where C58 ML cells were incubated in liquid ATGN as in (**Section 4.4.1**) to ensure normal cell growth across the population (**Figure 4.13Ai**). This control also allowed for verification that seeding density remained consistent with previous experiments

(approximately 90 CFU/mm²). To quantify the total number of bacteria cells that were screened in any trial, 10 separate areas on the positive control hydrogels were imaged. As a negative control, C58-GFP was also cultured in ATGN/CFCF, where no growth was expected (**Figure 4.13Aiii**), verifying that an inhibitory environment for normal cell growth was present. With these two controls in place, mutants within the seeded ML population that were able to grow in the presence of ATGN/CFCF were identified as candidate agrocin 84 resistant mutants (**Figure 4.13Aii**). Once each cell population was encapsulated in the respective hydrogels, they were immersed in ATGN or ATGN/CFCF media, incubated, and then imaged using fluorescence microscopy. ML cells seeded in positive control hydrogels consistently grew into fluorescent microcolonies (**Figure 4.13Bi**) at 28 °C within 24 h, as expected. C58 ML cells in the positive control were quantified at a density of 90 cells/mm², indicating that approximately 28,000 cells were present within the hydrogel. Test hydrogels were immersed in ATGN/CFCF solution for 72 h; fresh media were added to this solution every 24 h. After 72 h, the media was changed to ATGN only and incubated for an additional 48 h to enable the surviving, agrocin-resistant mutants to fully develop inside the hydrogels (**Figure 4.13Bii**). Resistant mutants appeared at a density of 0.057 microcolonies/mm² (18 ± 7 resistant mutants per hydrogel). The negative control hydrogel treated the same way as the test hydrogels, rarely produced microcolonies (<0.0011 microcolonies/mm²), verifying that parental C58-GFP cells very rarely survived when K84 CFCF was present. At the conclusion of the screen, the total number of rare microcolonies in a representative test hydrogel was 25, representing 0.089% of the cell population. Each rare colony was extracted from this hydrogel, plated, and recovered for genomic analysis; 23/25 microcolonies were successfully recovered.

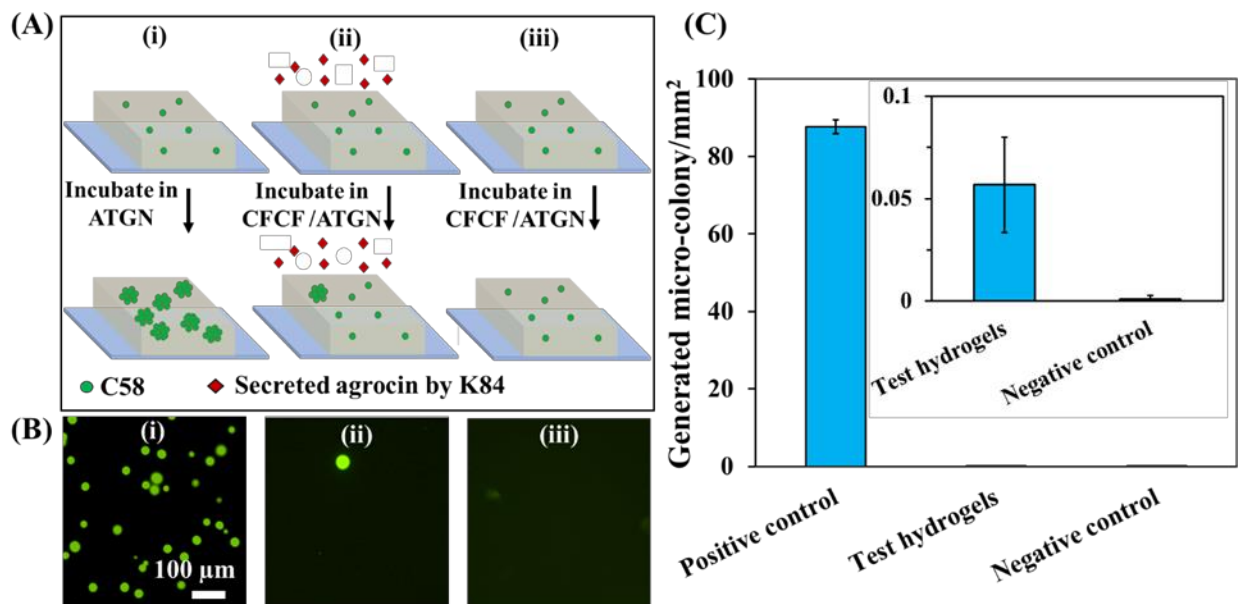


Figure 4.13. (A) Schematic of the ML screen: (i) positive control: growth of C58 ML cells within the hydrogel, (ii) hydrogel incubation in presence of CFCE/ATGN for growth of agrocin resistant C58 ML cells, (iii) negative control: C58-GFP incubated in CFCE/ATGN under identical conditions. (B) Representative fluorescent images of the fluorescent micro-colonies in (i) positive control, (ii) test hydrogels, and (iii) negative control. (C) Representative data for generated micro-colonies in each treatment ($n = 3$ independent trials).

4.4.5 Follow-up phenotypic and genotypic analysis of rare cells

Following cell retrieval and recovery, colonies were again streaked onto media containing kanamycin and spectinomycin. To corroborate phenotypic observations in the hydrogel with standard microbiological approaches, the agrocin 84 bioassay was performed as described in **Section 4.3.12**.^{197,198} For every extracted microcolony, a random subset ($n = 5$) of recovered colonies that showed resistance to the antibiotics, as well as a set of controls for every isolated mutant (**Figure 4.14A**), was tested for agrocin 84 resistance. The coculture of C58 with K84 was included as an agrocin 84 sensitive control for which we expected a zone of inhibition (a region near K84 with no bacterial growth due to inhibition) to form. Additionally, the coculture of *A.*

tumefaciens NT1 with K84, a bacterial strain that is known to be resistant to agrocin 84, was used to compare the degree of resistance/susceptibility of the hydrogel isolates. The agrocin 84 bioassay verified successful recovery of 9 resistant mutants. Four of these resistant mutants came from two recovered microcolonies, and we failed to recover resistant mutants from 16 of the 23 recovered microcolonies. These observations validate the agrocin 84 resistant phenotype observed in the hydrogel screen and also demonstrate that results observed in the screen can be corroborated using follow-up tests due to the ability to extract, isolate, and grow colonies of interest from the screening interface.

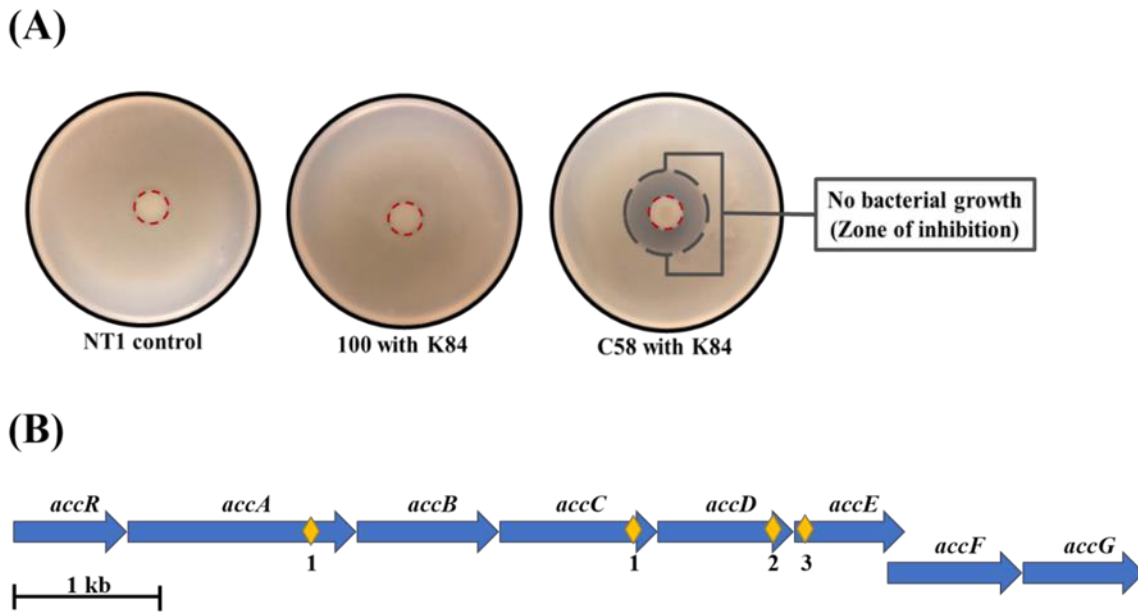


Figure 4.14. (A) Observations of the agrocin 84 bioassay. As expected, NT1 shows no inhibition when co-cultured with K84, and was used as the positive control. The isolated C58 mutant (herein referred to as 100) also shows no inhibition when co-cultured with K84, similar to NT1, while C58 bacteria show a clearing (zone of inhibition) surrounding the K84 at the plate center. K84 bacterial growth is contained inside the red dashed line. The boundary of the zone of inhibition, if present, is denoted by the gray dash line. (B) Most agrocin 84 resistant mutants carry mutations in the *acc* operon. The location of the *acc* operon mutations found in seven of the nine isolated mutants is represented with yellow diamonds, with numbers below indicating how many times a mutation in this position was observed. All *acc* mutants were recovered from different agrocin 84 resistant

microcolonies. Mutants with identical mutations were recovered from different hydrogels and so cannot be the result of cross-contamination during recovery. Each gene is shown as an arrow, and they all have been drawn to scale.

The final step was to connect the observed phenotype with a genotype of the extracted isolates using whole genome sequencing. Previous work identified that the *acc* operon of the Ti plasmid in C58 encodes for the utilization of agrocinopines A and B and for susceptibility to agrocin 84 with mutations in this region resulting in agrocin 84 resistant phenotypes.^{183,207,208} This gave a clear expectation for the location of genotypic mutations that should be present in the mutants isolated from the hydrogels. Whole genome sequence analysis showed that 78% (7/9) of the isolated mutants that were sequenced from the screen had mutations in genes within the *acc* locus (**Figure 4.14B**). About 20% of the isolated mutants (2/9) lacked a mutation in the *acc* locus; however, they had mutations in other membrane transporter genes. It has been previously shown that inhibitors like agrocin 84 can enter bacterial cells through these transporters; however, more research is required to determine the genetic basis of agrocin 84 resistance in these mutant strains. Taken together, our observations verify that successful genotype-to-phenotype determinations can be made from rare mutants isolated from the hydrogel screen.

4.5 Conclusion

Photodegradable hydrogels have been widely studied as matrices for biological applications due to their biocompatibility, tunable chemical and physical properties, and crosslinking abilities. These materials offer a unique set of advantages for cell screening applications: viable, high density cell encapsulation and monitoring, molecular exchange for cell growth and function, and spatiotemporal control of matrix degradation for cell release and retrieval

when a patterned light source is used. While these materials have been developed extensively toward drug delivery and tissue engineering applications and have been successfully used for capture and on-demand release of rare circulating tumor cells,¹²⁷ they have largely remained separate from application in microbiology. Here, we demonstrate the use of photodegradable hydrogels for high-throughput screening of bacterial populations. To our knowledge, this is also the first successful use of photodegradable hydrogel materials in a bacterial cell screening application. The novelty of the approach lies in the combination of high-density culture, allowing for parallel, microscopic observation of tens of thousands of cellular microcolonies, followed by sequential sampling of any desired microcolony at high resolution and with high purity, enabling follow-up genetic characterization of a rare or desired phenotype.

Given the pervasive knowledge gap between bacteria phenotype and genotype, we anticipate that this simple, materials-driven approach to screening and isolation will benefit a variety of different screens. The proof-of-principle for ML screening demonstrated here with a simple growth/no growth phenotype lays the foundation for more complex phenotypic screens, such as using fluorescence or colorimetric reporters to screen for mutations disrupting gene regulation,⁶³ or growth-based screening of auxotrophic mutants that have loss of enzymatic function leading to metabolic deficiencies.²⁰⁹ Using traditional approaches, these screens typically require observations of tens of thousands of macroscopic colonies in hundreds of agar or agarose plates. This throughput can be matched with a single photodegradable hydrogel when combined with a high-throughput image analysis tool to rapidly identify rare cellular phenotypes.¹⁸⁷ The high-throughput nature of our approach along with its repeatability and fast turnaround time also make this approach applicable to other cell separations in microbiomes, clinical samples, and mammalian cell lines.

4.6 Acknowledgements

This research was supported by the National Science Foundation (Award 1650187). N.F. would like to acknowledge the National Science Foundation Research Trainee Innovations in Food, Energy, and Water Systems (NRT-INFEWS) program (Award 1828571) and support from the Dr. Larry Erickson Fellowship Award (Kansas State University). P.A.N.- O. would like to acknowledge support from the National Science Foundation Graduate Research Fellowship (Award GGVP004842). We would like to thank Christopher Carter for help with the agrocin 84 bioassays. We also thank the Kansas IDeA Networks of Biomedical Research Excellence (KINBRE) Bioinformatics Core (P20GM103418) for help with using scripts used in the bioinformatic analyses. The computing for this project was performed on the Beocat Research Cluster at Kansas State University, which is funded in part by NSF grants CNS-1006860, EPS-1006860, EPS0919443, ACI-1440548, CHE-1726332, and NIH P20GM113109.

Chapter 5 - Polyethylene glycol-based Hydrogel Coating for Improved Performance of Microbial Electrochemical Cells

5.1 Overview

In bioelectrochemical systems, anode-bound electroactive biofilms play a crucial role in energy production. Electroactive bacteria in the anode biofilm are sensitive to environmental stressors, compromising their viability and metabolic activity in the long term. In this paper, we develop a polyethylene glycol (PEG) - based hydrogel over anode biofilms to serve as a protective barrier against environmental stressors while allowing for exchange of nutrients required for biofilm function. The PEG-based hydrogel utilized here is a crosslinked network of PEG-tetrathiol and PEG-divinyl sulfone macromers. Hydrolytic stability due to the presence of stable thioether sulfone bonds within the hydrogel provided long term (72 days) hydrolytic stability over a range of pH values (3 to 10). Finite element modeling was used to predict the concentration of the carbon source (acetate) throughout the hydrogel layer and at the hydrogel-biofilm interface at different coating thicknesses. Based on the model, coating thicknesses of 700-800 μm ensured sufficient acetate concentration at the hydrogel-biofilm interface to sustain biofilm function. Long-term, simultaneous monitoring of coated and uncoated electrodes experimentally confirmed that the coating did not significantly compromise the biofilm activity. Finally, an ammonia spike was used to evaluate the coating's potential for biofilm protection under harsh conditions. It was observed that the coating provided a sponge for the ammonia, inhibiting its diffusion to the biofilm to decrease its negative impact. Furthermore, after changing the condition back to a standard media, ammonia entrapped in the coating increased the buffering capacity of the media, which improved the metabolic activity of the biofilm, until the $\text{NH}_4\text{-N}$ was eventually released from the coating.

KEYWORDS: Anode biofilm, immobilization, protective coating, bioelectrochemical systems

5.2 Introduction

There is a widespread effort to find alternative energy sources that are environmentally friendly and more sustainable than fossil fuels.²¹⁰ Amongst different sources of green energy, bioelectrochemical systems (BESs) have obtained recent attention as an energy source useful for low-power applications. BESs utilize microorganisms to generate power by producing bioelectricity through direct biomass conversion. Biomass, unlike fossil fuels, is renewable and includes a wide spectrum of organics from woody biomass to waste materials.²¹¹ This energy can be utilized in several applications. Wastewater treatment is a widely studied example because of the complementary need to remediate the waste organics while sustainably recovering the products and energy from the waste. There are at least three categories of BESs: (1) microbial fuel cells (MFCs) that simultaneously remove the organic matter to treat wastewater, as well as generate electricity,²¹² (2) microbial electrolysis cells (MECs) that can generate value-added products such as hydrogen gas,²¹³ and (3) microbial peroxide producing cells (MPPCs) that generate hydrogen peroxide, a valuable chemical, by performing the truncated oxygen reduction reaction in the cathode. BESs also remove nutrients or heavy metals from wastewater using the electric current produced to drive them into concentrated solutions.^{212,214,215} These devices are also being studied as potential sensors in soil,²¹⁶ aquatic,²¹⁷ and wastewater environments.²¹⁸

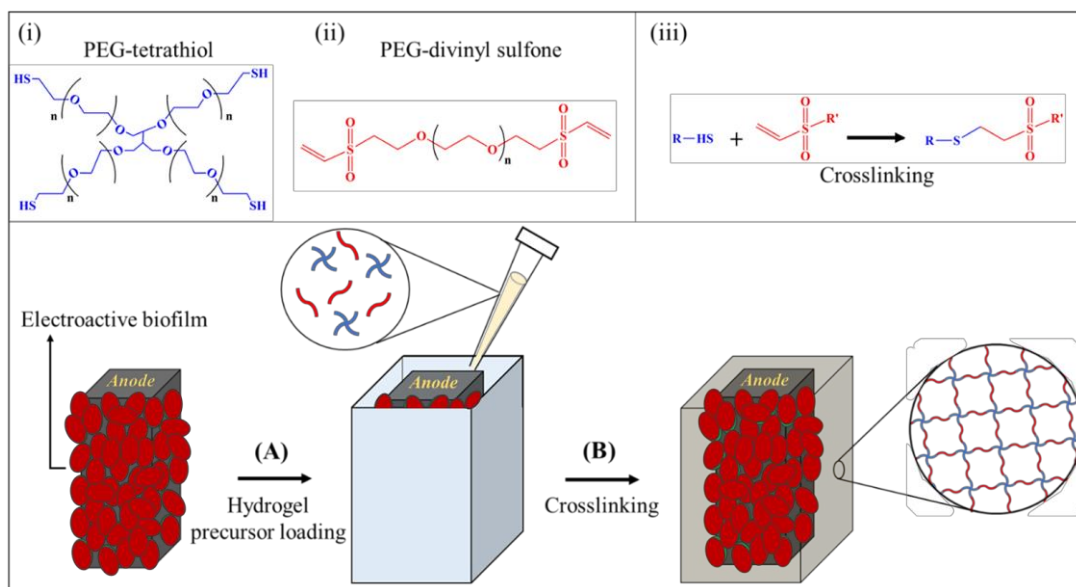
In BESs, the anode biofilm is one of the critical limiting factors in performance. The microbial community contains an abundance of electroactive bacteria (EAB) that play a crucial role in the electroactivity of the biofilm and the overall efficiency of these devices.²¹⁹ EAB or anode-respiring bacteria (ARB) are microorganisms capable of transferring electrons to or from a

solid substrate such as an electrode.²²⁰ Therefore, maintaining a well-balanced microbial community²²¹ with an abundance of EAB in the anode biofilm is crucial for maintaining efficient electron transfer and maximum current densities.¹⁴² However, recent studies have shown that EAB are highly sensitive to external stressors, such as heavy metal shock,²²² temperature fluctuations,²¹⁷ pH changes,²²³ organic solvents and other toxins.²²⁴ Electron generation and mass transfer within the EAB can be impacted by these stressors, which ultimately inhibits their electrocatalytic activity.²²⁵ Among these stressors, temperature fluctuations influence the BESs performance mainly by affecting the bacterial kinetics.²²⁶ Jadhav and Ghangrekar investigated the effect of temperature variations on their system. They demonstrated that an increase in ambient temperature favored the growth of the non-EAB, which affected the abundance of EAB and led to a decrease in current and coulombic efficiency of the system. They further studied the effect of pH variation on the performance of their MFC system by changing the anodic pH values between 5.5 and 7.5. They observed that a steady pH value of 6.5 increased the system performance to its maximum, whereas changing the pH value to more than 7 or less than 6 resulted in a decrease in efficiency.²²⁷ Accidental load of toxic shock can also change the microbial composition in the MFCs by affecting the EAB.²²⁸ This factor is especially crucial for MFCs operating as toxicity sensors. In MFC sensors, EAB act as a sensing element since the presence or a change in the concentration of the toxic substances affects their metabolic activity and resulting electrical signal.²²² Therefore, for MFC sensors' long-term operation in applications such as water monitoring, the decrease in metabolic activity of the biofilm caused by toxins should be reversible.²¹⁷ However, achieving a high degree of recovery, influenced by several factors such as toxic concentration, anode biofilm density, etc., is challenging.²²² To address the mentioned issues, it is crucial to develop methods

and materials that enhance the stability and long-term activity of BESs and specifically, their endurance upon environmental shocks.^{143,221,229}

Encapsulation of EAB with polymeric materials can be used as means of protection from environmental stress factors to extend the lifetime of EAB and stabilize their catalytic activity.²²⁴ Cell encapsulation techniques can also reduce the possibility of contamination, lower the ohmic losses between the cells and the anode, and increase metabolic activity.²³⁰ For instance, Du *et al.* encapsulated a living electroactive biofilm with artificial polydopamine (PDA) to protect the cells under extreme acid shock.¹⁴³ Luo *et al.* were also able to keep the activity of the anode biofilm and stabilize the MFC performance under harsh environmental conditions by immobilizing the anode biofilm using an agarose gel. Here, the small porosity of the hydrogel prevented the exogenous bacteria from disrupting the function of electroactive bacteria on the anode, preserving the performance of the MFC under severe conditions.¹⁴⁷ However, agarose is a natural polymer that cannot be tuned and modified and might not be a practical choice for BESs operated at various conditions. Unlike natural polymeric materials, synthetic hydrogels offer many advantages such as tunable porosity, stiffness, and stability.¹⁴⁷ Poly(ethylene glycol) (PEG) based hydrogels are a good candidate for protective BESs anode coatings. PEG is a chemically and biologically inert material with well-known antifouling properties that can inhibit fouling of exogenous microbes on the anode biofilm to maintain the balance of microbial community composition on the anode. PEG-based hydrogels have already been used for several bacteria interfaces various applications such as marine antifouling,^{231,232} bactericidal coatings,²³³ and antimicrobial wound dressing.²³⁴ Another importance of PEG hydrogels is their biocompatibility, making them suitable as a cell culture platform that is well-explored with mammalian cells,^{68,235} especially for biomedical and tissue engineering applications.^{236,237}

Although these interfaces have not been well studied for most microbial applications, we recently reported the use of PEG hydrogels for bacteria encapsulation and isolation. The results of these studies showed the compatibility of these materials as a 3-D matrix for bacterial cell culture.^{130,132} Despite the potential benefits of PEG, these materials have not been studied in BESs. In this report, the effect of PEG hydrogel protective coatings on anode biofilm efficiency is studied (**Scheme 5.1**). Coatings are designed to remain physically stable across anode surfaces, enable high stability across a range of pH values, and provide sufficient transport of small molecule metabolites to and from the biofilm interface. Comparing current densities in MECs with coated and uncoated anode biofilms revealed that the PEG-based coatings potential to reduce the environmental pressure on the biofilm, demonstrated here with an ammonia shock.



Scheme 5.1. Schematic of the anode coating procedure. (i) PEG-tetrathiol macromer, (ii) PEG-divinyl sulfone macromer, (iii) thiols and vinyl sulfone Michael-type addition reaction. (A) Loading the hydrogel precursor solution inside the parafilm mold. (B) Hydrogel formation at room temperature inside a vacuum glove box for one hour.

5.3 Materials and methods

5.3.1 Materials

Pentaerythritol tetra (mercaptoethyl) polyoxyethylene (PEG-tetrathiol, MW 10,000) was purchased from NOF America Corporation. Vinylsulfone-PEG-Vinylsulfone (PEG-divinyl sulfone, MW 3400) was purchased from Creative PEGWorks. Ethanol, and isopropanol were purchased from Fisher. (3-Mercaptopropyl) trimethoxysilane, sodium phosphate monobasic dihydrate ($\text{NaH}_2\text{PO}_4 \cdot 2\text{H}_2\text{O}$), sodium hydroxide (NaOH),alconox detergent, toluene anhydrous, Sodium hydrogen phosphate (Na_2HPO_4), potassium phosphate monobasic (KH_2PO_4), ammonium chloride (NH_4Cl), ethylenediaminetetraacetic acid (EDTA), cobalt chloride hexahydrate ($\text{CoCl}_2 \cdot 6\text{H}_2\text{O}$), calcium chloride dihydrate ($\text{CaCl}_2 \cdot 2\text{H}_2\text{O}$), boric acid (H_3BO_3), sodium molybdate dihydrate ($\text{Na}_2\text{MoO}_4 \cdot 2\text{H}_2\text{O}$), sodium selenite (Na_2SeO_3), sodium tungstate dihydrate ($\text{Na}_2\text{WO}_4 \cdot 2\text{H}_2\text{O}$), nickel chloride hexahydrate ($\text{NiCl}_2 \cdot 6\text{H}_2\text{O}$), magnesium chloride (MgCl_2), manganese chloride tetrahydrate ($\text{MnCl}_2 \cdot 4\text{H}_2\text{O}$), zinc chloride (ZnCl_2), copper sulfate pentahydrate ($\text{CuSO}_4 \cdot 5\text{H}_2\text{O}$) and aluminum potassium sulfate ($\text{AlK}(\text{SO}_4)_2$), ferrous chloride ($\text{Fe}(\text{II})\text{Cl}_2$), sodium sulfide nonahydrate ($\text{Na}_2\text{S} \cdot 9\text{H}_2\text{O}$), and sodium hydroxide (NaOH) were purchased from Sigma-Aldrich. Parafilm M was purchased from VWR. Rectangular graphite electrodes were ordered from GraphiteStore. Ag/AgCl reference electrodes were purchased from BASi.

5.3.2 Hydrogel crosslinking chemistry and hydrogel hydrolytic stability

experiments

The first stage in developing the hydrogel coating involved characterizing its long-term stability across a range of pH levels. Here, hydrogel stability experiments were done by

gravimetric analysis of the hydrogels adapted by Paez *et al.*⁹⁹ For this purpose, free hydrogels, not in the MEC setting, were prepared. The hydrolytic stability of PEGVS based hydrogels was also compared to PEG diacrylate (PEGDA) hydrogels that are susceptible to hydrolysis due to the presence of ester groups in acrylates.²³⁸ All hydrogels were prepared in the same manner by pipetting 95 μ l of hydrogel precursor solution on a flat parafilm surface. After gelation, hydrogels were immersed in Milli-Q water at room temperature for 48 hours to reach equilibrium, and then the initial mass of swollen hydrogels was measured. Hydrogels were then incubated in buffer at three different pH values (citric buffer, pH 3; phosphate buffer, pH 7; and carbonate buffer, pH 10) for 72 days at room temperature. The mass of the swollen hydrogels was measured at varied time points, and the normalized mass of swollen hydrogels (N_m) at each time point was calculated ($N_m = \text{weight at time } t / \text{initial weight}$). Increases in N_m from 1.0 indicate changes in hydrogel structure.

5.3.3 Diffusion coefficient measurements and COMSOL modeling

Thick coatings over the anode biofilm can hinder the substrate transfer to cells and affect cell viability, lowering the performance of the MEC.²²⁴ However, thick coatings (700-800 μ m) were desired here due to the ease of deposition and reproducibility of the coating technique (**Scheme 5.1**). The transport of the necessary carbon source was investigated to assure that the designed coating provided adequate flux to and from the growing bacteria and not compromise their viability. To model transport throughout the coatings, COMSOL modeling was used. First, the diffusion coefficient of the carbon source (acetate) through the coating was required as an input in the COMSOL model. Due to chemical interactions between the substrate and components in the PEG hydrogel, the diffusion coefficient was measured experimentally.

For quantitative analysis of the diffusion of molecules through the hydrogels, the analytical solution of Fick's second law of diffusion can be utilized. When the concentration gradient occurs in only one dimension, the release kinetics can be described by Fick's second law:²³⁹

$$\frac{dc}{dt} = D \cdot \frac{d^2c}{dx^2} \quad (1)$$

Where C is the concentration of the molecule within the polymeric system; t , x , and D are the time, position, and diffusion coefficient of the molecule in the bulk liquid, respectively. Generally, to measure the diffusion coefficient of the solute in a solution, the solute concentration is measured over time. Experimental data is then fit to the solution of Fick's equation to acquire the experimental diffusion coefficient.²³⁹ When molecules are molecularly dispersed in the hydrogel matrix, the hydrogels are considered monolithic systems.²⁴⁰ In this paper, as shown in **Figure 5.1**, a cylindrical setup is used for diffusion experiments with the monolithic acetate-loaded hydrogel at the bottom. Here we consider a perfect sink condition and no release from the edges of the cylindrical hydrogel, which means only the hydrogel surface is in contact with the release medium. Thus, only axial diffusion is considered, and the mathematical analysis can be limited to one dimension, where Fick's second law of diffusion can be solved analytically as follows:^{240,241}

$$\frac{M_t}{M_\infty} = 1 - \frac{8}{\pi^2} \sum_{n=0}^{\infty} \frac{\exp\left[-\frac{D(2n+1)^2\pi^2 t}{L^2}\right]}{(2n+1)^2} \quad (2)$$

Where M_t and M_∞ are the cumulative amounts of the released molecule at time t and infinite time, respectively; L denotes the height of the cylindrical gel, and D is the diffusion coefficient of the molecule within the system. This solution is similar to a cumulative molecule released over time

from a slab geometry.²⁴⁰ When $M_t/M_\infty \leq 0.6$, the early-time approximation is valid to calculate the diffusion rates by the equation below:

$$\frac{M_t}{M_\infty} = 4 \left(\frac{Dt}{\pi L^2} \right)^{0.5} \quad (3)$$

Here the PEGVS hydrogels were formed in buffer with an acetate solution concentration of 1-1.1 M. The hydrogel precursor solution (300 μ L) was then pipetted inside a 2 mL vial, resulting in a cylindrical hydrogel after gelation. Then, 1.5 mL of ultrapure water was added to the vial, and the vial was incubated at room temperature (215 rpm). Based on the geometry of the vial and the volume of the used hydrogel precursor solution, the height of the cylindrical gel was calculated to be 6 mm. At each data point, the solution was removed from the vial and replaced with fresh ultrapure water. The acetate concentration in each removed solution was measured at 210 nm using a ThermoScientific NanoDrop 1000 Spectrophotometer.

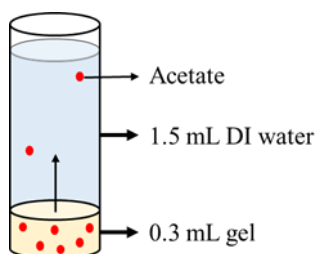


Figure 5.1. Setup used for diffusion coefficient measurements.

After calculating the diffusion coefficient of the substrate through PEGVS hydrogels, finite element modeling was used to generate concentration profiles for the substrate through the hydrogel. The goal here was to understand the hydrogel thickness, at which point diffusion limitations could inhibit the biofilm viability and function. The transport of diluted species in

porous media model in COMSOL Multiphysics® was developed considering the following assumptions: (1) hydrogel deformation is negligible, (2) hydrogel degradation throughout the studies based on stability results is not significant, (3) the ambient medium is infinite and well-stirred at all times, and thus, the concentration of the substrate does not change in the external media, (4) biofilm substrate consumption rate at the biofilm surface is 6.4×10^{-6} mol/m². s, calculated based on current density data, and remains the same throughout the study, (5) no flux from the bases.

5.3.4 MEC reactor setup and current monitoring

These experiments set up the microbial electrochemical cells as MECs to prevent oxygen diffusion that could inhibit microbial activity and to provide the optimum anode potential for maximizing ARB growth on the anode biofilm.²⁴² Two H-type reactors were used in the experiment, each containing an anode and a cathode compartment separated by an anion exchange membrane (AEM). The two compartments each held a volume of 585 mL. The anode compartment contained two rectangular graphite electrodes in the anode (www.graphitestore.com), with a total surface area of 32 cm², and the cathode compartment contained one 16 cm² rectangular electrode. The anode was maintained at a potential of -301 mV by an Ag/AgCl reference electrode. The reactors were kept in a temperature-controlled environment to maintain 30 °C conditions, while the anode was mixed at a rate of 100 rpm.

The biofilm in each of the two reactors was established by adding anaerobic sludge obtained from the Salina Wastewater Treatment Plant (Salina, Kansas) to the anode. The sludge was added at a concentration of 1% v/v to a phosphate buffer media containing the following composition per liter: 12.04 g Na₂HPO₄, 2.06 g KH₂PO₄, and 0.41 g NH₄Cl; 10 mL of a 1 L trace

mineral media containing 0.5 g EDTA, 0.082 g $\text{CoCl}_2 \cdot 6\text{H}_2\text{O}$, 0.114 g $\text{CaCl}_2 \cdot 2\text{H}_2\text{O}$, 0.01 g H_3BO_3 , 0.02 g $\text{Na}_2\text{MoO}_4 \cdot 2\text{H}_2\text{O}$, 0.001 g Na_2SeO_3 , 0.01 g $\text{Na}_2\text{WO}_4 \cdot 2\text{H}_2\text{O}$, 0.02 g $\text{NiCl}_2 \cdot 6\text{H}_2\text{O}$, 1.16 g MgCl_2 , 0.59 g $\text{MnCl}_2 \cdot 4\text{H}_2\text{O}$, 0.05 g ZnCl_2 , 0.01 g $\text{CuSO}_4 \cdot 5\text{H}_2\text{O}$, and 0.01 g $\text{AlK}(\text{SO}_4)_2$; 1 mL of a 4 g/L $\text{Fe}(\text{II})\text{Cl}_2$ stock solution; 0.5 mL of a 37.2 g/L $\text{Na}_2\text{S} \cdot 9\text{H}_2\text{O}$ stock solution.^{243,244} Acetate was then added as an electron donor to grow and condition the biofilm at a concentration of 40 mM. The cathode media was the same as the anode media, without the sludge or acetate, but was adjusted to a pH of 11.5 using sodium hydroxide. Once the biofilm began to grow on the anode electrodes, the media was replaced with the same composition described above, except the sludge. This was repeated until the reactor produced current densities of 5-8 A/m^2 . Once the reactor had reached this stable point, one of the two electrodes present could be coated with the hydrogel.

The electron donor concentrations were quantified by high-performance liquid chromatograph (HPLC) analysis (Shimadzu LC-20AT, USA) using an Aminex HPX-87H column (Bio-Rad Laboratories, USA) to separate the organic acids and sugars, which then were detected by a photodiode array and refractive index detectors. The current production from the reactors was continuously measured using a multichannel potentiostat, with current from both coated and uncoated electrodes monitored separately.

5.3.5 Parafilm holder for the coating process

After COMSOL modeling and finding the allowable thickness range for the hydrogel coating, a facile and reproducible method for depositing the hydrogel layer over the anode present in the MEC was developed. Parafilm is a cheap, flexible, waterproof sheet with hydrophobic properties used in most laboratories.²⁴⁵ For coating the anode biofilm, first, a plain electrode was used. Static tape (40 μm thick) was taped around the electrode to reach the desired thickness

(multiples of 40 μm). This process can be repeated until the full height of the electrode is covered. Then, a parafilm sheet was wrapped around the covered electrode until a stiff mold from the parafilm is obtained. Then, the mold is pressed on another parafilm sheet to close the base (**Figure 5.2**). Finally, the tape-covered electrode is gently pulled out of the parafilm mold, resulting in a hollow cuboid that is closed off from the base. This mold can then be placed on a petri dish or other solid surfaces for the coating procedure of the anode.



Figure 5.2. Preparation of the parafilm holder for coating process.

5.3.6 Hydrogel coating preparation

For preparing the hydrogel precursor solution, the crosslinking conditions are adopted from Fattahi *et al.*,¹³² which acquires the addition of 5.6 μL of PEGVS (M_n 3400 Da, 49 mM) in water into 12.5 μL of phosphate buffer, pH 8. Lastly, 6.9 μL of PEG-tetrathiol (M_n 10000 Da, 20 mM) in water needs to be added to the mixture to obtain equimolar ratio of vinyl sulfone:thiol. The concentrations of vinyl sulfone and thiol groups in the final mixture are each 22 mM, and the final

solution volume is 25 μL . In this paper, concentrations of the crosslinkers were kept the same at different volumes.

For the development of the coating procedure, a parafilm-based mold was used (**Figure 5.3A**). The mold is placed on a petri dish. Then the anode electrode is centered in the mold, at which point a gap between the anode and the mold is present. This gap length can be varied between 600 and 800 μm depending on the thickness of the biofilm present on the anode. The gap is then filled with the liquid hydrogel precursor solution and allowed to react for 1 hour at room temperature under vacuum condition to achieve hydrogel formation. After gelation, the parafilm holder is gently unwrapped from the anode electrode, and the hydrogel is stabilized to the anode (**Figure 5.3B**). The anode electrode is then placed back inside the MEC setup (**Figure 5.3C**).

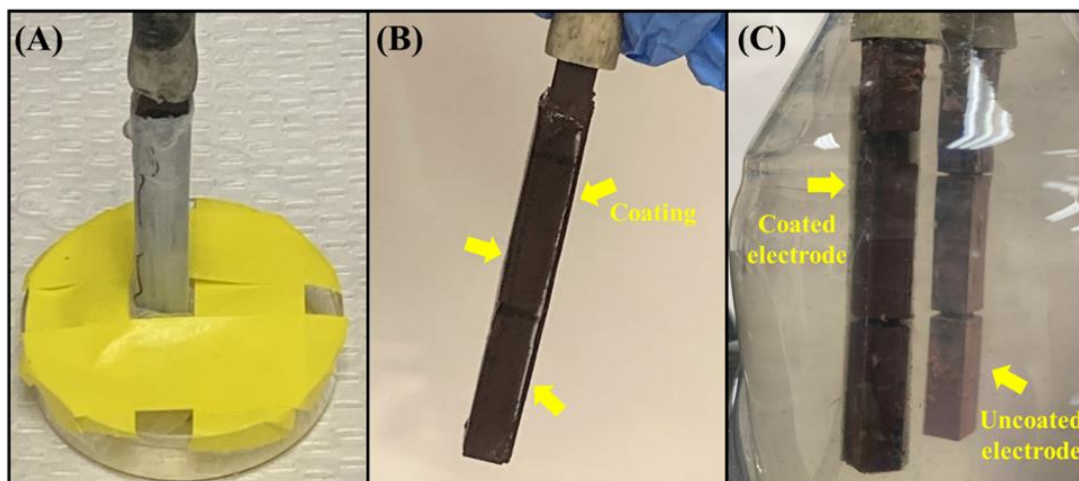


Figure 5.3. Anode coating procedure. (A) Coating formation over the anode inside the parafilm mold. (B) Coated hydrogel over the anode electrode after gelation. (C) Coated anode electrode placed back inside the reactor.

5.3.7 Initial testing of coating impacts on current production and longevity of coating

After allowing the biofilm-covered electrodes to reach high current density and coating one of the electrodes with hydrogel, two trials were conducted to compare the performance of the coated and uncoated electrodes. As previously described, the current production was continuously measured using a multichannel potentiostat that monitored each electrode. The current density was then compared, normalizing the current produced to the 16 cm² area of each electrode. The two trials took place over a period of at least two weeks to assess the sustained attachment and longevity of the coatings.

5.3.8 Ammonium spike experiments

To assess whether these coatings protect against ammonia toxicity, and to explore what effect previous ammonia exposure has on the future current production and future response to ammonia shocks. Once the MEC reactor had received new anode media and returned to stable, high current density for the coated and uncoated electrode, a shock load of ammonium chloride was added. Once again, using the multichannel potentiostat, the current production was then measured for the two electrodes to compare the inhibition of the coated and uncoated biofilm. The response from the two electrodes was also compared after providing the reactor a new media without the high ammonium level. The ammonium chloride spike and media replacement were then repeated to test how previous exposure to high ammonia levels affected the response of the coated and uncoated electrodes. The experiments were conducted using NH₄-N spikes that were 6.8 g/L NH₄-N and 10.8 g/L in concentration, which could also indicate whether the coating protects against other toxicants.

5.4 Results

5.4.1 Hydrolytic stability of the hydrogels

Click chemistries represent reactions with fast reaction kinetics with high efficiency for connecting two molecular units.¹⁰⁰ Bioclick reactions, including Michael-type addition, are a category of click reactions attractive for preparation of polymeric biomaterials. The reaction can be carried out in aqueous under physiological conditions with no harmful byproducts to cells.²⁴⁶ Thiol-Michael type addition reaction have been broadly utilized to synthesize biocompatible PEG-based hydrogels through step-growth polymerization mechanisms.^{247,248} Thiols are reactive with acrylates, maleimides, and vinyl sulfones through Michael addition.⁹⁹ These hydrogels have been broadly studied in tissue engineering and drug delivery. It is well-known that thiol-acrylate networks degrade due to hydrolysis of ester groups present in acrylates even at physiological pH²⁴⁹ and thiol-maleimide networks can also undergo hydrolysis under mild alkaline conditions.⁹⁹ Therefore, hydrogel stability for both thiol-acrylate and thiol-maleimide crosslinks cannot be sustained for a long operation time. However, thiols and vinyl sulfones form a highly stable thioether-sulfone bond that is not readily susceptible to hydrolysis, generating pH-stable hydrogels for long periods of time.^{91,250} Because use in a wide range of pH conditions is desired for broad BESs applications,^{251,252} PEG-divinyl sulfone (PEGVS) hydrogels were chosen for studies in this paper.

Hydrogel degradation happens upon reduction in crosslinking density due to breakage of the bonds within the crosslinking network. One method to investigate the crosslinking density alteration within the hydrogels is to measure the swelling ratio of the gels over time.²³⁸ An increase in swelling ratio is a result of a decrease in crosslinking density.²⁵³ Hennink *et al.* reported that

hydrolysis of a crosslink in the system leads to a longer chain networks among the remaining crosslinks, which allows for expansion and swelling in the hydrogel.²⁵⁴ Following **Section 5.3.2**, gravimetric analysis of the hydrogels was conducted for 72 days. At the end of this period, the mass of PEGVS hydrogels incubated in pH 3, pH 7, and pH 10 only reached 1.16, 1.08, and 1.18 times their initial mass, showing little hydrogel degradation and adequate long-term stability necessary for the coatings (**Figure 5.4A**).

In contrast, the PEGDA hydrogel was completely hydrolyzed and dissolved in medium solution after 24 hours in pH 10 buffer. Also, after 60 days, the mass of PEGDA hydrogels in pH 3 and pH 7 reached 1.64 and 2.44 times their initial mass, indicating significant degradation of the hydrogel structure (**Figure 5.4B, C**). Some fluctuations present in the trends of the provided data are due to instrument variability throughout the study (less than 2% error). Given the long-term (> 60 days) stability noted, these results suggest that PEGVS hydrogels are good candidates for a chemically stable, protective coating over the anode biofilm to study the MEC efficiency.

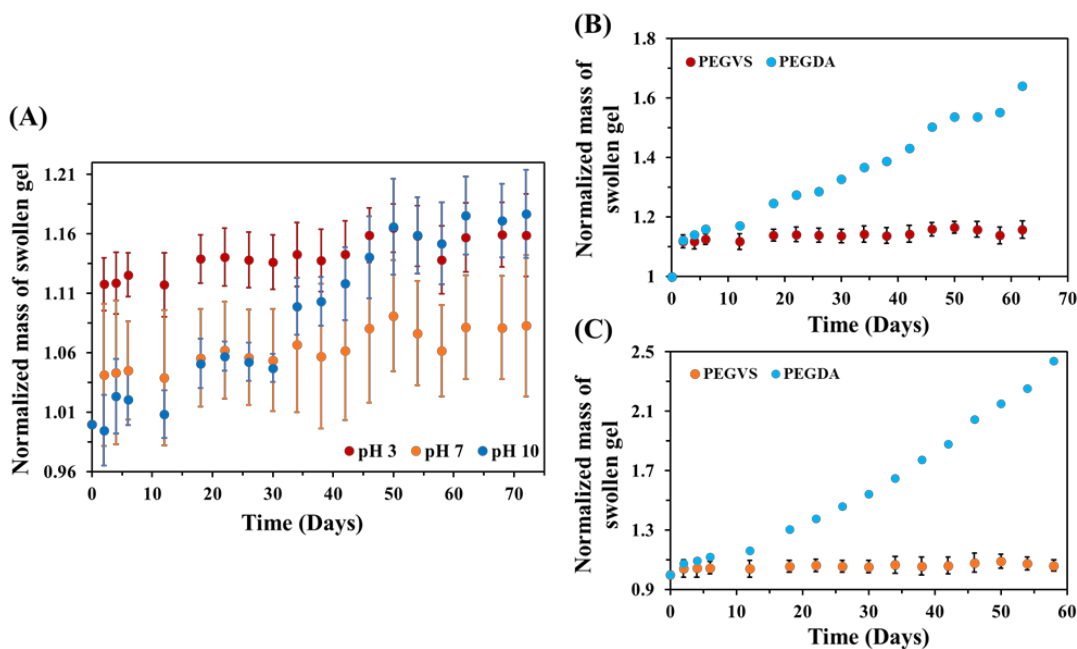


Figure 5.4. (A) Hydrolytic stability of PEGVS hydrogels at different pH values. Hydrogels (n=3) were incubated in pH 3, 7, and 10 at 25 °C for > 10 weeks. (B) Comparison of hydrolytic stability of PEGVS and PEGDA hydrogels at pH 3. (C) Comparison of hydrolytic stability of PEGVS and PEGDA hydrogels at pH 7.

5.4.2 Substrate diffusion coefficient and optimum coating thickness

NanoDrop measurements described in **Section 5.3.3**, were used to generate the release profile of acetate from the PEGVS and was plotted based on the released mass fraction of acetate using a mass balance (**Figure 5.5A**). Using Fick's law for early release time (**Figure 5.5B**), the effective diffusion coefficient of acetate through the PEGVS hydrogels was calculated to be $1.44 \times 10^{-10} \text{ m}^2/\text{s}$. This value is comparable with the diffusion coefficient of glucose through a similar PEG hydrogel reported in the literature, and takes into account physical and chemical interactions between acetate and the hydrogel that could cause diffusion limitations.²⁵⁵

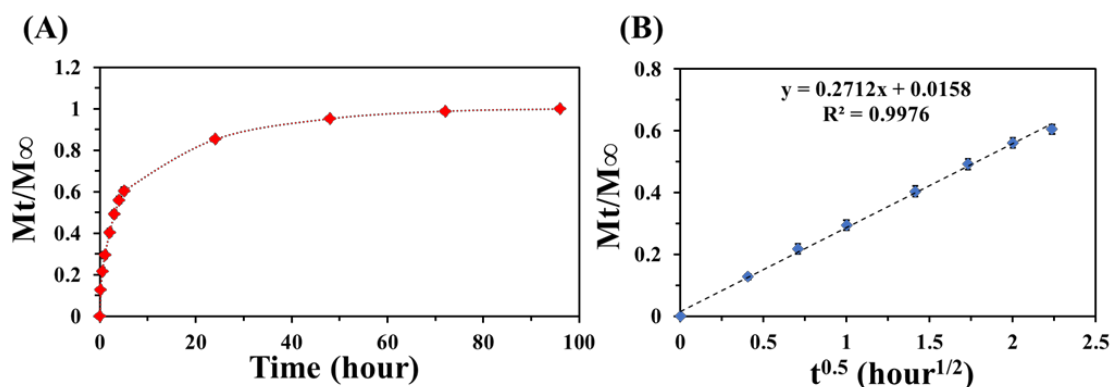


Figure 5.5. (A) The cumulative mass release of acetate from PEGVS hydrogels with the initial concentration of 0.3 mM. (B) Early time ($M_t/M_\infty < 0.6$) release profile plotted as a function of the square root of time that is used to determine the diffusion coefficient of the acetate through the PEGVS hydrogel using equations (2) and (3).

Considering the mentioned assumption for COMSOL modeling described in **Section 5.3.3**, the model allows for prediction of the concentration profile of acetate throughout the hydrogel (**Figure 5.6A, B**), and significantly, the maximum allowable thickness of the polymer coating that will supply an adequate flux of acetate to the biofilm for viability and growth with the given diffusion limitations of the hydrogel, based on the metabolic needs of the biofilm. For instance, in an MEC system with 40 mM of the substrate (acetate) and a mature anode biofilm with a metabolic consumption rate of 6.4×10^{-6} mol/m². s, the maximum allowable coating thickness is 900 μ m. **Figure 5.6C**, further shows the impact of biofilm maturity and its substrate consumption rate on the maximum allowable coating thickness.

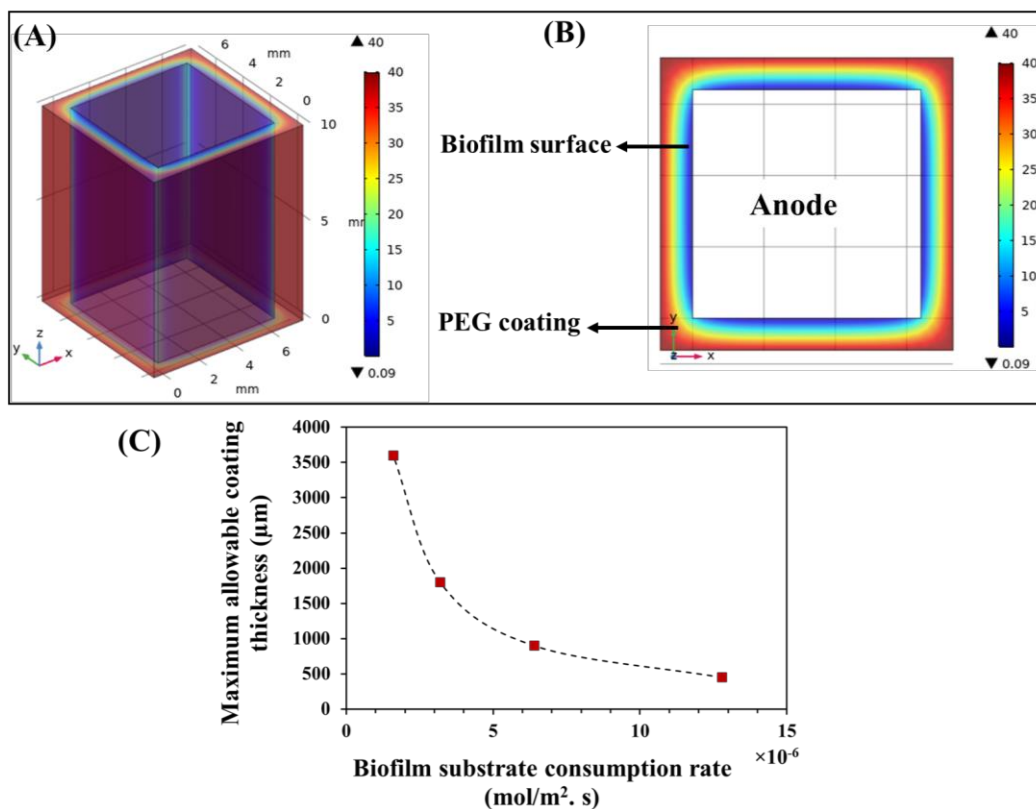


Figure 5.6. (A) Substrate concentration profile of a hollow cuboid representing the hydrogel coating over the anode biofilm, showing the diffusion of the substrate from the media through the walls. The dark red color on the outer surface of the cuboid shows the higher concentration of the substrate, which is the same as in the external solution. The dark blue color on the inside of the cuboid represents the lower concentration of the substrate available to the anode biofilm. (B) Two-dimensional concentration profile of the cuboid from the top view. (C) Effect of substrate consumption rate on maximum allowable coating thickness.

5.4.3 Hydrogel coating effect on microbial activity

To investigate the effect of the hydrogel coating on the long-term activity of the anode-bound biofilms, current density of two anodes was analyzed in side-by-side compartments, and all the environmental variables for both anodes were identical, other than presence of coating on one of the anodes. **Figure 5.7** shows the hydrogel coatings did not decrease the sustained microbial

electroactivity in the biofilm. The uncoated electrode produced current densities of 3.5-6 A/m², and the coated biofilm maintained current densities ranging from 30-70% of the uncoated electrode throughout the length of the trial. This amounted to a current density deficit of approximately 1.5-2.5 A/m². In **Figure 5.7B**, the current densities for the coated and uncoated electrodes return to these same levels when a slug load of acetate is provided after day 12 in trial 2, when the current production had gone to zero due to the depletion of the electron donor. The difference in current densities between the electrodes is likely due to diffusion limitations of the acetate through the hydrogel coating. The results from **Figure 5.7** demonstrate the longevity of the coatings. The coating was preserved for 30 days and 15 days in trials 1 and 2, respectively. It should be noted that the coatings did not reach the end of their useful lives, but the trials were ended to conduct further experiments on the electrodes.

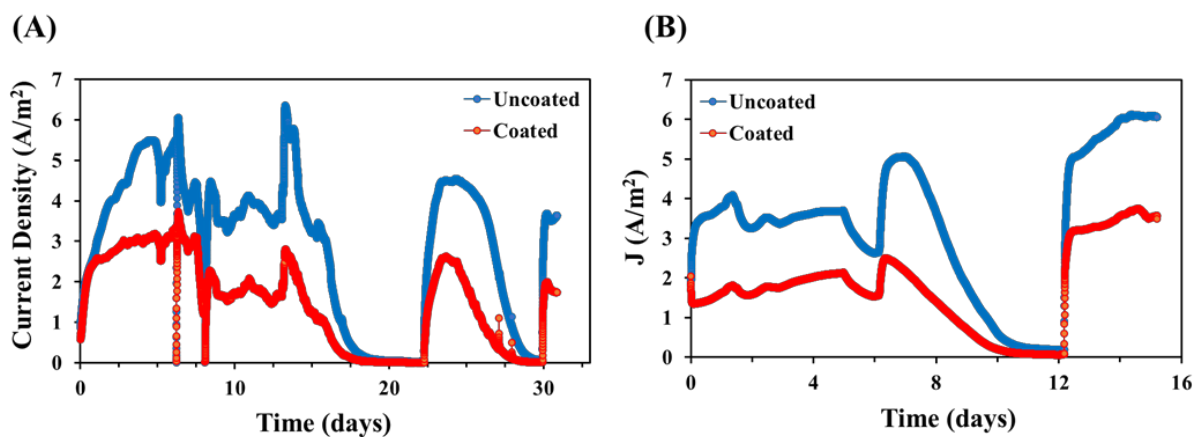


Figure 5.7. Current density comparisons between electrodes with and without a hydrogel coating for (A) trial 1 and (B) trial 2, showing a consistent 1.5-2.5 A/m² gap.

5.4.4 Protection of anode biofilm against ammonia shock

To investigate the effect of the coatings to protect from a chemical shock, anodes were exposed to ammonia-N in concentrations ranging from 6 – 10 g NH₄-N, this is representative of realistic industrial wastewaters such as fisheries, swine manure, etc.^{256,257} During the spike in concentration of 6.8 g/L NH₄-N into an acetate fed MEC with typical NH₄-N concentration of around 0.4 g N/L, there is an initial larger decrease in current density magnitude by the uncoated electrode than the coated electrode, with a slightly larger current density decrease as a percentage of pre-spike value (**Figure 5.8C**). After the electrodes are swapped into new reactors with regular NH₄-N concentrations, the coated electrode reaches high levels of current density, similar to its original value and faster than the uncoated reactor (**Figure 5.8F**), eventually surpassing its pre-spike current production. The current density gap between coated and uncoated reactors falls from 55-65% pre-spike to 75-85% post-spike in trial 1. This gap decrease is not as significant in trial 2 as the reactor has already been exposed to high concentrations of ammonia, reducing the pre-spike gap. Likely reasons for this observation could be connected to a modified pH buffering/transport through the coating which had likely retained some NH₄-N ions due to ion-dipole interactions.^{258,259} García-Jimen and Estelrich has previously reported a dipole–cation binding between the ether group of the PEG chain and the positive charge of iron oxide particles by disappearance of the stretching band characteristic of the C-O-C group (1080 cm⁻¹).²⁵⁸ The release of NH₄-N could help with added buffering capacity, as shown by previous research,²⁶⁰ which could lead to further increase in current density. Additional pH experiments could shed greater level of detail on the observed increase in current density in coated biofilm anodes after high NH₄-N exposure.

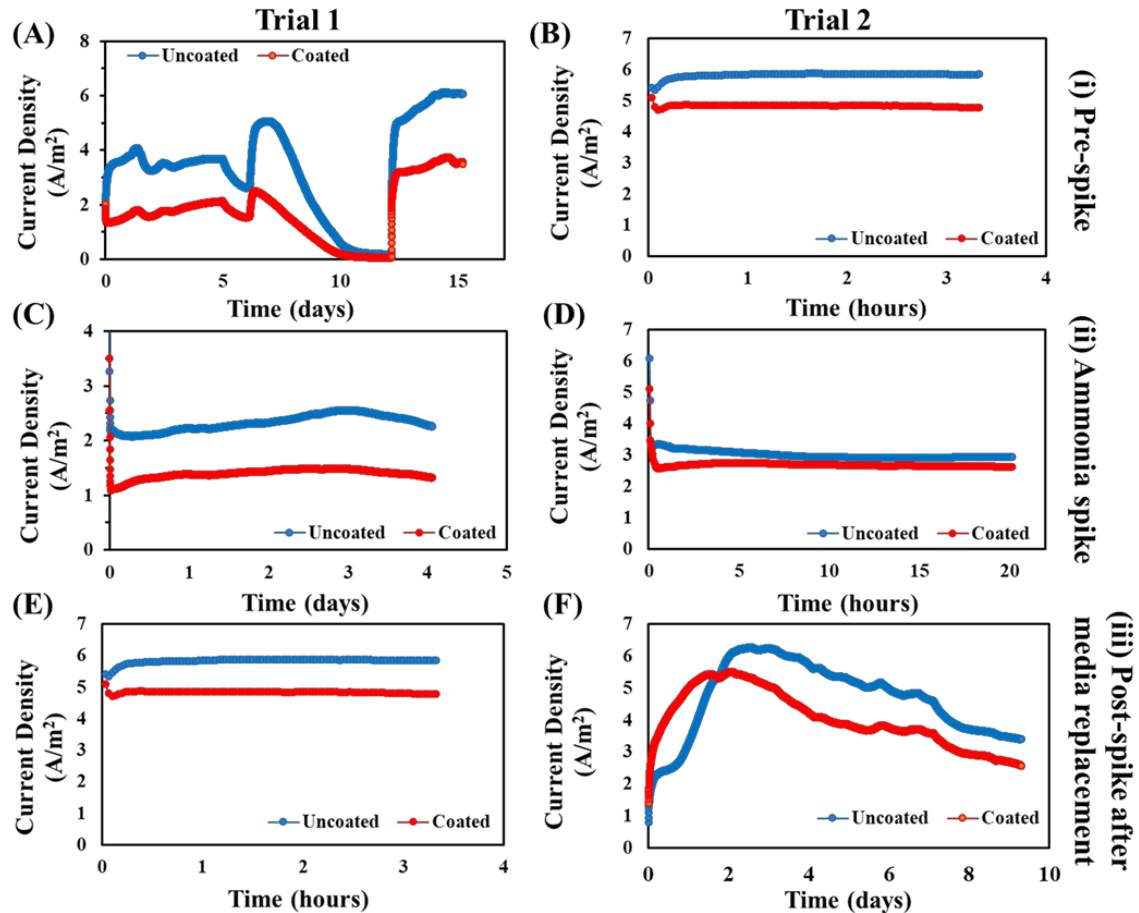


Figure 5.8. 6.8 g/L $\text{NH}_4\text{-N}$ spike. Pre-spike current density difference changes from 55-65% to 75-85% difference post spike and media replacement.

Figure 5.9 shows that at a higher ammonia concentration of 10.8 g/L, the results replicate that of the lower ammonia spike concentration and the coated electrodes show an even greater positive impact as $\text{NH}_4\text{-N}$ concentration increases. The coated electrode continues to have a more subdued reaction to the shock addition, while returning to high current density more quickly than the uncoated electrode. In fact, these effects are amplified at this higher ammonia level. The current density gap between the coated and uncoated electrodes narrows to 80-90%, conditioning the coating as with the lower ammonia addition. Additionally, during the period of exposure to the

high ammonia concentration, the coated reactor actually reaches a higher current density than the uncoated reactor. This shows that the coated electrode's response, relative to the uncoated electrode, improves as the ammonia concentration increases (**Figure 5.10**). This could be due to slower diffusion through the coating, and it suggests that the coating may provide some protection to the biofilm against other toxicants as well.

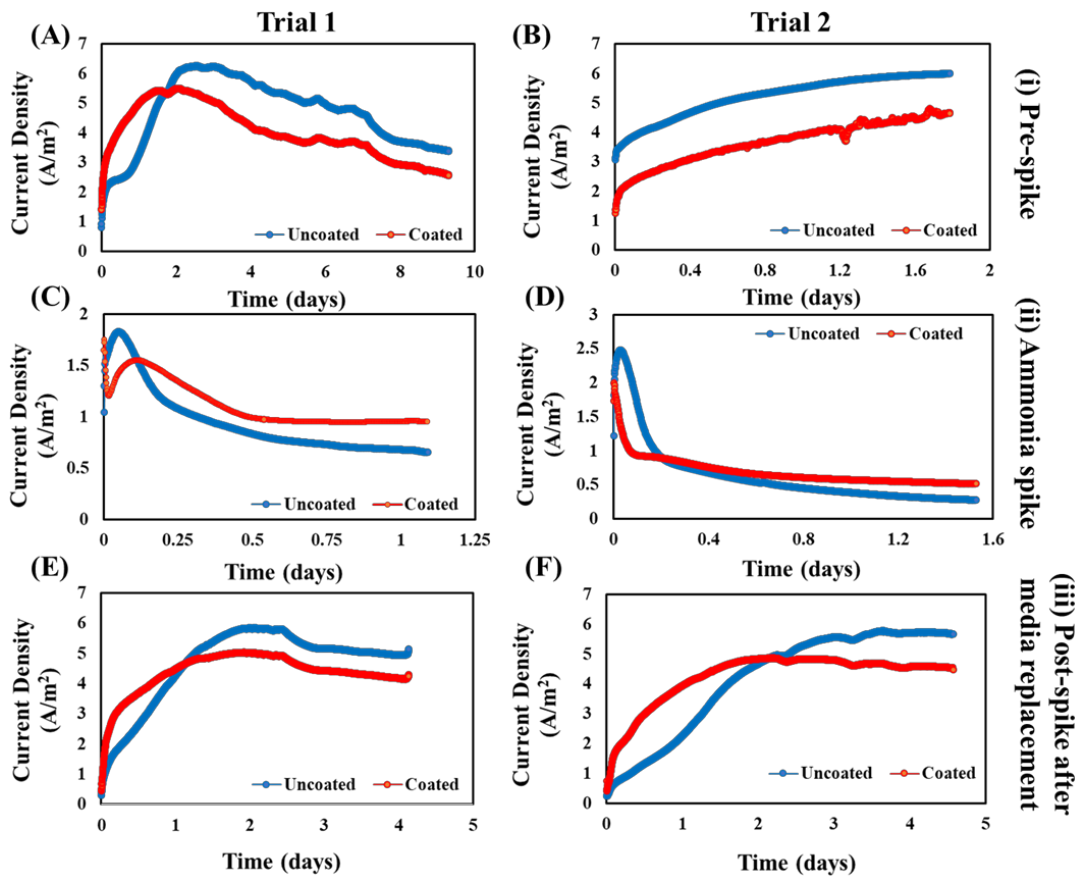


Figure 5.9. 10.8 g/L $\text{NH}_4\text{-N}$ spike. Post spike current difference from 75-85% to 80-90% in trial 1 and 67-77% to 80-90% in trial 2.

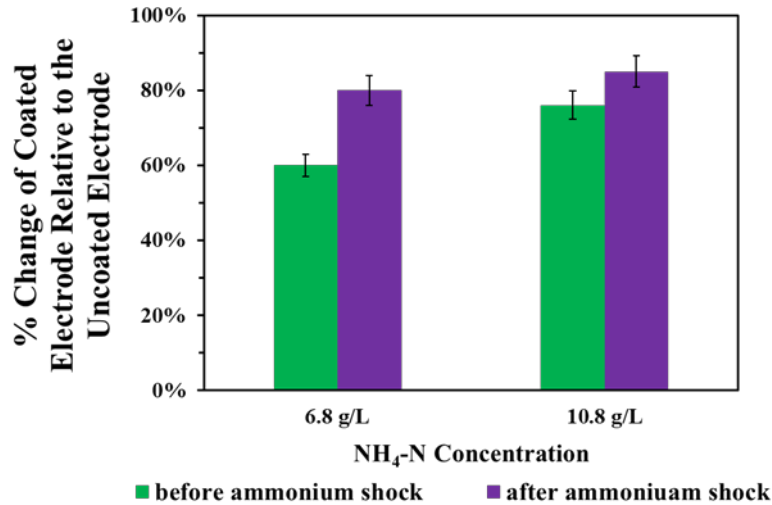


Figure 5.10. Variance reduction between the current density of the uncoated and coated electrode before and after ammonium spike.

5.5 Conclusion

For practical applications of BESs requiring long operation times, improving the long-term stability of EAB under environmental pressures is a high priority.²⁶¹ In this paper we demonstrated the use of PEG-divinyl sulfone hydrogels as coatings over anode biofilms for EAB protection from changes in the chemical environment. We have demonstrated the long-term stability of the proposed coating in the experimental setup for more than 30 days. For exploring the potential of the coating for biofilm protection from environmental stressors, as a model system, the response of coated electrode to ammonia toxicity was evaluated. To this end, different concentrations NH₄-N were introduced to the system and the changes in current density of the coated and uncoated electrode was monitored. Initially, before the ammonia spike, the uncoated electrode reached a higher current density and this difference remained consistent over time. However, during the ammonia spike, the coated electrode responded slower to the negative impact of the added

ammonia, and less reduction in current density was observed for this electrode, eventually resulting in a higher current density in the coated electrode. After replacing the media with new media without high concentrations of ammonia, the coated electrode reached an even higher current density for a period of time. Although the higher current density observed for the coated electrode did not last and the uncoated electrode eventually surpassed it, the current density difference that was observed initially in the system was narrowed. It was also observed that introducing higher concentrations of $\text{NH}_4\text{-N}$ to the system further decreases this difference. We believe the reason behind this observation is due to dipole interactions between the PEG-based coating and the $\text{NH}_4\text{-N}$ ions due to cation coordination with the ether oxygen of the PEG molecule, an effect noted with cationic molecules and PEG units in other reports.^{258,259} Based on this hypothesis, the coatings likely retain some $\text{NH}_4\text{-N}$ in its network and prevent the biofilm from experiencing the high amount of $\text{NH}_4\text{-N}$ that the uncoated electrode experiences. Moreover, after replacing the media, when high concentrations of ammonia are no longer present, the $\text{NH}_4\text{-N}$ that is retained within the coating can likely enhance the buffering capacity and have a positive impact on the biofilm metabolic activity. However, due to the concentration gradient of $\text{NH}_4\text{-N}$ in the coating and in the bulk, this positive response fades as $\text{NH}_4\text{-N}$ diffuses out of the coating and into the bulk media. Future experiments with changing the pH of the media can further confirm the pH buffering influence of $\text{NH}_4\text{-N}$ on the system.

Acknowledgment:

This work was supported by the National Science Foundation (Award #1841613)

Chapter 6 - Summary and Future Recommendations

6.1 Photodegradable hydrogels for high-throughput screening, identification, and on-demand isolation of rare microbial cells.

Hydrogels are hydrophilic polymeric materials with the ability to retain large amounts of water. These features, along with porous structure, allow for the exchange of oxygen, nutrients, and other biomolecules from these interfaces. Stimuli-responsive hydrogels are a category of hydrogels that can undergo changes in their physical and chemical traits in response to an external stimulus, enabling manipulation of the cell microenvironment. These properties make stimuli-responsive hydrogels ideal materials for applications such as drug delivery and tissue engineering.

The potentials of hydrogel materials have not been well explored in microbiology. Therefore, most of this dissertation (**Chapter 3 and 4**) emphasizes the biocompatibility of photodegradable polyethylene glycol (PEG) *o*-nitrobenzyl diacrylate hydrogels for high-throughput microbial cell growth and cell release with selectivity and specificity for downstream genetic analysis using a 365 nm light patterning device.

6.1.1 PEG-based hydrogels for high throughput screening of microbial cells.

Hydrogels are appropriate environments to interact with microbial cells because of their aqueous environment, tunable mechanical and chemical properties, and porous structure. In this thesis, the first portions are allocated to study the feasibility of using PEG-based hydrogels as a high-throughput cell culture platform. PEG-based hydrogels in these studies contained ester groups, which are susceptible to hydrolysis. It was observed that culturing entrapped cells within these hydrogels resulted in the formation of clonal microcolonies from the original individual cells.

We believe this is partially due to a bacteria dependent degradation in the hydrogel matrix, providing additional room for cell growth while remaining encapsulated in the matrix. The compatibility of the PEG-based hydrogel for cell growth favored the bacterial cell encapsulation at high-densities, allowing for the monitoring tens of thousands of cells parallelly, enabling genome-wide screening for bacterial cells with rare behavior. As a model system, we encapsulated *Agrobacterium tumefaciens* C58 bacterial cells within 13 μm thick hydrogels layers at a density of 90 cells/ mm^2 . This seeding density allowed parallel monitoring of 28,000 C58 cells in each hydrogel. Hydrogels were incubated in the presence of an inhibitory molecule, agrocin 84, produced by the biocontrol agent *Rhizobium rhizogenes* K84 to the growth of C58. Monitoring the growth of individual cells and screening for rare growth behavior, enabled the identification of rare C58 mutants resistant to agrocin 84. Here, screening 28,000 C58 cells resulted in identification of 9 mutants that were able to grow in the presence of agrocin 84. Identified rare colonies were exposed to a patterned UV light source and the cells were recovered from the hydrogel. To validate the observed phenotype, genomic analysis of the isolates was done, demonstrating that seven of the resistant strains had the gene mutation (acc locus of the Ti plasmid) that was previously reported. This confirmed the successful application of the platform for connecting observed phenotypes to genotype.

6.1.1.1 Future work

Future work can explore the mechanisms of bacteria degradation in the hydrogel network. We believe the ability of bacteria for colony formation can have several reasons including: (1) Ester hydrolysis in the hydrogel network; it is known that bacteria are able to produce esterase, an enzyme with the ability to hydrolyze esters, which are present in the PEG hydrogel crosslinker here,²⁶² and (2) pH change; metabolic activity of bacteria can also change the pH of the media, and

it is likely that they are able to change the localized pH and affect the hydrolysis.²⁶³ Therefore, it would be beneficial to investigate crosslinking chemistries that offer more stable hydrogels, such as thiol-maleimide, and thiol-vinyl sulfone hydrogels that do not contain ester groups and their susceptibility to bacteria degradation is not well characterized.

6.1.2 Light responsive PEG-based hydrogels for microbial cell isolation with spatiotemporal control.

In this thesis, PEG-based hydrogels incorporated with a light-responsive moiety, *o*-nitrobenzyl, were used for the controlled release of target cells upon light exposure. We investigated the degree of control over the hydrogel degradation and cell release mechanisms. The ability of the light patterning device to project high-resolution patterns for hydrogel degradation was confirmed by using various patterns enabling cell release with different morphology. Release kinetics were investigated to obtain the minimum light dose necessary for cell release for minimizing the DNA damage to the cells by the UV light. DNA quality of the released cells after light exposure was measured, showing that light exposure had no measurable impact on the DNA quality under the light dose used in these studies.

The isolation of individual microbes from a heterogeneous population or community at the single-cell level is critical for discovering and characterizing novel or rare organisms with essential functions. Also, with the advent of single-cell PCR and single-cell genomics, isolation of unculturable microbes for sequencing is an essential but overlooked step for discovering new microbes with unique functions. A new approach to screen and isolate cells at individual levels at high purity and into low (1 nL-1 pL) solution volumes for downstream analysis would serve as a valuable tool for single-cell studies. Micron-scale pattern resolution of the Polygon400 light

patterning tool also enables the potential for release at the single-cell level. A representative image showing the Polygon400 light patterning tool resolution that allows for single cells release from the hydrogels is shown in **Figure 6.1**. However, this result is limited to releasing the single cell into large solution volumes. Coupling these hydrogels with a microfluidic device that can capture single cells into pL water droplets would provide a solution and would offer an approach which would also have a broader impact in biomedical diagnostics, such as recovery of rare cells from blood (e.g., circulating tumor cells, fetal cells, or vascular endothelial cells)

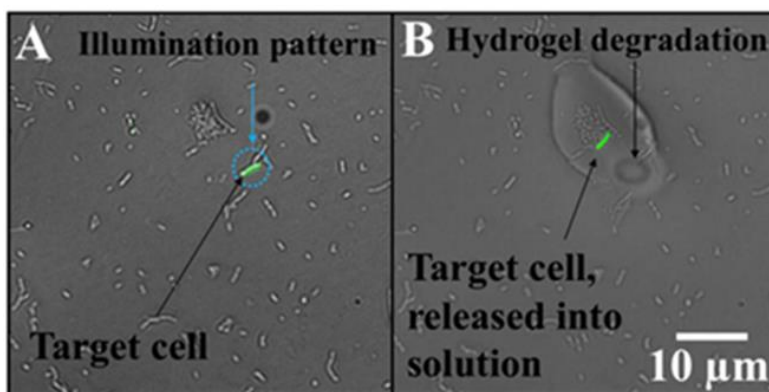


Figure 6.1 Single-cell isolation from the hydrogel. (A) 1:1,000 of fluorescently labeled *E. coli* - FM41:*E. coli* cells captured with the photodegradable hydrogel. The labeled *E. coli* represents the "rare" cell. (B) After identification, targeted cell is isolated in solution.

6.1.2.1 Future work

For future work, the photodegradable hydrogel interfaces previously developed in this thesis can be interfaced with a simple water-oil microfluidic device to isolate a single cell into pL solution volumes. For instance, the hydrogel area can overlay with a PDMS microfluidic device with a channel volume between 10-50 nL. This method could enable the identification of individual cells with rare behavior, which can then be targeted with the patterned illumination tool

for release into the channel. Once suspended in solution, the targeted cell could then be moved downstream of the hydrogel and confined in a water-oil plug using a microfluidic T-junction, commonly used in droplet microfluidics systems, where it can be inspected with microscopy. The high-purity droplet can then be removed from the device for downstream processing.

My second suggestion for future work is to investigate the near-infrared light source as an alternative to the UV light source for cell isolation. For cell release at the single-cell level, due to the need to use higher microscope magnifications such as 40X- 100X, the intensity of the light exposed by the Polygon400 device is extremely high, which could be damaging to the cell. An alternative could be purchasing a near-infrared light source and encapsulating upconversion nanoparticles (UCNPs) within the hydrogels. UCNPs are nanoparticles that can convert low-energy near-infrared (NIR) excitation into ultraviolet emission. Therefore, by entrapping UCNP inside the hydrogel and NIR irradiation, the UCNPs would generate the UV light required for cleaving the *o*-nitrobenzyl groups, enabling hydrogel degradation.

6.2 Hydrogel coatings for covering and protecting anode biofilm of bioelectrochemical systems from environmental pressure.

Cell immobilization techniques have shown to be beneficial to decrease the effect of environmental stressors on microbes. Specifically, using polymers to entrap the electroactive bacteria (EAB) on the anode electrode can provide additional mechanical strength and protect the biofilm. The porous structure of these biomaterials can also allow for nutrient transport to the biofilm, to preserve the biofilm viability. In the last portion of this thesis, we investigated the use of PEG-divinyl sulfone hydrogels for anode biofilm encapsulation and its effect on MEC efficiency. We demonstrated that hydrogel formation through Michael type addition reaction

between thiol and vinyl sulfone groups resulted in a stable hydrogel network. The developed hydrogel was stable in various pH values (pH 3 to pH 10) for over 70 days, confirming their potential for BESs application operating at multiple conditions for a long time. We also investigated the optimum way of depositing the hydrogel coating on the anode biofilm without damaging the biofilm. We showed that cuboid holders can be made from parafilm based on the electrode size to provide a simple encapsulation method. The electrode is placed inside the holder, and hydrogel polymerization occurs within one hour. After the polymerization, the parafilm holder is removed by unwrapping the parafilm sheet from the electrode. The hydrophobicity of parafilm inhibited the attachment of hydrogel solution to the holder, resulting in a clean coating stabilized to the biofilm functionalized anode. Current density response of the coated anode compared to the uncoated anode was monitored overtime to investigate the effect of coating on biofilm metabolic activity. The results showed that in a standard-setting and without an environmental shock, the uncoated electrode had a higher current density, while the coated electrode responded better when the system was introduced to a toxin such as ammonium. We believe reduction in the current density in the standard-setting is likely due to the substrate transport limitation throughout the thick coating. Specially, we hypothesis that the better performance of the coated electrode is due to the hydrogel acting as an ammonium sponge, which impedes ammonium from reaching the biofilm. We believe this is likely due to a dipole–cation binding between the ether group and the positive charge of NH_4^+ , resulting in delaying the NH_4^+ to reach the anode biofilm.

6.2.1 Future work

For future investigation, to take advantage of the full potential of hydrogel coatings for anode biofilm protection, it is vital to address the limitations they face. Achieving thin coatings is challenging and thick hydrogels such as those used here may result in substrate transport limitation,

reducing the current density. Therefore, it is important to explore pathways that can compensate for this limitation to achieve higher yields in BESs.

My first recommendation is including a systematic investigation of MEC performance after coating with hydrogels of different mesh sizes, as this will greatly impact diffusional mass transfer. This is beneficial for finding an optimum mesh size that better allow the substrate transport to the biofilm, while having a good mechanical stability over the course of the operation.

Another method to enhance the performance of these devices is the use of additives to the hydrogel such as enzymes and conductive materials. For example, by coupling enzymes throughout these hydrogels, we can better control the chemical environment at the hydrogel/biofilm interface. Glucose oxidase (GOx) is an enzyme that utilizes oxygen and produces hydrogen peroxide in return.²⁶⁴ Thus, we can couple this enzyme throughout the coating for oxygen depletion to ensure anaerobic conditions. Lactate dehydrogenase (LDH) is another enzyme that can be coupled throughout the coating to break down glucose into organic acids that are readily consumed by bacteria in the biofilm. Therefore, addition of these enzymes can be beneficial for biofilm metabolism which governs the performance of BESs.

Carbon nanotubes (CNTs) are another material that can be incorporated into the coating structure. These materials have been utilized to modify the anode electrode in BES, accelerating electron transfer to enhance the performance. Therefore, we hypothesize that adding this material to the coating could accelerate electron transfer and compensate for the reduction in current density due to the transport limitation, improving the efficiency. Furthermore, CNTs may also serve as an enhancer of the mechanical integrity of the coating, making it more stable.

References

- (1) Okamoto, M.; John, B. Synthetic Biopolymer Nanocomposites for Tissue Engineering Scaffolds. *Progress in Polymer Science*. Elsevier Ltd October 1, 2013, pp 1487–1503. <https://doi.org/10.1016/j.progpolymsci.2013.06.001>.
- (2) Hubbell, J. A. Synthetic Biodegradable Polymers for Tissue Engineering and Drug Delivery. *Curr. Opin. Solid State Mater. Sci.* **1998**, 3 (3), 246–251. [https://doi.org/10.1016/S1359-0286\(98\)80098-3](https://doi.org/10.1016/S1359-0286(98)80098-3).
- (3) Anakwenze, O. A.; Kancherla, V.; Baldwin, K.; Levine, W. N.; Mehta, S. Orthopaedic Residency Applications Increase after Implementation of 80-Hour Workweek General. *Clin. Orthop. Relat. Res.* **2013**, 471 (5), 1720–1724. <https://doi.org/10.1007/s11999-013-2785-1>.
- (4) Weisenberger, M. S.; Deans, T. L. Bottom-up Approaches in Synthetic Biology and Biomaterials for Tissue Engineering Applications. *Journal of Industrial Microbiology and Biotechnology*. Springer Verlag July 1, 2018, pp 599–614. <https://doi.org/10.1007/s10295-018-2027-3>.
- (5) Ergene, C.; Palermo, E. F. Antimicrobial Synthetic Polymers: An Update on Structure-Activity Relationships. *Curr. Pharm. Des.* **2018**, 24 (8), 855–865. <https://doi.org/10.2174/1381612824666180213140732>.
- (6) Mihindikulasuriya, S. D. F.; Lim, L. T. Nanotechnology Development in Food Packaging: A Review. *Trends Food Sci. Technol.* **2014**, 40 (2), 149–167. <https://doi.org/10.1016/j.tifs.2014.09.009>.
- (7) Zhao, S.; Huang, G.; Fu, H.; Wang, Y. Enhanced Coagulation/Flocculation by Combining Diatomite with Synthetic Polymers for Oily Wastewater Treatment. *Sep. Sci. Technol.* **2014**, 49 (7), 999–1007. <https://doi.org/10.1080/01496395.2013.877035>.
- (8) Cisneros, C. G.; Bloemen, V.; Mignon, A. Synthetic, Natural, and Semisynthetic Polymer Carriers for Controlled Nitric Oxide Release in Dermal Applications: A Review. *Polymers*. MDPI AG March 1, 2021, pp 1–26. <https://doi.org/10.3390/polym13050760>.
- (9) Bhatia, S. Natural Polymers vs Synthetic Polymer. In *Natural Polymer Drug Delivery Systems*; Springer International Publishing, 2016; pp 95–118. https://doi.org/10.1007/978-3-319-41129-3_3.
- (10) Bixler, G. D.; Bhushan, B. Review Article: Biofouling: Lessons from Nature. *Philosophical Transactions of the Royal Society A: Mathematical, Physical and Engineering Sciences*. Royal Society May 28, 2012, pp 2381–2417. <https://doi.org/10.1098/rsta.2011.0502>.

- (11) Lowe, S.; O'Brien-Simpson, N. M.; Connal, L. A. Antibiofouling Polymer Interfaces: Poly(Ethylene Glycol) and Other Promising Candidates. *Polymer Chemistry*. Royal Society of Chemistry January 14, 2015, pp 198–212. <https://doi.org/10.1039/c4py01356e>.
- (12) Brzozowska, A. M.; Parra-Velandia, F. J.; Quintana, R.; Xiaoying, Z.; Lee, S. S. C.; Chin-Sing, L.; Jańczewski, D.; Teo, S. L. M.; Vancso, J. G. Biomimicking Micropatterned Surfaces and Their Effect on Marine Biofouling. *Langmuir* **2014**, *30* (30), 9165–9175. <https://doi.org/10.1021/la502006s>.
- (13) Blackman, L. D.; Qu, Y.; Cass, P.; Locoock, K. E. S. Approaches for the Inhibition and Elimination of Microbial Biofilms Using Macromolecular Agents. *Chemical Society Reviews*. Royal Society of Chemistry February 7, 2021, pp 1587–1616. <https://doi.org/10.1039/d0cs00986e>.
- (14) Pasparakis, G.; Alexander, C. Synthetic Polymers for Capture and Detection of Microorganisms. *Analyst*. Royal Society of Chemistry October 22, 2007, pp 1075–1082. <https://doi.org/10.1039/b705097f>.
- (15) Welch, J. D.; Williams, L. A.; DiSalvo, M.; Brandt, A. T.; Marayati, R.; Sims, C. E.; Allbritton, N. L.; Prins, J. F.; Yeh, J. J.; Jones, C. D. Selective Single Cell Isolation for Genomics Using Microraft Arrays. *Nucleic Acids Res.* **2016**, *44* (17), 8292–8301. <https://doi.org/10.1093/nar/gkw700>.
- (16) Li, Y.; Ma, L.; Wu, D.; Chen, G. Advances in Bulk and Single-Cell Multi-Omics Approaches for Systems Biology and Precision Medicine. *Brief. Bioinform.* **2021**. <https://doi.org/10.1093/bib/bbab024>.
- (17) Chintapula, U.; M Iqbal, S.; Kim, Y.-T. A Compendium of Single Cell Analysis in Aging and Disease. *AIMS Mol. Sci.* **2020**, *7* (1), 49–69. <https://doi.org/10.3934/molsci.2020004>.
- (18) Ishii, S.; Tago, K.; Senoo, K. Single-Cell Analysis and Isolation for Microbiology and Biotechnology: Methods and Applications. *Appl. Microbiol. Biotechnol.* **2010**, *86* (5), 1281–1292. <https://doi.org/10.1007/s00253-010-2524-4>.
- (19) Katsuragi, T.; Tani, Y. Screening for Microorganisms with Specific Characteristics by Flow Cytometry and Single-Cell Sorting. *Journal of Bioscience and Bioengineering*. Elsevier Science Publishers B.V. January 1, 2000, pp 217–222. [https://doi.org/10.1016/S1389-1723\(00\)88822-2](https://doi.org/10.1016/S1389-1723(00)88822-2).
- (20) Johns, N. I.; Blazejewski, T.; Gomes, A. L. C.; Wang, H. H. Principles for Designing Synthetic Microbial Communities. *Current Opinion in Microbiology*. Elsevier Ltd June 1, 2016, pp 146–153. <https://doi.org/10.1016/j.mib.2016.03.010>.
- (21) Zhang, X.; Wei, X.; Wei, Y.; Chen, M.; Wang, J. The Up-to-Date Strategies for the Isolation and Manipulation of Single Cells. *Talanta*. Elsevier B.V. October 1, 2020, p 121147. <https://doi.org/10.1016/j.talanta.2020.121147>.
- (22) Parbhoo, T.; Sampson, S. L.; Mouton, J. M. Recent Developments in the Application of

- Flow Cytometry to Advance Our Understanding of Mycobacterium Tuberculosis Physiology and Pathogenesis. *Cytometry Part A*. Wiley-Liss Inc. July 1, 2020, pp 683–693. <https://doi.org/10.1002/cyto.a.24030>.
- (23) Daugherty, P. S.; Iverson, B. L.; Georgiou, G. Flow Cytometric Screening of Cell-Based Libraries. *J. Immunol. Methods* **2000**, *243* (1–2), 211–227. [https://doi.org/10.1016/S0022-1759\(00\)00236-2](https://doi.org/10.1016/S0022-1759(00)00236-2).
- (24) Jennings, C. D.; Foon, K. A. Recent Advances in Flow Cytometry: Application to the Diagnosis of Hematologic Malignancy. *Blood*. American Society of Hematology October 15, 1997, pp 2863–2892. <https://doi.org/10.1182/blood.v90.8.2863>.
- (25) Adan, A.; Alizada, G.; Kiraz, Y.; Baran, Y.; Nalbant, A. Flow Cytometry: Basic Principles and Applications. *Critical Reviews in Biotechnology*. Taylor and Francis Ltd February 17, 2017, pp 163–176. <https://doi.org/10.3109/07388551.2015.1128876>.
- (26) Macey, M. G. Principles of Flow Cytometry. In *Flow Cytometry: Principles and Applications*; Humana Press Inc., 2007; pp 1–15. https://doi.org/10.1007/978-1-59745-451-3_1.
- (27) Rajapaksha, P.; Elbourne, A.; Gangadoo, S.; Brown, R.; Cozzolino, D.; Chapman, J. A Review of Methods for the Detection of Pathogenic Microorganisms. *Analyst*. Royal Society of Chemistry January 21, 2019, pp 396–411. <https://doi.org/10.1039/c8an01488d>.
- (28) Czechowska, K.; Johnson, D. R.; van der Meer, J. R. Use of Flow Cytometric Methods for Single-Cell Analysis in Environmental Microbiology. *Current Opinion in Microbiology*. Elsevier Current Trends June 1, 2008, pp 205–212. <https://doi.org/10.1016/j.mib.2008.04.006>.
- (29) Ishii, S.; Tago, K.; Senoo, K. Single-Cell Analysis and Isolation for Microbiology and Biotechnology: Methods and Applications. *Applied Microbiology and Biotechnology*. Springer May 23, 2010, pp 1281–1292. <https://doi.org/10.1007/s00253-010-2524-4>.
- (30) Hoefel, D.; Monis, P. T.; Grooby, W. L.; Andrews, S.; Saint, C. P. Profiling Bacterial Survival through a Water Treatment Process and Subsequent Distribution System. *J. Appl. Microbiol.* **2005**, *99* (1), 175–186. <https://doi.org/10.1111/j.1365-2672.2005.02573.x>.
- (31) Beggah, S.; Vogne, C.; Zenaro, E.; Van Der Meer, J. R. Mutant HbpR Transcription Activator Isolation for 2-Chlorobiphenyl via Green Fluorescent Protein-Based Flow Cytometry and Cell Sorting. *Microb. Biotechnol.* **2008**, *1* (1), 68–78. <https://doi.org/10.1111/j.1751-7915.2007.00008.x>.
- (32) Matsuyoshi, Y.; Akahoshi, M.; Nakamura, M.; Tatsumi, R.; Mizunoya, W. Isolation and Purification of Satellite Cells from Young Rats by Percoll Density Gradient Centrifugation. In *Methods in Molecular Biology*; Humana Press Inc., 2019; Vol. 1889, pp 81–93. https://doi.org/10.1007/978-1-4939-8897-6_6.
- (33) Wang, Z.; Hansen, O.; Petersen, P. K.; Rogeberg, A.; Kutter, J. P.; Bang, D. D.; Wolff, A.

- Dielectrophoresis Microsystem with Integrated Flow Cytometers for On-Line Monitoring of Sorting Efficiency. *Electrophoresis* **2006**, *27* (24), 5081–5092. <https://doi.org/10.1002/elps.200600422>.
- (34) Zeb, Q.; Wang, C.; Shafiq, S.; Liu, L. An Overview of Single-Cell Isolation Techniques. In *Single-Cell Omics: Volume 1: Technological Advances and Applications*; Elsevier, 2019; pp 101–135. <https://doi.org/10.1016/B978-0-12-814919-5.00006-3>.
- (35) Ma, Z.; Zhou, Y.; Collins, D. J.; Ai, Y. Fluorescence Activated Cell Sorting: Via a Focused Traveling Surface Acoustic Beam. *Lab Chip* **2017**, *17* (18), 3176–3185. <https://doi.org/10.1039/c7lc00678k>.
- (36) DeMello, A. J. Control and Detection of Chemical Reactions in Microfluidic Systems. *Nature*. Nature Publishing Group July 27, 2006, pp 394–402. <https://doi.org/10.1038/nature05062>.
- (37) El-Ali, J.; Sorger, P. K.; Jensen, K. F. Cells on Chips. *Nature*. Nature Publishing Group July 27, 2006, pp 403–411. <https://doi.org/10.1038/nature05063>.
- (38) Psaltis, D.; Quake, S. R.; Yang, C. Developing Optofluidic Technology through the Fusion of Microfluidics and Optics. *Nature*. Nature Publishing Group July 27, 2006, pp 381–386. <https://doi.org/10.1038/nature05060>.
- (39) Thiele, J.; Steinhauser, D.; Pfohl, T.; Förster, S. Preparation of Monodisperse Block Copolymer Vesicles via Flow Focusing in Microfluidics. *Langmuir* **2010**, *26* (9), 6860–6863. <https://doi.org/10.1021/la904163v>.
- (40) Chun, B.; Chun, M. S. Effects of Channel Aspect Ratio on Microfluidic-Chip Design of Hydrodynamic Filtration for Particle Sorting. *J. Phys. D. Appl. Phys.* **2019**, *52* (22). <https://doi.org/10.1088/1361-6463/ab0d78>.
- (41) Asghari, M.; Cao, X.; Mateescu, B.; Van Leeuwen, D.; Aslan, M. K.; Stavarakis, S.; Demello, A. J. Oscillatory Viscoelastic Microfluidics for Efficient Focusing and Separation of Nanoscale Species. *ACS Nano* **2020**, *14* (1), 422–433. <https://doi.org/10.1021/acsnano.9b06123>.
- (42) Costello, C. M.; Yeung, C. L.; Rawson, F. J.; Mendes, P. M. Application of Nanotechnology to Control Bacterial Adhesion and Patterning on Material Surfaces. *Journal of Experimental Nanoscience*. 2012, pp 634–651. <https://doi.org/10.1080/17458080.2012.740640>.
- (43) Andersson, H.; Van den Berg, A. Microfluidic Devices for Cellomics: A Review. *Sensors Actuators, B Chem.* **2003**, *92* (3), 315–325. [https://doi.org/10.1016/S0925-4005\(03\)00266-1](https://doi.org/10.1016/S0925-4005(03)00266-1).
- (44) Chao, T. C.; Ros, A. Microfluidic Single-Cell Analysis of Intracellular Compounds. *Journal of the Royal Society Interface*. Royal Society 2008. <https://doi.org/10.1098/rsif.2008.0233.focus>.

- (45) Zhou, P.; He, J.; Huang, L.; Yu, Z.; Su, Z.; Shi, X.; Zhou, J. Microfluidic High-Throughput Platforms for Discovery of Novel Materials. *Nanomaterials*. MDPI AG December 1, 2020, pp 1–17. <https://doi.org/10.3390/nano10122514>.
- (46) Sohrabi, S.; Kassir, N.; Keshavarz Moraveji, M. Droplet Microfluidics: Fundamentals and Its Advanced Applications. *RSC Adv.* **2020**, *10* (46), 27560–27574. <https://doi.org/10.1039/d0ra04566g>.
- (47) Kaminski, T. S.; Scheler, O.; Garstecki, P. Droplet Microfluidics for Microbiology: Techniques, Applications and Challenges. *Lab on a Chip*. Royal Society of Chemistry June 7, 2016, pp 2168–2187. <https://doi.org/10.1039/c6lc00367b>.
- (48) Guo, M. T.; Rotem, A.; Heyman, J. A.; Weitz, D. A. Droplet Microfluidics for High-Throughput Biological Assays. *Lab on a Chip*. Royal Society of Chemistry June 21, 2012, pp 2146–2155. <https://doi.org/10.1039/c2lc21147e>.
- (49) Huebner, A.; Bratton, D.; Whyte, G.; Yang, M.; Demello, A. J.; Abell, C.; Hollfelder, F. Static Microdroplet Arrays: A Microfluidic Device for Droplet Trapping, Incubation and Release for Enzymatic and Cell-Based Assays. *Lab Chip* **2009**, *9* (5), 692–698. <https://doi.org/10.1039/b813709a>.
- (50) Kaminski, T. S.; Scheler, O.; Garstecki, P. Droplet Microfluidics for Microbiology: Techniques, Applications and Challenges. *Lab on a Chip*. Royal Society of Chemistry June 7, 2016, pp 2168–2187. <https://doi.org/10.1039/c6lc00367b>.
- (51) Vincent, M. E.; Liu, W.; Haney, E. B.; Ismagilov, R. F. Microfluidic Stochastic Confinement Enhances Analysis of Rare Cells by Isolating Cells and Creating High Density Environments for Control of Diffusible Signals. *Chem. Soc. Rev.* **2010**, *39* (3), 974–984. <https://doi.org/10.1039/b917851a>.
- (52) Zhang, D.; Bi, H.; Liu, B.; Qiao, L. Detection of Pathogenic Microorganisms by Microfluidics Based Analytical Methods. *Anal. Chem.* **2018**, *90* (9), 5512–5520. <https://doi.org/10.1021/acs.analchem.8b00399>.
- (53) Zhang, Q.; Lambert, G.; Liao, D.; Kim, H.; Robin, K.; Tung, C. K.; Pourmand, N.; Austin, R. H. Acceleration of Emergence of Bacterial Antibiotic Resistance in Connected Microenvironments. *Science (80-.)*. **2011**, *333* (6050), 1764–1767. <https://doi.org/10.1126/science.1208747>.
- (54) Hu, B.; Xu, P.; Ma, L.; Chen, D.; Wang, J.; Dai, X.; Huang, L.; Du, W. One Cell at a Time: Droplet-Based Microbial Cultivation, Screening and Sequencing. *Mar. Life Sci. Technol.* **2021**, *3* (2), 169–188. <https://doi.org/10.1007/s42995-020-00082-8>.
- (55) Burmeister, A.; Hilgers, F.; Langner, A.; Westerwalbesloh, C.; Kerkhoff, Y.; Tenhaef, N.; Drepper, T.; Kohlheyer, D.; Von Lieres, E.; Noack, S.; Grünberger, A. A Microfluidic Co-Cultivation Platform to Investigate Microbial Interactions at Defined Microenvironments. *Lab Chip* **2019**, *19* (1), 98–110. <https://doi.org/10.1039/c8lc00977e>.

- (56) Pratt, S. L.; Zath, G. K.; Akiyama, T.; Williamson, K. S.; Franklin, M. J.; Chang, C. B. DropSOAC: Stabilizing Microfluidic Drops for Time-Lapse Quantification of Single-Cell Bacterial Physiology. *Front. Microbiol.* **2019**, *10* (SEP), 2112. <https://doi.org/10.3389/fmicb.2019.02112>.
- (57) Krämer, C. E. M.; Singh, A.; Helfrich, S.; Grünberger, A.; Wiechert, W.; Nöh, K.; Kohlheyer, D. Non-Invasive Microbial Metabolic Activity Sensing at Single Cell Level by Perfusion of Calcein Acetoxymethyl Ester. *PLoS One* **2015**, *10* (10). <https://doi.org/10.1371/JOURNAL.PONE.0141768>.
- (58) Mao, H.; Cremer, P. S.; Manson, M. D. A Sensitive, Versatile Microfluidic Assay for Bacterial Chemotaxis. *Proc. Natl. Acad. Sci. U. S. A.* **2003**, *100* (9), 5449–5454. <https://doi.org/10.1073/pnas.0931258100>.
- (59) Boedicker, J. Q.; Vincent, M. E.; Ismagilov, R. F. Microfluidic Confinement of Single Cells of Bacteria in Small Volumes Initiates High-Density Behavior of Quorum Sensing and Growth and Reveals Its Variability. *Angew. Chemie - Int. Ed.* **2009**, *48* (32), 5908–5911. <https://doi.org/10.1002/anie.200901550>.
- (60) Cottinet, D.; Condamine, F.; Bremond, N.; Griffiths, A. D.; Rainey, P. B.; De Visser, J. A. G. M.; Baudry, J.; Bibette, J. Lineage Tracking for Probing Heritable Phenotypes at Single-Cell Resolution. *PLoS One* **2016**, *11* (4). <https://doi.org/10.1371/journal.pone.0152395>.
- (61) Jeong, H. H.; Jin, S. H.; Lee, B. J.; Kim, T.; Lee, C. S. Microfluidic Static Droplet Array for Analyzing Microbial Communication on a Population Gradient. *Lab Chip* **2015**, *15* (3), 889–899. <https://doi.org/10.1039/c4lc01097c>.
- (62) Leung, K.; Zahn, H.; Leaver, T.; Konwar, K. M.; Hanson, N. W.; Pagé, A. P.; Lo, C. C.; Chain, P. S.; Hallam, S. J.; Hansen, C. L. A Programmable Droplet-Based Microfluidic Device Applied to Multiparameter Analysis of Single Microbes and Microbial Communities. *Proc. Natl. Acad. Sci. U. S. A.* **2012**, *109* (20), 7665–7670. <https://doi.org/10.1073/pnas.1106752109>.
- (63) Lim, J. W.; Shin, K. S.; Moon, J.; Lee, S. K.; Kim, T. A Microfluidic Platform for High-Throughput Screening of Small Mutant Libraries. *Anal. Chem.* **2016**, *88* (10), 5234–5242. <https://doi.org/10.1021/acs.analchem.6b00317>.
- (64) Molter, T. W.; McQuaide, S. C.; Suchorolski, M. T.; Strovas, T. J.; Burgess, L. W.; Meldrum, D. R.; Lidstrom, M. E. A Microwell Array Device Capable of Measuring Single-Cell Oxygen Consumption Rates. *Sensors Actuators, B Chem.* **2009**, *135* (2), 678–686. <https://doi.org/10.1016/j.snb.2008.10.036>.
- (65) Meek, C. C.; Pantano, P. Spatial Confinement of Avidin Domains in Microwell Arrays. *Lab Chip* **2001**, *1* (2), 158–163. <https://doi.org/10.1039/b107733c>.
- (66) Zhang, L.; Chen, P.; Zhou, Z.; Hu, Y.; Sha, Q.; Zhang, H.; Liu, X.; Du, W.; Feng, X.; Liu, B. F. Agarose-Based Microwell Array Chip for High-Throughput Screening of Functional

- Microorganisms. *Talanta* **2019**, *191*, 342–349.
<https://doi.org/10.1016/j.talanta.2018.08.090>.
- (67) Lin, C. C.; Metters, A. T. Hydrogels in Controlled Release Formulations: Network Design and Mathematical Modeling. *Advanced Drug Delivery Reviews*. Elsevier November 30, 2006, pp 1379–1408. <https://doi.org/10.1016/j.addr.2006.09.004>.
- (68) Tibbitt, M. W.; Anseth, K. S. Hydrogels as Extracellular Matrix Mimics for 3D Cell Culture. *Biotechnology and Bioengineering*. John Wiley & Sons, Ltd July 1, 2009, pp 655–663. <https://doi.org/10.1002/bit.22361>.
- (69) Ullah, F.; Othman, M. B. H.; Javed, F.; Ahmad, Z.; Akil, H. M. Classification, Processing and Application of Hydrogels: A Review. *Materials Science and Engineering C*. Elsevier Ltd December 1, 2015, pp 414–433. <https://doi.org/10.1016/j.msec.2015.07.053>.
- (70) Fechler, N.; Badi, N.; Schade, K.; Pfeifer, S.; Lutz, J. F. Thermogelation of PEG-Based Macromolecules of Controlled Architecture. *Macromolecules* **2009**, *42* (1), 33–36. <https://doi.org/10.1021/ma8025173>.
- (71) Lutolf, M. P.; Hubbell, J. A. Synthetic Biomaterials as Instructive Extracellular Microenvironments for Morphogenesis in Tissue Engineering. *Nature Biotechnology*. Nature Publishing Group January 1, 2005, pp 47–55. <https://doi.org/10.1038/nbt1055>.
- (72) Veronese, F. M.; Pasut, G. PEGylation, Successful Approach to Drug Delivery. *Drug Discovery Today*. Elsevier Current Trends November 1, 2005, pp 1451–1458. [https://doi.org/10.1016/S1359-6446\(05\)03575-0](https://doi.org/10.1016/S1359-6446(05)03575-0).
- (73) Bryant, S. J.; Nuttelman, C. R.; Anseth, K. S. Cytocompatibility of UV and Visible Light Photoinitiating Systems on Cultured NIH/3T3 Fibroblasts in Vitro. *J. Biomater. Sci. Polym. Ed.* **2000**, *11* (5), 439–457. <https://doi.org/10.1163/156856200743805>.
- (74) Del Grosso, C. A.; Leng, C.; Zhang, K.; Hung, H. C.; Jiang, S.; Chen, Z.; Wilker, J. J. Surface Hydration for Antifouling and Bio-Adhesion. *Chem. Sci.* **2020**, *11* (38), 10367–10377. <https://doi.org/10.1039/d0sc03690k>.
- (75) Pidhatika, B.; Rodenstein, M.; Chen, Y.; Rakhmatullina, E.; Mühlebach, A.; Acikgöz, C.; Textor, M.; Konradi, R. Comparative Stability Studies of Poly(2-Methyl-2-Oxazoline) and Poly(Ethylene Glycol) Brush Coatings. *Biointerphases* **2012**, *7* (1–4), 1–15. <https://doi.org/10.1007/s13758-011-0001-y>.
- (76) Christensen, L. H.; Breiting, V. B.; Aasted, A.; Jørgensen, A.; Kebuladze, I. Long-Term Effects of Polyacrylamide Hydrogel on Human Breast Tissue. *Plast. Reconstr. Surg.* **2003**, *111* (6), 1883–1890. <https://doi.org/10.1097/01.PRS.0000056873.87165.5A>.
- (77) Tuson, H. H.; Renner, L. D.; Weibel, D. B. Polyacrylamide Hydrogels as Substrates for Studying Bacteria. *Chem. Commun.* **2012**, *48* (10), 1595–1597. <https://doi.org/10.1039/c1cc14705f>.

- (78) Maitra, J.; Kumar Shukla, V. Cross-Linking in Hydrogels-A Review. *Am. J. Polym. Sci.* **2014**, *2014* (2), 25–31. <https://doi.org/10.5923/j.ajps.20140402.01>.
- (79) Wu, J.; Zhao, Z.; Hamel, C. M.; Mu, X.; Kuang, X.; Guo, Z.; Qi, H. J. Evolution of Material Properties during Free Radical Photopolymerization. *J. Mech. Phys. Solids* **2018**, *112*, 25–49. <https://doi.org/10.1016/j.jmps.2017.11.018>.
- (80) Papavasiliou, G.; Sonja Sokic, M. T. Synthetic PEG Hydrogels as Extracellular Matrix Mimics for Tissue Engineering Applications; 2012; pp 111–134.
- (81) Schieber, M.; Chandel, N. S. ROS Function in Redox Signaling and Oxidative Stress. *Current Biology*. Cell Press May 19, 2014, pp R453–R462. <https://doi.org/10.1016/j.cub.2014.03.034>.
- (82) Fairbanks, B. D.; Schwartz, M. P.; Bowman, C. N.; Anseth, K. S. Photoinitiated Polymerization of PEG-Diacrylate with Lithium Phenyl-2,4,6-Trimethylbenzoylphosphinate: Polymerization Rate and Cytocompatibility. *Biomaterials* **2009**, *30* (35), 6702–6707. <https://doi.org/10.1016/j.biomaterials.2009.08.055>.
- (83) Nguyen, K. T.; West, J. L. Photopolymerizable Hydrogels for Tissue Engineering Applications. *Biomaterials* **2002**, *23* (22), 4307–4314. [https://doi.org/10.1016/S0142-9612\(02\)00175-8](https://doi.org/10.1016/S0142-9612(02)00175-8).
- (84) Lin, C. C.; Anseth, K. S. PEG Hydrogels for the Controlled Release of Biomolecules in Regenerative Medicine. *Pharmaceutical Research*. Springer March 18, 2009, pp 631–643. <https://doi.org/10.1007/s11095-008-9801-2>.
- (85) Lee, S.; Tong, X.; Yang, F. Effects of the Poly(Ethylene Glycol) Hydrogel Crosslinking Mechanism on Protein Release. *Biomater. Sci.* **2016**, *4* (3), 405–411. <https://doi.org/10.1039/c5bm00256g>.
- (86) Tibbitt, M. W.; Kloxin, A. M.; Sawicki, L. A.; Anseth, K. S. Mechanical Properties and Degradation of Chain and Step-Polymerized Photodegradable Hydrogels. *Macromolecules* **2013**, *46* (7), 2785–2792. <https://doi.org/10.1021/ma302522x>.
- (87) Malkoch, M.; Vestberg, R.; Gupta, N.; Mespouille, L.; Dubois, P.; Mason, A. F.; Hedrick, J. L.; Liao, Q.; Frank, C. W.; Kingsbury, K.; Hawker, C. J. Synthesis of Well-Defined Hydrogel Networks Using Click Chemistry. *Chem. Commun.* **2006**, No. 26, 2774–2776. <https://doi.org/10.1039/b603438a>.
- (88) Echalié, C.; Valot, L.; Martinez, J.; Mehdi, A.; Subra, G. Chemical Cross-Linking Methods for Cell Encapsulation in Hydrogels. *Mater. Today Commun.* **2019**, *20*, 100536. <https://doi.org/10.1016/j.mtcomm.2019.05.012>.
- (89) Mather, B. D.; Viswanathan, K.; Miller, K. M.; Long, T. E. Michael Addition Reactions in Macromolecular Design for Emerging Technologies. *Progress in Polymer Science (Oxford)*. Pergamon May 1, 2006, pp 487–531. <https://doi.org/10.1016/j.progpolymsci.2006.03.001>.

- (90) Gennari, A.; Wedgwood, J.; Lallana, E.; Francini, N.; Tirelli, N. Thiol-Based Michael-Type Addition. A Systematic Evaluation of Its Controlling Factors. *Tetrahedron* **2020**, *76* (47), 131637. <https://doi.org/10.1016/j.tet.2020.131637>.
- (91) Nair, D. P.; Podgórski, M.; Chatani, S.; Gong, T.; Xi, W.; Fenoli, C. R.; Bowman, C. N. The Thiol-Michael Addition Click Reaction: A Powerful and Widely Used Tool in Materials Chemistry. *Chemistry of Materials*. American Chemical Society January 14, 2014, pp 724–744. <https://doi.org/10.1021/cm402180t>.
- (92) Rizzi, S. C.; Hubbell, J. A. Recombinant Protein-Co-PEG Networks as Cell-Adhesive and Proteolytically Degradable Hydrogel Matrixes. Part I: Development and Physicochemical Characteristics. *Biomacromolecules* **2005**, *6* (3), 1226–1238. <https://doi.org/10.1021/bm049614c>.
- (93) Yom-Tov, O.; Seliktar, D.; Bianco-Peled, H. PEG-Thiol Based Hydrogels with Controllable Properties. *Eur. Polym. J.* **2016**, *74*, 1–12. <https://doi.org/10.1016/j.eurpolymj.2015.11.002>.
- (94) Khan, A. H.; Cook, J. K.; Wortmann, W. J.; Kersker, N. D.; Rao, A.; Pojman, J. A.; Melvin, A. T. Synthesis and Characterization of Thiol-Acrylate Hydrogels Using a Base-Catalyzed Michael Addition for 3D Cell Culture Applications. *J. Biomed. Mater. Res. - Part B Appl. Biomater.* **2020**, *108* (5), 2294–2307. <https://doi.org/10.1002/jbm.b.34565>.
- (95) Elbert, D. L.; Pratt, A. B.; Lutolf, M. P.; Halstenberg, S.; Hubbell, J. A. Protein Delivery from Materials Formed by Self-Selective Conjugate Addition Reactions. *J. Control. Release* **2001**, *76* (1–2), 11–25. [https://doi.org/10.1016/S0168-3659\(01\)00398-4](https://doi.org/10.1016/S0168-3659(01)00398-4).
- (96) Elia, R.; Fuegy, P. W.; VanDelden, A.; Firpo, M. A.; Prestwich, G. D.; Peattie, R. A. Stimulation of in Vivo Angiogenesis by in Situ Crosslinked, Dual Growth Factor-Loaded, Glycosaminoglycan Hydrogels. *Biomaterials* **2010**, *31* (17), 4630–4638. <https://doi.org/10.1016/j.biomaterials.2010.02.043>.
- (97) Hermanson, G. *Bioconjugate Techniques*; 2013.
- (98) Jansen, L. E.; Negrón-Piñeiro, L. J.; Galarza, S.; Peyton, S. R. Control of Thiol-Maleimide Reaction Kinetics in PEG Hydrogel Networks. *Acta Biomater.* **2018**, *70*, 120–128. <https://doi.org/10.1016/j.actbio.2018.01.043>.
- (99) Paez, J. I.; Farrukh, A.; Valbuena-Mendoza, R.; Włodarczyk-Biegun, M. K.; Del Campo, A. Thiol-Methylsulfone-Based Hydrogels for 3D Cell Encapsulation. *ACS Appl. Mater. Interfaces* **2020**, *12* (7), 8062–8072. <https://doi.org/10.1021/acsami.0c00709>.
- (100) Kharkar, P. M.; Rehmann, M. S.; Skeens, K. M.; Maverakis, E.; Kloxin, A. M. Thiol-ene Click Hydrogels for Therapeutic Delivery. **2016**. <https://doi.org/10.1021/acsbiomaterials.5b00420>.
- (101) Liu, Y.; Liu, B.; Riesberg, J. J.; Shen, W. In Situ Forming Physical Hydrogels for Three-Dimensional Tissue Morphogenesis. *Macromol. Biosci.* **2011**, *11* (10), 1325–1330.

<https://doi.org/10.1002/mabi.201100119>.

- (102) Soppimath, K. S.; Aminabhavi, T. M.; Dave, A. M.; Kumbar, S. G.; Rudzinski, W. E. Stimulus-Responsive “Smart” Hydrogels as Novel Drug Delivery Systems. *Drug Dev. Ind. Pharm.* **2002**, *28* (8), 957–974. <https://doi.org/10.1081/DDC-120006428>.
- (103) Plunkett, K. N.; Berkowski, K. L.; Moore, J. S. Chymotrypsin Responsive Hydrogel: Application of a Disulfide Exchange Protocol for the Preparation of Methacrylamide Containing Peptides. *Biomacromolecules* **2005**, *6* (2), 632–637. <https://doi.org/10.1021/bm049349v>.
- (104) Bhattarai, N.; Ramay, H. R.; Gunn, J.; Matsen, F. A.; Zhang, M. PEG-Grafted Chitosan as an Injectable Thermosensitive Hydrogel for Sustained Protein Release. *J. Control. Release* **2005**, *103* (3), 609–624. <https://doi.org/10.1016/j.jconrel.2004.12.019>.
- (105) Xu, F. J.; Kang, E. T.; Neoh, K. G. PH- and Temperature-Responsive Hydrogels from Crosslinked Triblock Copolymers Prepared via Consecutive Atom Transfer Radical Polymerizations. *Biomaterials* **2006**, *27* (14), 2787–2797. <https://doi.org/10.1016/j.biomaterials.2006.01.003>.
- (106) Richter, A. *Hydrogels for Actuators*; Springer, Berlin, Heidelberg, 2009; pp 221–248. https://doi.org/10.1007/978-3-540-75645-3_7.
- (107) Serra, L.; Doménech, J.; Peppas, N. A. Drug Transport Mechanisms and Release Kinetics from Molecularly Designed Poly(Acrylic Acid-g-Ethylene Glycol) Hydrogels. *Biomaterials* **2006**, *27* (31), 5440–5451. <https://doi.org/10.1016/j.biomaterials.2006.06.011>.
- (108) Laftah, W. A.; Hashim, S.; Ibrahim, A. N. Polymer Hydrogels: A Review. *Polymer - Plastics Technology and Engineering*. Taylor & Francis Group October 2011, pp 1475–1486. <https://doi.org/10.1080/03602559.2011.593082>.
- (109) Kotsuchibashi, Y. Recent Advances in Multi-Temperature-Responsive Polymeric Materials. *Polymer Journal*. Springer Nature July 1, 2020, pp 681–689. <https://doi.org/10.1038/s41428-020-0330-0>.
- (110) Prabakaran, M.; Mano, J. F. Stimuli-Responsive Hydrogels Based on Polysaccharides Incorporated with Thermo-Responsive Polymers as Novel Biomaterials. *Macromol. Biosci.* **2006**, *6* (12), 991–1008. <https://doi.org/10.1002/mabi.200600164>.
- (111) Guenther, M.; Gerlach, G.; Kuckling, D.; Kretschmer, K.; Corten, C.; Weber, J.; Sorber, J.; Suchanek, G.; Arndt, K.-F. Chemical Sensors Based on Temperature-Responsive Hydrogels. In *Smart Structures and Materials 2006: Smart Sensor Monitoring Systems and Applications*; SPIE, 2006; Vol. 6167, p 61670T. <https://doi.org/10.1117/12.657126>.
- (112) Okabe, K.; Inada, N.; Gota, C.; Harada, Y.; Funatsu, T.; Uchiyama, S. Intracellular Temperature Mapping with a Fluorescent Polymeric Thermometer and Fluorescence Lifetime Imaging Microscopy. *Nat. Commun.* **2012**, *3* (1), 1–9.

<https://doi.org/10.1038/ncomms1714>.

- (113) Kotsuchibashi, Y.; Ebara, M.; Aoyagi, T.; Narain, R. Recent Advances in Dual Temperature Responsive Block Copolymers and Their Potential as Biomedical Applications. *Polymers (Basel)*. **2016**, *8* (11), 380. <https://doi.org/10.3390/polym8110380>.
- (114) Danko, M.; Kroneková, Z.; Mrlik, M.; Osicka, J.; Bin Yousaf, A.; Mihálová, A.; Tkac, J.; Kasak, P. Sulfobetaines Meet Carboxybetaines: Modulation of Thermo- and Ion-Responsivity, Water Structure, Mechanical Properties, and Cell Adhesion. *Langmuir* **2019**, *35* (5), 1391–1403. <https://doi.org/10.1021/acs.langmuir.8b01592>.
- (115) Gupta, P.; Vermani, K.; Garg, S. Hydrogels: From Controlled Release to PH-Responsive Drug Delivery. *Drug Discovery Today*. Elsevier Current Trends May 15, 2002, pp 569–579. [https://doi.org/10.1016/S1359-6446\(02\)02255-9](https://doi.org/10.1016/S1359-6446(02)02255-9).
- (116) Hilmi, B.; Hamid, Z. A. A.; Akil, H. M.; Yahaya, B. H. The Characteristics of the Smart Polymeras Temperature or PH-Responsive Hydrogel. *Procedia Chem.* **2016**, *19*, 406–409. <https://doi.org/10.1016/j.proche.2016.03.031>.
- (117) Xu, L.; Qiu, L.; Sheng, Y.; Sun, Y.; Deng, L.; Li, X.; Bradley, M.; Zhang, R. Biodegradable PH-Responsive Hydrogels for Controlled Dual-Drug Release. *J. Mater. Chem. B* **2018**, *6* (3), 510–517. <https://doi.org/10.1039/c7tb01851g>.
- (118) Patel, N. G.; Zhang, G. Responsive Systems for Cell Sheet Detachment. *Organogenesis* **2013**, *9* (2), 93–100. <https://doi.org/10.4161/org.25149>.
- (119) Yang, H.; Yuan, B.; Zhang, X.; Scherman, O. A. Supramolecular Chemistry at Interfaces: Host-Guest Interactions for Fabricating Multifunctional Biointerfaces. *Acc. Chem. Res.* **2014**, *47* (7), 2106–2115. <https://doi.org/10.1021/ar500105t>.
- (120) Katz, J. S.; Burdick, J. A. Light-Responsive Biomaterials: Development and Applications. *Macromolecular Bioscience*. Macromol Biosci April 8, 2010, pp 339–348. <https://doi.org/10.1002/mabi.200900297>.
- (121) Koetting, M. C.; Peters, J. T.; Steichen, S. D.; Peppas, N. A. Stimulus-Responsive Hydrogels: Theory, Modern Advances, and Applications. *Materials Science and Engineering R: Reports*. Elsevier Ltd June 1, 2015, pp 1–49. <https://doi.org/10.1016/j.mser.2015.04.001>.
- (122) Thomas, S. W. New Applications of Photolabile Nitrobenzyl Groups in Polymers. *Macromol. Chem. Phys.* **2012**, *213* (23), 2443–2449. <https://doi.org/10.1002/macp.201200486>.
- (123) Zhu, H.; Yang, H.; Ma, Y.; Lu, T. J.; Xu, F.; Genin, G. M.; Lin, M. Spatiotemporally Controlled Photoresponsive Hydrogels: Design and Predictive Modeling from Processing through Application. *Advanced Functional Materials*. Wiley-VCH Verlag August 1, 2020, p 2000639. <https://doi.org/10.1002/adfm.202000639>.

- (124) Ozcelik, B. Degradable Hydrogel Systems for Biomedical Applications. In *Biosynthetic Polymers for Medical Applications*; Elsevier Inc., 2016; pp 173–188. <https://doi.org/10.1016/B978-1-78242-105-4.00007-9>.
- (125) Li, L.; Scheiger, J. M.; Levkin, P. A. Design and Applications of Photoresponsive Hydrogels. *Adv. Mater.* **2019**, *31* (26), 1807333. <https://doi.org/10.1002/adma.201807333>.
- (126) Villiou, M.; Paez, J. I.; Del Campo, A. Photodegradable Hydrogels for Cell Encapsulation and Tissue Adhesion. *ACS Appl. Mater. Interfaces* **2020**, *12* (34), 37862–37872. <https://doi.org/10.1021/acsami.0c08568>.
- (127) LeValley, P. J.; Tibbitt, M. W.; Noren, B.; Kharkar, P.; Kloxin, A. M.; Anseth, K. S.; Toner, M.; Oakey, J. Immunofunctional Photodegradable Poly(Ethylene Glycol) Hydrogel Surfaces for the Capture and Release of Rare Cells. *Colloids Surf., B* **2019**, *174*, 483–492. <https://doi.org/10.1016/j.colsurfb.2018.11.049>.
- (128) Shin, D.-S.; You, J.; Rahimian, A.; Vu, T.; Siltanen, C.; Ehsanipour, A.; Stybayeva, G.; Sutcliffe, J.; Revzin, A. Photodegradable Hydrogels for Capture, Detection, and Release of Live Cells. *Angew. Chemie Int. Ed.* **2014**, *53* (31), 8221–8224. <https://doi.org/10.1002/anie.201404323>.
- (129) Griffin, D. R.; Kasko, A. M. Photodegradable Macromers and Hydrogels for Live Cell Encapsulation and Release. *J. Am. Chem. Soc.* **2012**, *134* (31), 13103–13107. <https://doi.org/10.1021/ja305280w>.
- (130) Van Der Vlies, A. J.; Barua, N.; Nieves-Otero, P. A.; Platt, T. G.; Hansen, R. R. On Demand Release and Retrieval of Bacteria from Microwell Arrays Using Photodegradable Hydrogel Membranes. *ACS Appl. Bio Mater.* **2019**, *2* (1), 266–276. <https://doi.org/10.1021/acsabm.8b00592>.
- (131) Barua, N.; Herken, A. M.; Stern, K. R.; Reese, S.; Powers, R. L.; Morrell-Falvey, J. L.; Platt, T. G.; Hansen, R. R. Simultaneous Discovery of Positive and Negative Interactions among Root Microbiome Bacteria Using Microwell Recovery Arrays. *Front. Microbiol.* **2021**, *11*, 3361. <https://doi.org/10.3389/fmicb.2020.601788>.
- (132) Fattahi, N.; Nieves-Otero, P. A.; Masigol, M.; Van der Vlies, A. J.; Jensen, R. S.; Hansen, R. R.; Platt, T. G. Photodegradable Hydrogels for Rapid Screening, Isolation, and Genetic Characterization of Bacteria with Rare Phenotypes. *Biomacromolecules* **2020**. <https://doi.org/10.1021/acs.biomac.0c00543>.
- (133) Gul, M. M.; Ahmad, K. S. Bioelectrochemical Systems: Sustainable Bio-Energy Powerhouses. *Biosensors and Bioelectronics*. Elsevier Ltd October 1, 2019, p 111576. <https://doi.org/10.1016/j.bios.2019.111576>.
- (134) Ghangrekar, M. M.; Chatterjee, P. A Systematic Review on Bioelectrochemical Systems Research. *Current Pollution Reports*. Springer December 1, 2017, pp 281–288. <https://doi.org/10.1007/s40726-017-0071-7>.

- (135) Kelly, P. T.; He, Z. Nutrients Removal and Recovery in Bioelectrochemical Systems: A Review. *Bioresource Technology*. Elsevier Ltd February 1, 2014, pp 351–360. <https://doi.org/10.1016/j.biortech.2013.12.046>.
- (136) Sleutels, T. H. J. A.; Ter Heijne, A.; Buisman, C. J. N.; Hamelers, H. V. M. Bioelectrochemical Systems: An Outlook for Practical Applications. *ChemSusChem*. Wiley-VCH Verlag June 1, 2012, pp 1012–1019. <https://doi.org/10.1002/cssc.201100732>.
- (137) Kadier, A.; Kalil, M. S.; Chandrasekhar, K.; Mohanakrishna, G.; Saratale, G. D.; Saratale, R. G.; Kumar, G.; Pugazhendhi, A.; Sivagurunathan, P. Surpassing the Current Limitations of High Purity H₂ Production in Microbial Electrolysis Cell (MECs): Strategies for Inhibiting Growth of Methanogens. *Bioelectrochemistry*. Elsevier B.V. February 1, 2018, pp 211–219. <https://doi.org/10.1016/j.bioelechem.2017.09.014>.
- (138) Wilberforce, T.; Sayed, E. T.; Abdelkareem, M. A.; Elsaid, K.; Olabi, A. G. Value Added Products from Wastewater Using Bioelectrochemical Systems: Current Trends and Perspectives. *J. Water Process Eng.* **2021**, *39*, 101737. <https://doi.org/10.1016/j.jwpe.2020.101737>.
- (139) Sleutels, T. H. J. A.; Ter Heijne, A.; Buisman, C. J. N.; Hamelers, H. V. M. Bioelectrochemical Systems: An Outlook for Practical Applications. *ChemSusChem*. Wiley-VCH Verlag 2012, pp 1012–1019. <https://doi.org/10.1002/cssc.201100732>.
- (140) Shi, J.; Zhao, S.; Yu, X.; Zhou, T.; Khan, A.; Yu, Z.; Feng, P.; Wang, J.; Liu, P.; Li, X. Enhanced Performance of Sediment Microbial Fuel Cell by Immobilization of *Shewanella Oneidensis* MR-1 on an Anode Surface. *Int. J. Hydrogen Energy* **2019**, *44* (20), 10091–10101. <https://doi.org/10.1016/j.ijhydene.2018.11.225>.
- (141) Borole, A. P.; Reguera, G.; Ringeisen, B.; Wang, Z. W.; Feng, Y.; Kim, B. H. Electroactive Biofilms: Current Status and Future Research Needs. *Energy and Environmental Science*. The Royal Society of Chemistry December 22, 2011, pp 4813–4834. <https://doi.org/10.1039/c1ee02511b>.
- (142) Gandu, B.; Rozenfeld, S.; Ouaknin Hirsch, L.; Schechter, A.; Cahan, R. Immobilization of Bacterial Cells on Carbon-Cloth Anode Using Alginate for Hydrogen Generation in a Microbial Electrolysis Cell. *J. Power Sources* **2020**, *455*, 227986. <https://doi.org/10.1016/j.jpowsour.2020.227986>.
- (143) Du, Q.; Li, T.; Li, N.; Wang, X. Protection of Electroactive Biofilm from Extreme Acid Shock by Polydopamine Encapsulation. *Environ. Sci. Technol. Lett.* **2017**, *4* (8), 345–349. <https://doi.org/10.1021/acs.estlett.7b00242>.
- (144) Zhang, Y.; Sun, J.; Hu, Y.; Wang, Z.; Li, S. Effects of Periodically Alternating Temperatures on Performance of Single-Chamber Microbial Fuel Cells. *Int. J. Hydrogen Energy* **2014**, *39* (15), 8048–8054. <https://doi.org/10.1016/j.ijhydene.2014.03.110>.
- (145) Wang, J.; Liu, Q.; Wu, B.; Hu, H.; Dong, D.; Yin, J.; Ren, H. Effect of Salinity on Mature Wastewater Treatment Biofilm Microbial Community Assembly and Metabolite

- Characteristics. *Sci. Total Environ.* **2020**, *711*, 134437.
<https://doi.org/10.1016/j.scitotenv.2019.134437>.
- (146) Alkayyali, T.; Cameron, T.; Haltli, B.; Kerr, R. G.; Ahmadi, A. Microfluidic and Cross-Linking Methods for Encapsulation of Living Cells and Bacteria - A Review. *Analytica Chimica Acta*. Elsevier B.V. April 11, 2019, pp 1–21.
<https://doi.org/10.1016/j.aca.2018.12.056>.
- (147) Luo, H.; Yu, S.; Liu, G.; Zhang, R.; Teng, W. Effect of In-Situ Immobilized Anode on Performance of the Microbial Fuel Cell with High Concentration of Sodium Acetate. *Fuel* **2016**, *182*, 732–739. <https://doi.org/10.1016/j.fuel.2016.06.032>.
- (148) Roy, S.; Pandit, S. Microbial Electrochemical System: Principles and Application. In *Biomass, Biofuels, Biochemicals: Microbial Electrochemical Technology: Sustainable Platform for Fuels, Chemicals and Remediation*; Elsevier, 2018; pp 19–48.
<https://doi.org/10.1016/B978-0-444-64052-9.00002-9>.
- (149) Xu, M.; Li, J.; Liu, B.; Yang, C.; Hou, H.; Hu, J.; Yang, J.; Xiao, K.; Liang, S.; Wang, D. The Evaluation of Long Term Performance of Microbial Fuel Cell Based Pb Toxicity Shock Sensor. *Chemosphere* **2021**, *270*.
<https://doi.org/10.1016/j.chemosphere.2020.129455>.
- (150) Welch, J. D.; Williams, L. A.; DiSalvo, M.; Brandt, A. T.; Marayati, R.; Sims, C. E.; Allbritton, N. L.; Prins, J. F.; Yeh, J. J.; Jones, C. D. Selective Single Cell Isolation for Genomics Using Microarray Arrays. *Nucleic Acids Res.* **2016**, *44* (17), 8292–8301.
<https://doi.org/10.1093/nar/gkw700>.
- (151) Blainey, P. C. The Future Is Now: Single-Cell Genomics of Bacteria and Archaea. *FEMS Microbiology Reviews*. John Wiley & Sons, Ltd May 1, 2013, pp 407–427.
<https://doi.org/10.1111/1574-6976.12015>.
- (152) Swennenhuis, J. F.; Tibbe, A. G. J.; Stevens, M.; Katika, M. R.; Van Dalum, J.; Duy Tong, H.; Van Rijn, C. J. M.; Terstappen, L. W. M. M. Self-Seeding Microwell Chip for the Isolation and Characterization of Single Cells. *Lab Chip* **2015**, *15* (14), 3039–3046.
<https://doi.org/10.1039/c5lc00304k>.
- (153) Shrirao, A. B.; Fritz, Z.; Novik, E. M.; Yarmush, G. M.; Schloss, R. S.; Zahn, J. D.; Yarmush, M. L. Microfluidic Flow Cytometry: The Role of Microfabrication Methodologies, Performance and Functional Specification. *TECHNOLOGY* **2018**, *06* (01), 1–23. <https://doi.org/10.1142/s2339547818300019>.
- (154) Nichols, D.; Cahoon, N.; Trakhtenberg, E. M.; Pham, L.; Mehta, A.; Belanger, A.; Kanigan, T.; Lewis, K.; Epstein, S. S. Use of Ichip for High-Throughput in Situ Cultivation of "uncultivable Microbial Species". *Appl. Environ. Microbiol.* **2010**, *76* (8), 2445–2450. <https://doi.org/10.1128/AEM.01754-09>.
- (155) Oliver, J. D. Recent Findings on the Viable but Nonculturable State in Pathogenic Bacteria. *FEMS Microbiology Reviews*. Blackwell Publishing Ltd 2010, pp 415–425.

<https://doi.org/10.1111/j.1574-6976.2009.00200.x>.

- (156) Zhao, X.; Zhong, J.; Wei, C.; Lin, C. W.; Ding, T. Current Perspectives on Viable but Non-Culturable State in Foodborne Pathogens. *Frontiers in Microbiology*. Frontiers Research Foundation April 4, 2017, p 580. <https://doi.org/10.3389/fmicb.2017.00580>.
- (157) Wang, X.; Gou, X.; Chen, S.; Yan, X.; Sun, D. Cell Manipulation Tool with Combined Microwell Array and Optical Tweezers for Cell Isolation and Deposition. *J. Micromechanics Microengineering* **2013**, *23* (7), 075006. <https://doi.org/10.1088/0960-1317/23/7/075006>.
- (158) Kloxin, A. M.; Kasko, A. M.; Salinas, C. N.; Anseth, K. S. Photodegradable Hydrogels for Dynamic Tuning of Physical and Chemical Properties. *Science* (80-.). **2009**, *324* (5923), 59–63. <https://doi.org/10.1126/science.1169494>.
- (159) Masigol, M.; Barua, N.; Retterer, S. T.; Lokitz, B. S.; Hansen, R. R. Chemical Copatterning Strategies Using Azlactone-Based Block Copolymers. *J. Vac. Sci. Technol. B, Nanotechnol. Microelectron. Mater. Process. Meas. Phenom.* **2017**, *35* (6), 06GJ01. <https://doi.org/10.1116/1.4991881>.
- (160) Masigol, M.; Barua, N.; Lokitz, B. S.; Hansen, R. R. Fabricating Reactive Surfaces with Brush-like and Crosslinked Films of Azlactone-Functionalized Block Co-Polymers. *J. Vis. Exp.* **2018**, *2018* (136), 1–10. <https://doi.org/10.3791/57562>.
- (161) Timm, A. C.; Halsted, M. C.; Wilmoth, J. L.; Retterer, S. T. Assembly and Tracking of Microbial Community Development within a Microwell Array Platform. *J. Vis. Exp.* **2017**, No. 124, 6:e55701. <https://doi.org/10.3791/55701>.
- (162) Shokrzadeh, M.; Mohammadpour, A. Evaluation of a Modified Salt-out Method for DNA Extraction from Whole Blood Lymphocytes: A Simple and Economical Method for Gene Polymorphism. *Pharm. Biomed. Res.* **2018**, *4* (2), 28. <https://doi.org/10.18502/pbr.v4i2.218>.
- (163) Hansen, R. H.; Timm, A. C.; Timm, C. M.; Bible, A. N.; Morrell-Falvey, J. L.; Pelletier, D. A.; Simpson, M. L.; Doktycz, M. J.; Retterer, S. T. Stochastic Assembly of Bacteria in Microwell Arrays Reveals the Importance of Confinement in Community Development. *PLoS One* **2016**, *11* (5), e0155080. <https://doi.org/10.1371/journal.pone.0155080>.
- (164) Halsted, M.; Wilmoth, J. L.; Briggs, P. A.; Hansen, R. R.; Briggs, D. P.; Timm, A. C.; Retterer, S. T. Development of Transparent Microwell Arrays for Optical Monitoring and Dissection of Microbial Communities. *J. Vac. Sci. Technol. B, Nanotechnol. Microelectron. Mater. Process. Meas. Phenom.* **2016**, *34* (6), 06KI03. <https://doi.org/10.1116/1.4962739>.
- (165) Holland, S. L.; Reader, T.; Dyer, P. S.; Avery, S. V. Phenotypic Heterogeneity Is a Selected Trait in Natural Yeast Populations Subject to Environmental Stress. *Environ. Microbiol.* **2014**, *16* (6), 1729–1740. <https://doi.org/10.1111/1462-2920.12243>.

- (166) Huys, G. R.; Raes, J. Go with the Flow or Solitary Confinement: A Look inside the Single-Cell Toolbox for Isolation of Rare and Uncultured Microbes. *Curr. Opin. Microbiol* **2018**, *44*, 1–8. <https://doi.org/10.1016/j.mib.2018.05.002>.
- (167) Brehm-Stecher, B. F.; Johnson, E. A. Single-Cell Microbiology: Tools, Technologies, and Applications. *Microbiol. Mol. Biol. Rev.* **2004**, *68* (3), 538–559. <https://doi.org/10.1128/MMBR.68.3.538-559.2004>.
- (168) Czechowska, K.; ... D. J.-C. opinion in; 2008, undefined. Use of Flow Cytometric Methods for Single-Cell Analysis in Environmental Microbiology. *Elsevier*.
- (169) Faraghat, S. A.; Hoettges, K. F.; Steinbach, M. K.; Van Der Veen, D. R.; Brackenbury, W. J.; Henslee, E. A.; Labeed, F. H.; Hughes, M. P. High-Throughput, Low-Loss, Low-Cost, and Label-Free Cell Separation Using Electrophysiology-Activated Cell Enrichment. *Proc. Natl. Acad. Sci. U. S. A.* **2017**, *114* (18), 4591–4596. <https://doi.org/10.1073/pnas.1700773114>.
- (170) Tatematsu, K.; Kuroda, S. Automated Single-Cell Analysis and Isolation System: A Paradigm Shift in Cell Screening Methods for Bio-Medicines. In *Advances in Experimental Medicine and Biology*; Springer New York LLC, 2018; Vol. 1068, pp 7–17. https://doi.org/10.1007/978-981-13-0502-3_2.
- (171) DeMello, A. J. Control and Detection of Chemical Reactions in Microfluidic Systems. *Nature* **2006**, *442* (7101), 394–402. <https://doi.org/10.1038/nature05062>.
- (172) El-Ali, J.; Sorger, P. K.; Jensen, K. F. Cells on Chips. *Nature* **2006**, *442* (7101), 403–411. <https://doi.org/10.1038/nature05063>.
- (173) Psaltis, D.; Quake, S. R.; Yang, C. Developing Optofluidic Technology through the Fusion of Microfluidics and Optics. *Nature* **2006**, *442* (7101), 381–386. <https://doi.org/10.1038/nature05060>.
- (174) Kou, S.; Cheng, D.; Sun, F.; Hsing, I. M. Microfluidics and Microbial Engineering. *Lab Chip* **2016**, *16* (3), 432–446. <https://doi.org/10.1039/c5lc01039j>.
- (175) Nam, S.; Stowers, R.; Lou, J.; Xia, Y.; Biomaterials, O. C.-; 2019, undefined. Varying PEG Density to Control Stress Relaxation in Alginate-PEG Hydrogels for 3D Cell Culture Studies. *Elsevier*.
- (176) Sergeeva, A.; Vikulina, A. S.; Volodkin, D. Porous Alginate Scaffolds Assembled Using Vaterite CaCO₃ Crystals. *Micromachines* **2019**, *10* (6), 357. <https://doi.org/10.3390/mi10060357>.
- (177) Duarte, J. M.; Barbier, I.; Schaerli, Y. Bacterial Microcolonies in Gel Beads for High-Throughput Screening of Libraries in Synthetic Biology. *ACS Synth. Biol.* **2017**, *6* (11), 1988–1995. <https://doi.org/10.1021/acssynbio.7b00111>.
- (178) Connell, J. L.; Ritschdorff, E. T.; Whiteley, M.; Shear, J. B. 3D Printing of Microscopic

- Bacterial Communities. **2013**, *110* (46), 18380–18385.
<https://doi.org/10.1073/pnas.1309729110>.
- (179) Zengler, K.; Toledo, G.; Rappé, M.; Elkins, J.; Mathur, E. J.; Short, J. M.; Keller, M. Cultivating the Uncultured. *Proc. Natl. Acad. Sci. U. S. A.* **2002**, *99* (24), 15681–15686.
<https://doi.org/10.1073/pnas.252630999>.
- (180) Kloxin, A. M.; Tibbitt, M. W.; Anseth, K. S. Synthesis of Photodegradable Hydrogels as Dynamically Tunable Cell Culture Platforms. *Nat. Protoc.* **2010**, *5* (12), 1867–1887.
<https://doi.org/10.1038/nprot.2010.139>.
- (181) Peppas, N. A.; Hilt, J. Z.; Khademhosseini, A.; Langer, R. Hydrogels in Biology and Medicine: From Molecular Principles to Bionanotechnology. *Adv. Mater.* **2006**, *18* (11), 1345–1360. <https://doi.org/10.1002/adma.200501612>.
- (182) Harrison, J.; Studholme, D. J. Recently Published Streptomyces Genome Sequences. *Microb. Biotechnol.* **2014**, *7* (5), 373–380. <https://doi.org/10.1111/1751-7915.12143>.
- (183) Reader, J. S.; Ordoukhanian, P. T.; Kim, J. C.; De Crécy-Lagard, V.; Hwang, I.; Farrand, S.; Schimmel, P. Virology: Major Biocontrol of Plant Tumors Targets TRNA Synthetase. *Science (80-.)*. **2005**, *309* (5740), 1533. <https://doi.org/10.1126/science.1116841>.
- (184) Holsters, M.; de Waele, D.; Depicker, A.; Messens, E.; van Montagu, M.; Schell, J. Transfection and Transformation of Agrobacterium Tumefaciens. *Mol. Gen. Genet.* **1978**, *163* (2), 181–187. <https://doi.org/10.1007/BF00267408>.
- (185) Tempe, J.; Petit, A.; Holsters, M.; Montagu, M. v.; Schell, J. Thermosensitive Step Associated with Transfer of the Ti Plasmid during Conjugation: Possible Relation to Transformation in Crown Gall. *Proc. Natl. Acad. Sci. U. S. A.* **1977**, *74* (7), 2848–2849.
<https://doi.org/10.1073/pnas.74.7.2848>.
- (186) Lampe, D. J.; Akerley, B. J.; Rubin, E. J.; Mekalanos, J. J.; Robertson, H. M. Hyperactive Transposase Mutants of the Himar1 Mariner Transposon. *Proc. Natl. Acad. Sci. U. S. A.* **1999**, *96* (20), 11428–11433. <https://doi.org/10.1073/pnas.96.20.11428>.
- (187) Watson, B.; Currier, T. C.; Gordon, M. P.; Chilton, M. D.; Nester, E. W. Plasmid Required for Virulence of Agrobacterium Tumefaciens. *J. Bacteriol.* **1975**, *123* (1), 255–264. <https://doi.org/10.1128/jb.123.1.255-264.1975>.
- (188) Danhorn, T.; Hentzer, M.; Givskov, M.; Parsek, M. R.; Fuqua, C. Phosphorus Limitation Enhances Biofilm Formation of the Plant Pathogen Agrobacterium Tumefaciens through the PhoR-PhoB Regulatory System. *J. Bacteriol.* **2004**, *186* (14), 4492–4501.
<https://doi.org/10.1128/JB.186.14.4492-4501.2004>.
- (189) Kerr, A.; Htay, K. Biological Control of Crown Gall through Bacteriocin Production. *Physiol. Plant Pathol.* **1974**, *4* (1), 37–44. [https://doi.org/10.1016/0048-4059\(74\)90042-3](https://doi.org/10.1016/0048-4059(74)90042-3).
- (190) Cormack, B. P.; Valdivia, R. H.; Falkow, S. FACS-Optimized Mutants of the Green

- Fluorescent Protein (GFP). In *Gene*; Elsevier B.V., 1996; Vol. 173, pp 33–38.
[https://doi.org/10.1016/0378-1119\(95\)00685-0](https://doi.org/10.1016/0378-1119(95)00685-0).
- (191) Grant, W. M.; Thomas, C. C. Toxicology of the Eye, Third Edition. *Cutan. Ocul. Toxicol.* **1987**, *6* (2), 155–156. <https://doi.org/10.3109/15569528709052171>.
- (192) Khire, V. S.; Lee, T. Y.; Bowman, C. N. Surface Modification Using Thiol–Acrylate Conjugate Addition Reactions. *Macromolecules* **2007**, *40* (16), 5669–5677.
<https://doi.org/10.1021/ma070146j>.
- (193) Hu, M.; Noda, S.; Okubo, T.; Yamaguchi, Y.; Komiyama, H. Structure and Morphology of Self-Assembled 3-Mercaptopropyltrimethoxysilane Layers on Silicon Oxide. *Appl. Surf. Sci.* **2001**, *181* (3–4), 307–316. [https://doi.org/10.1016/S0169-4332\(01\)00399-3](https://doi.org/10.1016/S0169-4332(01)00399-3).
- (194) Sprouffske, K.; Wagner, A. Growthcurver: An R Package for Obtaining Interpretable Metrics from Microbial Growth Curves. *BMC Bioinf.* **2016**, *17* (1), 172.
<https://doi.org/10.1186/s12859-016-1016-7>.
- (195) Baldwin, A. D.; Kiick, K. L. Tunable Degradation of Maleimide–Thiol Adducts in Reducing Environments. *Bioconjug. Chem.* **2011**, *22* (10), 1946–1953.
<https://doi.org/10.1021/bc200148v>.
- (196) Masigol, M.; Fattahi, N.; Barua, N.; Lokitz, B. S.; Retterer, S. T.; Platt, T. G.; Hansen, R. R. Identification of Critical Surface Parameters Driving Lectin-Mediated Capture of Bacteria from Solution. *Biomacromolecules* **2019**, *20* (7), 2852–2863.
<https://doi.org/10.1021/acs.biomac.9b00609>.
- (197) Hayman, G. T.; Farrand, S. K. Characterization and Mapping of the Agrocinopine-Agrocin 84 Locus on the Nopaline Ti Plasmid PTiC58. *J. Bacteriol.* **1988**, *170* (4), 1759–1767. <https://doi.org/10.1128/jb.170.4.1759-1767.1988>.
- (198) Hayman, G. T.; Von Bodman, S. B.; Kim, H.; Jiang, P.; Farrand, S. K. Genetic Analysis of the Agrocinopine Catabolic Region of *Agrobacterium tumefaciens* Ti Plasmid PTiC58, Which Encodes Genes Required for Opine and Agrocin 84 Transport. *J. Bacteriol.* **1993**, *175* (17), 5575–5584. <https://doi.org/10.1128/jb.175.17.5575-5584.1993>.
- (199) Li, H.; Durbin, R. Fast and Accurate Short Read Alignment with Burrows-Wheeler Transform. *Bioinformatics* **2009**, *25* (14), 1754–1760.
<https://doi.org/10.1093/bioinformatics/btp324>.
- (200) McKenna, A.; Hanna, M.; Banks, E.; Sivachenko, A.; Cibulskis, K.; Kernytzky, A.; Garimella, K.; Altshuler, D.; Gabriel, S.; Daly, M.; DePristo, M. A. The Genome Analysis Toolkit: A MapReduce Framework for Analyzing next-Generation DNA Sequencing Data. *Genome Res.* **2010**, *20* (9), 1297–1303. <https://doi.org/10.1101/gr.107524.110>.
- (201) Allardet-Servent, A.; Michaux-Charachon, S.; Jumas-Bilak, E.; Karayan, L.; Ramuz, M. Presence of One Linear and One Circular Chromosome in the *Agrobacterium tumefaciens* C58 Genome. *J. Bacteriol.* **1993**, *175* (24), 7869–7874.

<https://doi.org/10.1128/jb.175.24.7869-7874.1993>.

- (202) Sambrook, J.; Russell, D. *Molecular Cloning: A Laboratory Manual Fourth Edition* Ed Cold Spring Harbor. **2001**.
- (203) Weber, L. M.; Lopez, C. G.; Anseth, K. S. Effects of PEG Hydrogel Crosslinking Density on Protein Diffusion and Encapsulated Islet Survival and Function. *J. Biomed. Mater. Res. Part A* **2009**, *90A* (3), 720–729. <https://doi.org/10.1002/jbm.a.32134>.
- (204) Canal, T.; Peppas, N. A. Correlation between Mesh Size and Equilibrium Degree of Swelling of Polymeric Networks. *J. Biomed. Mater. Res.* **1989**, *23* (10), 1183–1193. <https://doi.org/10.1002/jbm.820231007>.
- (205) Zustiak, S. P.; Leach, J. B. Hydrolytically Degradable Poly(Ethylene Glycol) Hydrogel Scaffolds with Tunable Degradation and Mechanical Properties. *Biomacromolecules* **2010**, *11* (5), 1348–1357. <https://doi.org/10.1021/bm100137q>.
- (206) Metters, A.; Hubbell, J. Network Formation and Degradation Behavior of Hydrogels Formed by Michael-Type Addition Reactions. *Biomacromolecules* **2005**, *6* (1), 290–301. <https://doi.org/10.1021/bm049607o>.
- (207) Hayman, G. T.; Farrand, S. K. Agrobacterium Plasmids Encode Structurally and Functionally Different Loci for Catabolism of Agrocinopine-Type Opines. *Mol. Gen. Genet.* **1990**, *223* (3), 465–473. <https://doi.org/10.1007/BF00264455>.
- (208) Kim, H.; Farrand, S. K. Characterization of the Acc Operon from the Nopaline-Type Ti Plasmid PTiC58, Which Encodes Utilization of Agrocinopines A and B and Susceptibility to Agrocin 84. *J. Bacteriol.* **1997**, *179* (23), 7559–7572. <https://doi.org/10.1128/jb.179.23.7559-7572.1997>.
- (209) Connon, S. A.; Giovannoni, S. J. High-Throughput Methods for Culturing Microorganisms in Very-Low-Nutrient Media Yield Diverse New Marine Isolates. *Appl. Environ. Microbiol.* **2002**, *68* (8), 3878–3885. <https://doi.org/10.1128/AEM.68.8.3878-3885.2002>.
- (210) Hindatu, Y.; Annuar, M. S. M.; Gumel, A. M. Mini-Review: Anode Modification for Improved Performance of Microbial Fuel Cell. *Renewable and Sustainable Energy Reviews*. Elsevier Ltd June 1, 2017, pp 236–248. <https://doi.org/10.1016/j.rser.2017.01.138>.
- (211) Watanabe, K. Recent Developments in Microbial Fuel Cell Technologies for Sustainable Bioenergy. *J. Biosci. Bioeng.* **2008**, *106* (6), 528–536. <https://doi.org/10.1263/jbb.106.528>.
- (212) Rahimnejad, M.; Adhami, A.; Darvari, S.; Zirepour, A.; Oh, S. E. Microbial Fuel Cell as New Technology for Bioelectricity Generation: A Review. *Alexandria Engineering Journal*. Elsevier B.V. September 1, 2015, pp 745–756. <https://doi.org/10.1016/j.aej.2015.03.031>.

- (213) Call, D.; Logan, B. E. Hydrogen Production in a Single Chamber Microbial Electrolysis Cell Lacking a Membrane. *Environ. Sci. Technol.* **2008**, *42* (9), 3401–3406. <https://doi.org/10.1021/es8001822>.
- (214) Ge, Z.; Chen, X.; Huang, X.; Ren, Z. J. Capacitive Deionization for Nutrient Recovery from Wastewater with Disinfection Capability. *Environ. Sci. Water Res. Technol.* **2018**, *4* (1), 33–39. <https://doi.org/10.1039/c7ew00350a>.
- (215) Li, N.; Wan, Y.; Wang, X. Nutrient Conversion and Recovery from Wastewater Using Electroactive Bacteria. *Science of the Total Environment*. Elsevier B.V. March 1, 2020, p 135690. <https://doi.org/10.1016/j.scitotenv.2019.135690>.
- (216) Deng, H.; Jiang, Y. B.; Zhou, Y. W.; Shen, K.; Zhong, W. H. Using Electrical Signals of Microbial Fuel Cells to Detect Copper Stress on Soil Microorganisms. *Eur. J. Soil Sci.* **2015**, *66* (2), 369–377. <https://doi.org/10.1111/ejss.12215>.
- (217) Jiang, Y.; Yang, X.; Liang, P.; Liu, P.; Huang, X. Microbial Fuel Cell Sensors for Water Quality Early Warning Systems: Fundamentals, Signal Resolution, Optimization and Future Challenges. *Renewable and Sustainable Energy Reviews*. Elsevier Ltd January 1, 2018, pp 292–305. <https://doi.org/10.1016/j.rser.2017.06.099>.
- (218) Sonawane, J. M.; Ezugwu, C. I.; Ghosh, P. C. Microbial Fuel Cell-Based Biological Oxygen Demand Sensors for Monitoring Wastewater: State-of-the-Art and Practical Applications. *ACS Sensors* **2020**, *5* (8), 2297–2316. <https://doi.org/10.1021/acssensors.0c01299>.
- (219) Cao, M.; Feng, Y.; Wang, N.; Li, Y.; Li, N.; Liu, J.; He, W. Electrochemical Regulation on the Metabolism of Anode Biofilms under Persistent Exogenous Bacteria Interference. *Electrochim. Acta* **2020**, *340*. <https://doi.org/10.1016/j.electacta.2020.135922>.
- (220) Borole, A. P.; Reguera, G.; Ringeisen, B.; Wang, Z. W.; Feng, Y.; Kim, B. H. Electroactive Biofilms: Current Status and Future Research Needs. *Energy and Environmental Science*. The Royal Society of Chemistry December 22, 2011, pp 4813–4834. <https://doi.org/10.1039/c1ee02511b>.
- (221) Yang, X. Y.; Tian, G.; Jiang, N.; Su, B. L. Immobilization Technology: A Sustainable Solution for Biofuel Cell Design. *Energy and Environmental Science*. The Royal Society of Chemistry February 25, 2012, pp 5540–5563. <https://doi.org/10.1039/c1ee02391h>.
- (222) Pan, J.; Hu, J.; Liu, B.; Li, J.; Wang, D.; Bu, C.; Wang, X.; Xiao, K.; Liang, S.; Yang, J.; Hou, H. Enhanced Quorum Sensing of Anode Biofilm for Better Sensing Linearity and Recovery Capability of Microbial Fuel Cell Toxicity Sensor. *Environ. Res.* **2020**, *181*, 108906. <https://doi.org/10.1016/j.envres.2019.108906>.
- (223) Du, Q.; Li, T.; Li, N.; Wang, X. Protection of Electroactive Biofilm from Extreme Acid Shock by Polydopamine Encapsulation. *Environ. Sci. Technol. Lett.* **2017**, *4* (8), 345–349. <https://doi.org/10.1021/acs.estlett.7b00242>.

- (224) Yong, Y. C.; Liao, Z. H.; Sun, J. Z.; Zheng, T.; Jiang, R. R.; Song, H. Enhancement of Coulombic Efficiency and Salt Tolerance in Microbial Fuel Cells by Graphite/Alginate Granules Immobilization of *Shewanella Oneidensis* MR-1. *Process Biochem.* **2013**, *48* (12), 1947–1951. <https://doi.org/10.1016/j.procbio.2013.09.008>.
- (225) Logan, B. E. Exoelectrogenic Bacteria That Power Microbial Fuel Cells. *Nat. Rev. Microbiol.* **2009**, *7* (5), 375–381. <https://doi.org/10.1038/nrmicro2113>.
- (226) Liu, H.; Cheng, S.; Logan, B. E. Power Generation in Fed-Batch Microbial Fuel Cells as a Function of Ionic Strength, Temperature, and Reactor Configuration. *Environ. Sci. Technol.* **2005**, *39* (14), 5488–5493. <https://doi.org/10.1021/es050316c>.
- (227) Jadhav, G. S.; Ghangrekar, M. M. Performance of Microbial Fuel Cell Subjected to Variation in PH, Temperature, External Load and Substrate Concentration. *Bioresour. Technol.* **2009**, *100* (2), 717–723. <https://doi.org/10.1016/j.biortech.2008.07.041>.
- (228) Feng, C.; Li, J.; Qin, D.; Chen, L.; Zhao, F.; Chen, S.; Hu, H.; Yu, C. P. Characterization of Exoelectrogenic Bacteria *Enterobacter* Strains Isolated from a Microbial Fuel Cell Exposed to Copper Shock Load. *PLoS One* **2014**, *9* (11), e113379. <https://doi.org/10.1371/journal.pone.0113379>.
- (229) Mei, X.; Xing, D.; Yang, Y.; Liu, Q.; Zhou, H.; Guo, C.; Ren, N. Adaptation of Microbial Community of the Anode Biofilm in Microbial Fuel Cells to Temperature. *Bioelectrochemistry* **2017**, *117*, 29–33. <https://doi.org/10.1016/j.bioelechem.2017.04.005>.
- (230) Lakshmidevi, R.; Nagendra Gandhi, N.; Muthukumar, K. Bioelectricity and Bioactive Compound Production in an Algal-Assisted Microbial Fuel Cell with Immobilized Bioanode. *Biomass Convers. Biorefinery* **2020**, 1–17. <https://doi.org/10.1007/s13399-020-00916-6>.
- (231) Lundberg, P.; Bruin, A.; Klijnstra, J. W.; Nyström, A. M.; Johansson, M.; Malkoch, M.; Hult, A. Poly(Ethylene Glycol)-Based Thiol-Ene Hydrogel Coatings? Curing Chemistry, Aqueous Stability, and Potential Marine Antifouling Applications. *ACS Appl. Mater. Interfaces* **2010**, *2* (3), 903–912. <https://doi.org/10.1021/am900875g>.
- (232) Ekblad, T.; Bergström, G.; Ederth, T.; Conlan, S. L.; Mutton, R.; Clare, A. S.; Wang, S.; Liu, Y.; Zhao, Q.; D'Souza, F.; Donnelly, G. T.; Willemsen, P. R.; Pettitt, M. E.; Callow, M. E.; Callow, J. A.; Liedberg, B. Poly(Ethylene Glycol)-Containing Hydrogel Surfaces for Antifouling Applications in Marine and Freshwater Environments. *Biomacromolecules* **2008**, *9* (10), 2775–2783. <https://doi.org/10.1021/bm800547m>.
- (233) Cleophas, R. T. C.; Sjollem, J.; Busscher, H. J.; Kruijtz, J. A. W.; Liskamp, R. M. J. Characterization and Activity of an Immobilized Antimicrobial Peptide Containing Bactericidal PEG-Hydrogel. *Biomacromolecules* **2014**, *15* (9), 3390–3395. <https://doi.org/10.1021/bm500899r>.
- (234) Wang, L.; Li, X.; Sun, T.; Tsou, Y.-H.; Chen, H.; Xu, X. Dual-Functional Dextran-PEG Hydrogel as an Antimicrobial Biomedical Material. *Macromol. Biosci.* **2018**, *18* (2),

1700325. <https://doi.org/10.1002/mabi.201700325>.

- (235) Khan, A. H.; Cook, J. K.; Wortmann, W. J.; Kersker, N. D.; Rao, A.; Pojman, J. A.; Melvin, A. T. Synthesis and Characterization of Thiol-acrylate Hydrogels Using a Base-catalyzed Michael Addition for 3D Cell Culture Applications. *J. Biomed. Mater. Res. Part B Appl. Biomater.* **2020**, *108* (5), 2294–2307. <https://doi.org/10.1002/jbm.b.34565>.
- (236) Forghani, A.; Garber, L.; Chen, C.; Tavangarian, F.; Tighe, T. B.; Devireddy, R.; Pojman, J. A.; Hayes, D. Fabrication and Characterization of Thiol-Triacrylate Polymer via Michael Addition Reaction for Biomedical Applications. *Biomed. Mater.* **2019**, *14* (1), 15001. <https://doi.org/10.1088/1748-605X/aae684>.
- (237) Gavira, J. A.; Cera-Manjarres, A.; Ortiz, K.; Mendez, J.; Jimenez-Torres, J. A.; Patiño-Lopez, L. D.; Torres-Lugo, M. Use of Cross-Linked Poly(Ethylene Glycol)-Based Hydrogels for Protein Crystallization. *Cryst. Growth Des.* **2014**, *14* (7), 3239–3248. <https://doi.org/10.1021/cg401668z>.
- (238) Browning, M. B.; Cereceres, S. N.; Luong, P. T.; Cosgriff-Hernandez, E. M. Determination of the *in Vivo* Degradation Mechanism of PEGDA Hydrogels. *J. Biomed. Mater. Res. Part A* **2014**, *102* (12), n/a-n/a. <https://doi.org/10.1002/jbm.a.35096>.
- (239) Takahashi, R.; Sato, S.; Sodesawa, T.; Kamomae, Y. Measurement of the Diffusion Coefficient of Nickel Nitrate in Wet Silica Gel Using UV/VIS Spectroscopy Equipped with a Flow Cell. *Phys. Chem. Chem. Phys.* **2000**, *2* (6), 1199–1204. <https://doi.org/10.1039/a909375c>.
- (240) Siepmann, J.; Siepmann, F. Modeling of Diffusion Controlled Drug Delivery. *Journal of Controlled Release*. J Control Release July 20, 2012, pp 351–362. <https://doi.org/10.1016/j.jconrel.2011.10.006>.
- (241) Crank, J. *THE MATHEMATICS OF DIFFUSION CLARENDON PRESS OXFORD 1975*.
- (242) Torres, C. I.; Krajmalnik-Brown, R.; Parameswaran, P.; Marcus, A. K.; Wanger, G.; Gorby, Y. A.; Rittmann, B. E. Selecting Anode-Respiring Bacteria Based on Anode Potential: Phylogenetic, Electrochemical, and Microscopic Characterization. *Environ. Sci. Technol.* **2009**, *43* (24), 9519–9524. <https://doi.org/10.1021/es902165y>.
- (243) Parameswaran, P.; Torres, C. I.; Lee, H. S.; Rittmann, B. E.; Krajmalnik-Brown, R. Hydrogen Consumption in Microbial Electrochemical Systems (MXCs): The Role of Homo-Acetogenic Bacteria. *Bioresour. Technol.* **2011**, *102* (1), 263–271. <https://doi.org/10.1016/j.biortech.2010.03.133>.
- (244) Parameswaran, P.; Torres, C. I.; Lee, H. S.; Krajmalnik-Brown, R.; Rittmann, B. E. Syntrophic Interactions among Anode Respiring Bacteria (ARB) and Non-ARB in a Biofilm Anode: Electron Balances. *Biotechnol. Bioeng.* **2009**, *103* (3), 513–523. <https://doi.org/10.1002/bit.22267>.
- (245) Zhu, S.; Miller, W. G.; Scriven, L. E.; Davis, H. T. Superspreading of Water-Silicone

- Surfactant on Hydrophobic Surfaces. *Colloids Surfaces A Physicochem. Eng. Asp.* **1994**, *90* (1), 63–78. [https://doi.org/10.1016/0927-7757\(94\)02904-0](https://doi.org/10.1016/0927-7757(94)02904-0).
- (246) Anseth, K. S.; Klok, H. A. Click Chemistry in Biomaterials, Nanomedicine, and Drug Delivery. *Biomacromolecules*. American Chemical Society January 11, 2016, pp 1–3. <https://doi.org/10.1021/acs.biomac.5b01660>.
- (247) Jansen, L. E.; Negrón-Piñero, L. J.; Galarza, S.; Peyton, S. R. Control of Thiol-Maleimide Reaction Kinetics in PEG Hydrogel Networks. *Acta Biomater.* **2018**, *70*, 120–128. <https://doi.org/10.1016/j.actbio.2018.01.043>.
- (248) Moon, N. G.; Pekkanen, A. M.; Long, T. E.; Showalter, T. N.; Libby, B. Thiol-Michael ‘Click’ Hydrogels as an Imageable Packing Material for Cancer Therapy. *Polymer (Guildf)*. **2017**, *125*, 66–75. <https://doi.org/10.1016/j.polymer.2017.07.078>.
- (249) Rydholm, A. E.; Anseth, K. S.; Bowman, C. N. Effects of Neighboring Sulfides and PH on Ester Hydrolysis in Thiol-Acrylate Photopolymers. *Acta Biomater.* **2007**, *3* (4), 449–455. <https://doi.org/10.1016/j.actbio.2006.12.001>.
- (250) Chatani, S.; Nair, D. P.; Bowman, C. N. Relative Reactivity and Selectivity of Vinyl Sulfones and Acrylates towards the Thiol-Michael Addition Reaction and Polymerization. *Polym. Chem.* **2013**, *4* (4), 1048–1055. <https://doi.org/10.1039/c2py20826a>.
- (251) Rojas-Flores, S.; De La Cruz Noriega, M.; Benites, S. M.; Aguirre Gonzales, G.; Salvador Salinas, A.; Silva Palacios, F. Generation of Bioelectricity from Fruit Waste. *Energy Reports* **2020**, *6*, 37–42. <https://doi.org/10.1016/j.egy.2020.10.025>.
- (252) Fan, Y.; Hu, H.; Liu, H. Sustainable Power Generation in Microbial Fuel Cells Using Bicarbonate Buffer and Proton Transfer Mechanisms. *Environ. Sci. Technol.* **2007**, *41* (23), 8154–8158. <https://doi.org/10.1021/es071739c>.
- (253) Nutan, B.; Chandel, A. K. S.; Bhalani, D. V.; Jewrajka, S. K. Synthesis and Tailoring the Degradation of Multi-Responsive Amphiphilic Conetwork Gels and Hydrogels of Poly(β -Amino Ester) and Poly(Amido Amine). *Polymer (Guildf)*. **2017**, *111*, 265–274. <https://doi.org/10.1016/j.polymer.2017.01.057>.
- (254) Meyvis, T. K. L.; De Smedt, S. C.; Demeester, J.; Hennink, W. E. Influence of the Degradation Mechanism of Hydrogels on Their Elastic and Swelling Properties during Degradation. *Macromolecules* **2000**, *33* (13), 4717–4725. <https://doi.org/10.1021/ma992131u>.
- (255) Cavallo, A.; Madaghiele, M.; Masullo, U.; Lionetto, M. G.; Sannino, A. Photo-Crosslinked Poly(Ethylene Glycol) Diacrylate (PEGDA) Hydrogels from Low Molecular Weight Prepolymer: Swelling and Permeation Studies. *J. Appl. Polym. Sci.* **2017**, *134* (2). <https://doi.org/10.1002/app.44380>.
- (256) Garcia, M. L.; Angenent, L. T. Interaction between Temperature and Ammonia in Mesophilic Digesters for Animal Waste Treatment. *Water Res.* **2009**, *43* (9), 2373–2382.

- <https://doi.org/10.1016/j.watres.2009.02.036>.
- (257) Wakida, F. T.; Lerner, D. N. Non-Agricultural Sources of Groundwater Nitrate: A Review and Case Study. *Water Res.* **2005**, *39* (1), 3–16.
<https://doi.org/10.1016/j.watres.2004.07.026>.
- (258) García-Jimeno, S.; Estelrich, J. Ferrofluid Based on Polyethylene Glycol-Coated Iron Oxide Nanoparticles: Characterization and Properties. *Colloids Surfaces A Physicochem. Eng. Asp.* **2013**, *420*, 74–81. <https://doi.org/10.1016/j.colsurfa.2012.12.022>.
- (259) Volkov, V. I.; Marinin, A. A. NMR Methods for Studying Ion and Molecular Transport in Polymer Electrolytes. *Russ. Chem. Rev.* **2013**, *82* (3), 248–272.
<https://doi.org/10.1070/rc2013v082n03abeh004278>.
- (260) Mahmoud, M.; Parameswaran, P.; Torres, C. I.; Rittmann, B. E. Electrochemical Techniques Reveal That Total Ammonium Stress Increases Electron Flow to Anode Respiration in Mixed-Species Bacterial Anode Biofilms. *Biotechnol. Bioeng.* **2017**, *114* (6), 1151–1159. <https://doi.org/10.1002/bit.26246>.
- (261) Hou, R.; Luo, C.; Zhou, S.; Wang, Y.; Yuan, Y.; Zhou, S. Anode Potential-Dependent Protection of Electroactive Biofilms against Metal Ion Shock via Regulating Extracellular Polymeric Substances. *Water Res.* **2020**, *178*.
<https://doi.org/10.1016/j.watres.2020.115845>.
- (262) Larsen, E. M.; Johnson, R. J. Microbial Esterases and Ester Prodrugs: An Unlikely Marriage for Combating Antibiotic Resistance. *Drug Development Research*. Wiley-Liss Inc. February 1, 2019, pp 33–47. <https://doi.org/10.1002/ddr.21468>.
- (263) Uria, N.; Abramova, N.; Bratov, A.; Muñoz-Pascual, F. X.; Baldrich, E. Miniaturized Metal Oxide PH Sensors for Bacteria Detection. *Talanta* **2016**, *147*, 364–369.
<https://doi.org/10.1016/j.talanta.2015.10.011>.
- (264) Bankar, S. B.; Bule, M. V.; Singhal, R. S.; Ananthanarayan, L. Glucose Oxidase - An Overview. *Biotechnology Advances*. Elsevier July 1, 2009, pp 489–501.
<https://doi.org/10.1016/j.biotechadv.2009.04.003>.

Appendix A - List of materials from Chapter 3

Name	Company
Material	
(3-Mercaptopropyl)triethoxysilane	Sigma-Aldrich
Alconox Detergent Powder	Alconox
Ammonium Sulfate	Fisher Chemical
Calcium Chloride, Anhydrous	Fisher Chemical
Citric acid monohydrate	Sigma-Aldrich
D-Glucose (Dextrose)	VWR Amresco Life Science
Dneasy Blood & Tissue Kit (50)	
DOWSIL 184 Silicone Elastomer Base	The Dow Chemical Company
DOWSIL 184 Silicone Elastomer Curing Agent	DOW SILICONES CORPORATION
Ethanol, Anhydrous	Fisher Chemical
Fisherbrand Microscope Cover Glass	Fisher Scientific
Fisherfinest Premium Microscop Slides Plain	Fisher Scientific
Hydrogen peroxide solution	Sigma-Aldrich
Isopropanol	Sigma-Aldrich
Magnesium Sulfate, 7-Hydrate	Macron Fine Chemicals
Methanol	Sigma-Aldrich
Nitrogen, Compressed	Matheson
PBS Phosphate Buffer Sali 10X	
Pentaerythritol tetra(mercaptoethyl) polyoxyethylene (4 arm-PEG)	NOF America Corporation
Phosphate Buffered Saline (PBS), 10X	VWR Amresco Life Science
Polydimethyl Siloxane (PDMS) Slygard 184	Dow Corning
Premium Microscope Slides	Fisher Scientific
Sodium chloride	Sigma Life Science
Sodium hydroxide	Sigma-Aldrich
Sodium phosphate monobasic dihydrate	Sigma-Aldrich
Stainless Steel Thickness Gage	Precision Brand Products
Sulfuric acid	Sigma-Aldrich
Toluene, anhydrous, 99.8%	Sigma-Aldrich
Trichloro (1H,1H,2H,2Hperfluorooctyl) silane (TPS), 97%	Sigma-Aldrich
Tryptic Soy Broth	Sigma-Aldrich
Name	
Equipment	
Autoclave SK300C	Yamato Scientific
BioStack Microplate Stacker	BioTek Instruments
Brightfield Upright Microscope	Olympus Corporation
Centrifuge 5702	Eppendorf

Incu-Shaker Mini

NanoDrop One^C Spectrophotometer

Oxygen Plasma Cleaner

Plasma Cleaner

Polygon400

Ultrasonic Sonicator

Benchmark

Thermo Scientific

Harrick Plasma

Harrick Plasma

Mightex

Fischer Scientific

Appendix B - List of Abbreviation

Name	Abbreviation
Lead (II) ion	Pb ²⁺
(3-mercaptopropyl) trimethoxysilane	MPTS
<i>A. tumefaciens</i> C58-GFP Himar1 mutant library	C58 ML
Acetic acid	AcOH
<i>Agrobacterium tumefaciens</i>	<i>A. tumefaciens</i>
Ammonium ion	NH ₄ ⁺
Ammonium ion nitrogen content	NH ₄ -N
Anhydrous sodium sulfate	Na ₂ SO ₄
Anion exchange membrane	AEM
Anode-respiring bacteria	ARB
Arg–Gly–Asp	RGD
Bioelectrochemical systems	BESs
Cell free culture fluid	CFCF
Chemical oxygen demand	COD
Colony formation units	CFU
Deionized water	DI water
Deoxyribonucleic Acid	DNA
Deuterated chloroform	CDCl ₃
Dichloromethane	CH ₂ Cl ₂
Dicyclohexyl carbodiimide	DCC
Diethyl ether	Et ₂ O
Dimethylformamide	DMF
Electroactive bacteria	EAB
<i>Escherichia coli</i>	<i>E. coli</i>
Ethanol	EtOH
Extracellular electron transfer	EET
Fluorescein isothiocyanate	FITC
Fluorescent activated cell sorting	FACS
Glucose oxidase	Gox
High-performance liquid chromatograph	HPLC
High-throughput screening assays	THS
Hydrogen peroxide	H ₂ O ₂
Lactate dehydrogenase	LDH
Lower critical solution temperature	LCST
Microbial electrolysis cells	MEC
Microbial fuel cells	MFC

Microbial Genomic Sequencing Center	MiGS
Microbial peroxide producing cells	(MPPCs)
Mutant libraries	ML
Near-infrared light	NIR light
N-hydroxysuccinimide	NHS
<i>o</i> -nitrobenzyl	<i>o</i> -NB
PEG-divinyl sulfone	PEGVS
Pentaerythritol tetra (mercaptoethyl) polyoxyethylene	PEG-tetrathiol
Poly(ethylene glycol) diacrylate	PEGDA
Polyacrylamide	PAA
Polydimethylsiloxane	PDMS
Polydopamine	PDA
Polyethylene glycol	PEG
Polymerase chain reaction	PCR
<i>Rhizobium rhizogenes</i> K84	K84
Signal sender cells	SCs
Sodium hydrogen phosphate	NaH ₂ PO ₄
Sodium hydrogen sulfate	NaHSO ₄
Sodium hydroxide	NaOH
Sodium phosphate monobasic dihydrate	NaH ₂ PO ₄ ·2H ₂ O
Sulfuric acid	H ₂ SO ₄
Triethylamine	Et ₃ N
Ultraviolet light	UV light
Upconversion nanoparticles	UCNPs
Upper critical solution temperature	UCST
Viable but non-culturable cells	VBNC
Weight average molecular weight	MW
Wildtype <i>A. tumefaciens</i> C58	C58